Tests on GFRP Reinforced Concrete Knee-Joints Subjected to Negative Moments

by

Nader Sleiman

A thesis
presented to the University of Waterloo
in fulfillment of the
thesis requirement for the degree of
Master of Applied Science
in
Civil Engineering

Waterloo, Ontario, Canada, 2017

AUTHOR'S DECLARATION

I hereby declare that I am the sole author of this thesis. This is a true copy of the thesis, including any required final revisions, as accepted by my examiners.

I understand that my thesis may be made electronically available to the public.

Abstract

The use of glass-fibre reinforced polymers as main reinforcement in concrete structures has become an appealing option for structures in aggressive environments. Concrete knee-joints are joints where the beam and column both terminate at the joint. The application GFRP reinforcement in knee-joints may be problematic considering the weak link at the reinforcement bend. This is critical because there is a risk of premature failure in the joint due to bar rupture, regardless of adjoining member designs. The behaviour of knee-joints reinforced with GFRP has not been studied before.

The presented experimental program consists of eight full scale specimens which were tested under monotonic closing loads. The variables studied are the effect of varying reinforcement ratio, the effect of confinement stirrups in the joint, and the effect of corner geometry. The eight specimens are divided into two groups, confined and unconfined specimens. Of the eight specimens, two are designed with an altered geometry to include an interior chamfer.

Test results indicate that an increase in reinforcement ratio improves the strength efficiency while directly altering the failure mode: Failure by bar rupture as the reinforcement ratio increased was prevented and occurred by failure of diagonal strut. The addition of confinement stirrups significantly increased the ultimate strength as well as the maximum deflection. The effect of changing corner geometry has a minor effect on the specimen strength; however, brittle failure in the joint was prevented.

Further studies must be conducted including different confinement techniques, different FRP types and suppliers, as well as different loading types such as opening moments and load reversals.

Acknowledgements

First, I would like to thank my supervising professor, Professor M.A. Polak, for her continuous guidance and support. Thank you for inviting me to the world of research. I would also like to thank my readers Prof. A. Al-Mayah and Prof. D. Basu for their comments.

Special thanks go out to the technical staff at the Structures Lab. To Richard Morrison, whose innovative ideas and solutions played a big part in my work. To Doug Hirst, who always encouraged me to do things right without cutting corners. Finally, Peter Volcic, whose expertise in instrumentation allowed me to quickly get setup.

I would like to extend my gratitude to all of my colleagues at the University of Waterloo whose help and support was invaluable: Ryan Barrage, my dear friend and colleague, for the continuous words of encouragement during my time as a student and for always lending a friendly ear. Graeme Milligan for always being the first to offer help during all the stages of my experimental program. Ayman Shihata, for being an exemplary mentor, I am so grateful you took me under your wing when I first started. Piotr Wiciak, my friend and office mate, for all the philosophical and insightful discussions we've shared. Mikhail Laguta, my friend and classmate since 2010, for all the laughs we've shared looking at funny pictures while sharing a coffee. Colin Van Niejenhuis, for his continued advice when I got stuck, and for channeling his inner farmer to help me figure things out. Hisham Abduljabbar for the words of advice and for leading my formwork construction. Finally, Navan Chawla for her invaluable assistance during as a URA.

I'd like to acknowledge the help from all who've helped me at any point during my studies: Kyle Balkos, Dylan Dowling, Peter Loudfoot, and Adam Felinczak. Thank you.

Finally, I would like to thanks my parents, Samia and Hassan, and my sisters Sarah and Mira for the endless love and support they've bestowed. I would not be the person I am today without you.

Dedication

To my mother, my father, and my sisters.

Table of Contents

List of Figures

List of Tables

Chapter 1
Introduction

1.1 General

Reinforced concrete knee joints, also known as frame corners, are beam column joints which meet and terminate at the joint. Typical locations for knee joints include joints present in building rooftops, bridges, box culverts, as well as bridge pier caps, shown in Figure 1.1.

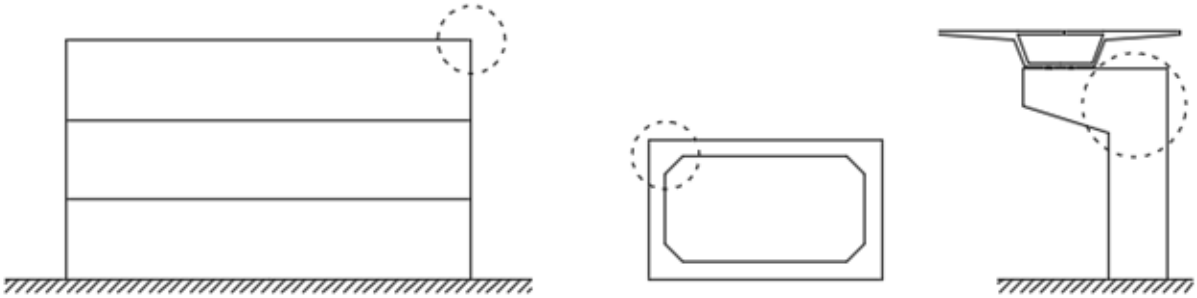

Figure 1.1: Knee-joints in (a) Parking Garage Rooftop, (b) Box Culverts, (c) Bridge Pier Caps

The main purpose of a joint in reinforced concrete structures is to transfer loads and moments from adjoining members to the column. Joints in a structural system are often the weakest link between adjoining members (Park & Paulay, 1975). As such, the design and detailing of the joint is critical to prevent their premature failure and potential subsequent collapse of structure.

Nilsson (1973) summarizes design criteria for frame corners and joints as follows:

- The strength of the joint should at least be as strong as the adjoining members.
- If the first condition is not met, sufficient ductility must be present to prevent brittle failure.
- Crack widths in the corner should be limited to an acceptable value under service loads.
- Fabrication and positioning of reinforcement in the joint must be easy.

Reinforced concrete structures are typically reinforced with steel. However, structures present in aggressive environments such as bridges, culverts, and other marine structures are highly

susceptible to corrosion. The corrosion of steel reinforcement leads to the deterioration and loss of load carrying capability of the structure. Solutions to this problem have been proposed, including the use of stainless steel reinforcement, epoxy coatings, and concrete additives. However, these methods are not perfect and, in the case of stainless steel, can be particularly expensive.

The use of fibre reinforced polymer (FRP) reinforcement is a viable alternative to steel as main reinforcement. Given that it is a fibre embedded in a polymer matrix, this material is completely non-metallic and does not corrode. In addition to the resistance to corrosion, FRP reinforcement exhibits higher tensile strengths, low thermal and electric conductivity, are nonmagnetic, and are lightweight (20 – 25%of steel density) (ACI Committee 440, 2015). Conversely, FRPs possess a lower modulus of elasticity and, unlike steel, does not show a yield plateau. These properties must be taken into account and alter the design philosophy of concrete structures reinforced with this material.

1.2 Research Motivation

Extensive research has been performed on knee joints reinforced with steel, in both opening and closing moments. The material behaviour in this joint type is well understood and detailing schemes are put into place. This is not true for glass fibre reinforced polymer (GFRP) reinforcing bars.

The reinforcement used in knee joints consists of continuous longitudinal bars running from the beam into the column, with a 90^{o} bend in the corner. GFRP bars exhibit high tensile strengths when loaded in the direction of the fibres and are significantly weaker when loaded perpendicularly. In the joint, the bent portion of the bar experiences forces acting perpendicular to the fibre orientation. This means that the bent portion is the weakest section in the bar and may be prone to premature failure at a load less than the ultimate strength.

Extensive tests must be performed in order to develop design guidelines for GFRP use in knee joints. Although tests exist for determining the strength of the bend, it is not certain that the

bends in actual structures will behave as tested. Currently, no tests have been performed on knee joints reinforced with FRP reinforcement (GFRP or other types). This presents a gap in literature that must be filled in order to better understand the behaviour of GFRP in knee joints.

1.3 Objectives and Scope

The main goal of this experimental program is to investigate the behaviour of GFRP longitudinal bars used in knee joints, namely under closing (or negative) moments. The weak link in the bend combined with the lack of yield plateau of GFRP must be accounted for in this investigation.

As a program that has not been undertaken before, one must consider the vast areas available to be studied – including, but not limited to, joints with closing and opening moments, joints loaded statically or cyclically, joints with angles other than 90^o, and also joints reinforced with FRP materials other than GFRP. As a starting point, the experimental program was selected to be tested under monotonic static loads with closing moments.

In order to facilitate the investigation, a number of parameters were considered: The effect of reinforcement ratio, joint confinement, and corner geometry. Eight full scale specimens were studied and divided into two groups, confined and unconfined specimens. Within each group, one specimen was designed with a chamfer in the interior corner, commonly seen in box culverts – while others were designed with 90^o corners. Within the unconfined group, the reinforcement ratio was varied.

The specimens were tested using static load applied at the beam free end while fixed at the base of the column. Analysis of the tests results were based on failure modes, moment-deflection curves, strain gauge readings, and crack patterns.

1.4 Thesis Organization

The thesis is organized in six chapters as follows:

Chapter 1 introduces the research and discusses the motivation behind the work

Chapter 2 presents the background and review of literature. FRP as a material is discussed, including the effect of bends. Previous work done on knee joints reinforced with steel is reviewed, with particular reference to the effect of reinforcement detail, reinforcement ratio, and joint confinement.

Chapter 3 describes the experimental program, including the fabrication of specimens, instrumentation used, and testing setup.

Chapter 4 presents the experimental results including test observations and failure modes.

Chapter 5 presents the discussion of data and examines the effect of reinforcement ratio, joint confinement, and corner geometry on the behaviour of the specimens.

Chapter 6 presents the main conclusions of the research work done and provides recommendations for future work.

Chapter 2
Background and Literature Review

This section presents the background on GFRP as a material, and reviews literature on GFRP bends. Review of literature regarding tests performed on steel reinforced knee joints is also presented.

2.1 Fibre Reinforced Polymers

FRPs are composite materials that consist of high strength fibres embedded in a polymeric resin matrix. Early uses of FRPs were adopted in the 1940's in the aircraft industry. After commercialization, better performing fibres were used to meet the challenges faced in the aerospace industry in the 1960s and 1970s (Bakis, et al., 2002). In the civil engineering industry, it was speculated as early as 1954 that the use of FRP as concrete reinforcement is viable given its corrosive resistance property (Bank, 2006). It was not until the 1970s that FRPs were considered for structural engineering applications (ISIS Canada, 2007). Since then, the use of FRPs as primary reinforcement has become more popular in reinforced concrete. Since FRPs are composed of separate components, the behaviour of the composite as a whole depends on the properties of the components.

2.1.1 Fibres

Fibres are the main component providing strength and stiffness in the FRP composite. Typically for structural applications, fibres are continuous with large length to diameter ratios. Due to their exceptional strength along their length, the fibre orientation is placed in line with applied loads. In civil engineering applications, three main fibre types are used: Glass, carbon, and aramid fibres (ISIS Educational Committee, 2006).

2.1.1.1 Glass

Many types of glass fibres are available for use, with E-glass being the most widely used. The benefits of using glass fibres include a relatively low cost, high strength, as well as electrical and

acid resistance (Benmokrane, Chaallal, & Masmoudi, 1995). However, the main disadvantages include a relatively low modulus of elasticity, as well as lower resistance to moisture and alkaline environments (Bai, 2013).

2.1.1.2 Carbon

Carbon fibres are the most expensive option; however, their use presents numerous advantages. This includes high tensile strength, high modulus of elasticity, as well as remarkable resistance to thermal, chemical, and environmental effects (ISIS Educational Committee, 2003). Their low density also makes their use appealing in situations where weight or deflections are sensitive. Conversely, in addition to their high cost, their production requires large amounts of energy (Bai, 2013).

2.1.1.3 Aramid

Aramid fibres (aromatic polyamide) are the least prevalent fibres used in FRP reinforcement. These fibres show the highest average tensile strength – relative to carbon and glass fibres – while possessing an intermediate modulus of elasticity (Bai, 2013). Due to their anisotropic nature, aramid fibres have a lower compressive and shear strength and is very sensitive to ultraviolet radiation and moisture (ISIS Educational Committee, 2003) which makes them a less popular civil engineering application.

2.1.2 Matrix

The second main component in FRPs is the matrix. In addition to carrying some loads, the matrix has four functions (Keller, 2003):

- Maintaining the orientation of the fibres in the desired position.
- Facilitating the transfer of forces to the fibres.
- Supporting the fibres against buckling under compressive loads.
- Protecting the fibres from environmental and chemical effects.

Two main types of resins are used: thermoplastics and thermosets. Thermoplastics, due to their non-crosslinked nature, do not form an irreversible chemical structure. This gives the ability of the material to withstand reprocessing. The use of thermoplastics as matrix for FRP reinforcement is uncommon due to their higher viscosity – which makes processing more difficult as well as allowing worse adhesion to the fibres (Bai, 2013).

Due to the crosslinked nature of thermosets, the resin cannot be reformed once it is cured. The low viscosity of thermosets provides ease of manufacturing while also possessing good adhesion to the fibres (Bai, 2013). For this reason, resin matrices used in structural engineering are almost exclusively thermosets.

The three main thermosets used in the manufacture of FRP reinforcement are polyesters, vinylesters, and epoxies. Since vinylesters are unsaturated esters of epoxy resin, their mechanical properties are similar to epoxy resins while their processing is akin to the processing of polyesters. Fewer crosslinks found in vinyl ester allows it to achieve higher flexibility and fracture toughness when compared with polyester. Vinylester offers high resistance in aggressive acidic and caustic environments, which makes it a good choice for civil engineering applications where harsh chemical environments are a concern (Bai, 2013). Although the cost of vinylester is higher relative to polyesters (ISIS Educational Committee, 2003), and Micelli & Nanni (2004) recommend avoiding the use of polyesters in the construction industry due to their inadequate protection of fibres in an alkaline environment.

2.1.3 Manufacturing

Several FRP manufacturing techniques are available, including pultrusion, filament winding, and wet lay-up. The common manufacturing method for FRP reinforcing bars with uniform sections is by pultrusion. This process involves pulling the continuous fibres into a resin bath and through a heated die. The resin coated fibres harden into the shape of the die after passing through. Fibres aligned with the length of the reinforcing bar as a result of this technique (ISIS Educational Committee, 2003). A schematic of the pultrusion process is shown in Figure 2.1.

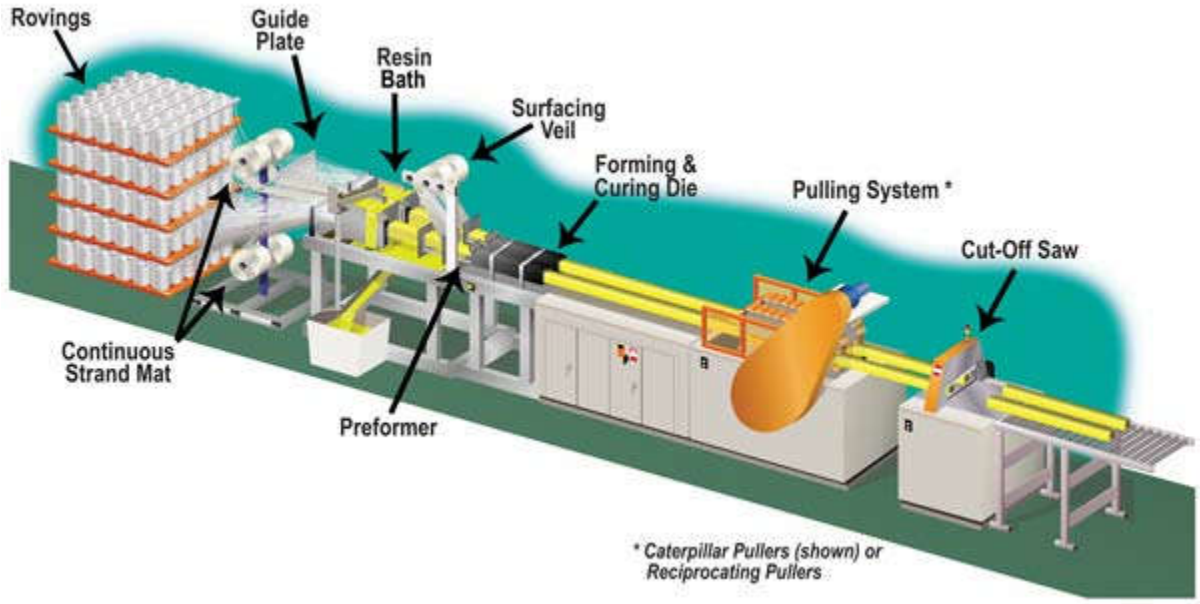

Figure 2.1: Process of Pultrusion (Strongwell, 2017)

2.1.4 GFRP Bends

The use of GFRP as main reinforcement in concrete structures required the development and use of bent bars. This includes the use of stirrups, looped bars, hooked bars, as well as special bends for use in bridge barriers (Benmokrane, El-Salakawy, El-Gamal, & Goulet, 2007). Compared to the straight portion of the reinforcement bar, the tensile strength of the bent portion is significantly less. The American Concrete Institute (ACI) committee 440 (2015) presents a relationship predicting the tensile strength of the bar at bends, which depends on the radius of bend to diameter ratio, r_b/d_b. For $r_b/d_b = 4$, the tensile strength is predicted to be 50% of the straight portion.

It is no surprise that the strength of the bend is less than the straight portion. The high strength of FRP bars comes from the load carrying ability of the bars parallel to the fibres. At the bend, these fibres are experiencing loads transverse to their orientation. The process of bending also introduces kinking of the innermost fibres which also reduces the strength of the bend, shown in Figure 2.2.

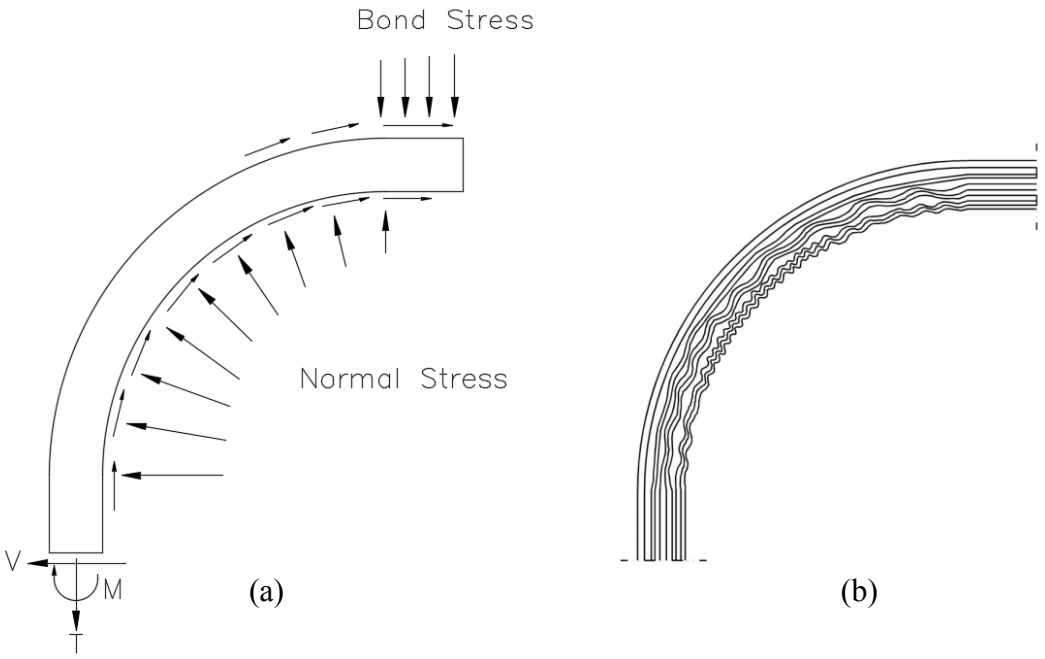

Figure 2.2: (a) Stresses and (b) Kinking of Fibres Occurring at the Bend (Ahmed et al. 2010)

On the microscopic level, the bending of individual aramid fibres has been seen to cause permanent deformation on the compression face (Hull & Clyne, 1996) and consequently contributing to lower strength of the bend as a whole.

Maruyama, Honma, & Okamur (1993) conducted tests on carbon and aramid FRP bent bars to investigate the effect of varying the radius of bend and strength of concrete on the performance of the bend.

The FRP bars considered in the investigation were seven strand CFRP, CFRP bars manufactured by pultrusion, and braided AFRP bars. Three different radii of bend were considered: 5 mm, 15 mm, and 25 mm measured from the inside face of the bend. The concrete strengths considered were 50 MPa and 100 MPa.

Results from testing indicated that as the radius of bend decreased, the capacity of the bend also decreased. It was found that the pultruded bars showed a sharper drop in tensile capacity relative

to the strand CFRP and braided AFRP bars. This was attributed mainly to the resulting slackness in the inside of the bend; which does not carry tensile stresses as effectively. Test results showed that an increase in concrete strength results in higher bend capacities. This was explained by the presence of better bond between the bars and concrete, which resulted in a decrease in the tensile forces transferred to the bent portion of the bars.

Ehsani, Saadatmanesh, & Tao (1995) performed tests on GFRP hooked bars to examine the effect of concrete compressive strength, radius of bend, tail length, and straight embedment length on the bond behaviour. The concrete compressive strength considered were 28 MPa and 56 MPa, and the radius of bends studied were 0 and 3; measured as a ratio of radius to diameter of bar. The straight embedment lengths and tail lengths were varied between 0 to 12 and 12 to 20 times the diameter of bar, respectively.

Test results for $r/d_b = 3$ showed a small increase in maximum tensile strength of the bar with increased concrete strength; however, with r/d_b of zero, there was little influence on the maximum tensile strength.

Increasing the hook radius showed a significant increase in maximum load – from 6.5 kips (28.9 kN) to 22.3 kips (99.2 kN) for r/d_b of zero and three, respectively. Strengths for r/d_b of zero were as low as 21% of the straight portion strength and did not exceed 27%. However for $r/d_b = 3$, strengths ranged from 53% to 97%. All specimens with low radius of bend failed by fracture of reinforcement by shear, whereas the higher radius of bend specimens failed by splitting of concrete or axial fracture.

A comparison between the bend strength testing methods was performed by Ahmed, El-Sayed, El-Salakawy, & Benmokrane (2010). Two testing methods are approved by the American Concrete Institute, the B.5 and B.12 test methods. The B.5 test method involves embedding a "C" shaped stirrup in two blocks of concrete and testing by pushing the blocks of concrete as shown in Figure 2.3. The B.12 test method involves testing of a "U" shaped specimen that is anchored as at the ends using the apparatus as shown in Figure 2.4.

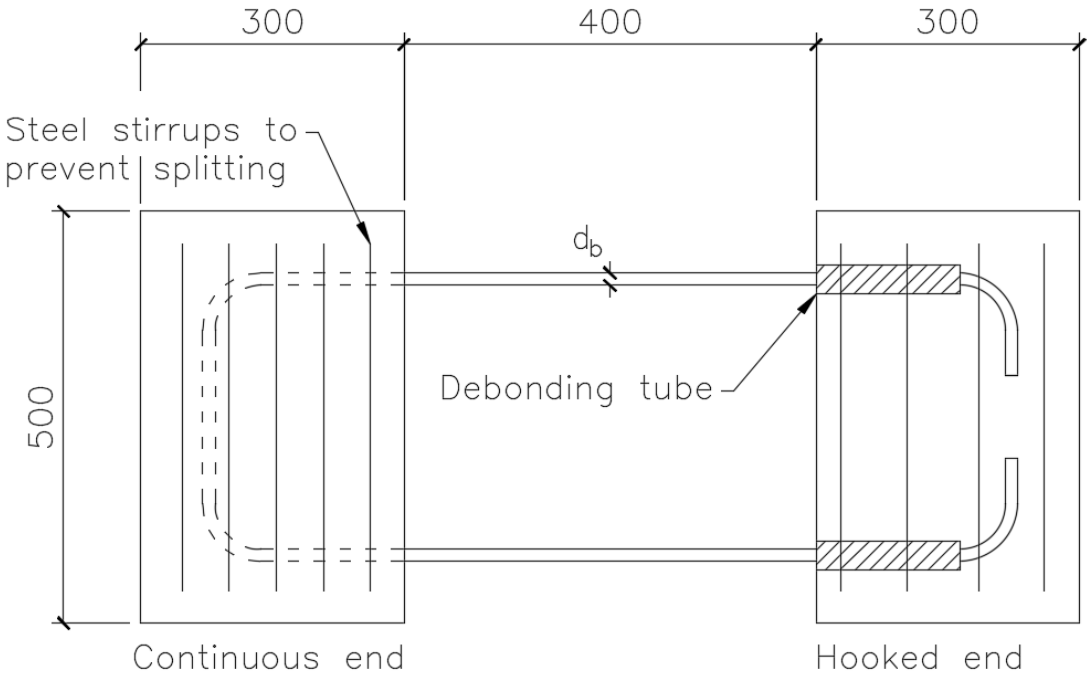

Figure 2.3: ACI B.5 Test Apparatus

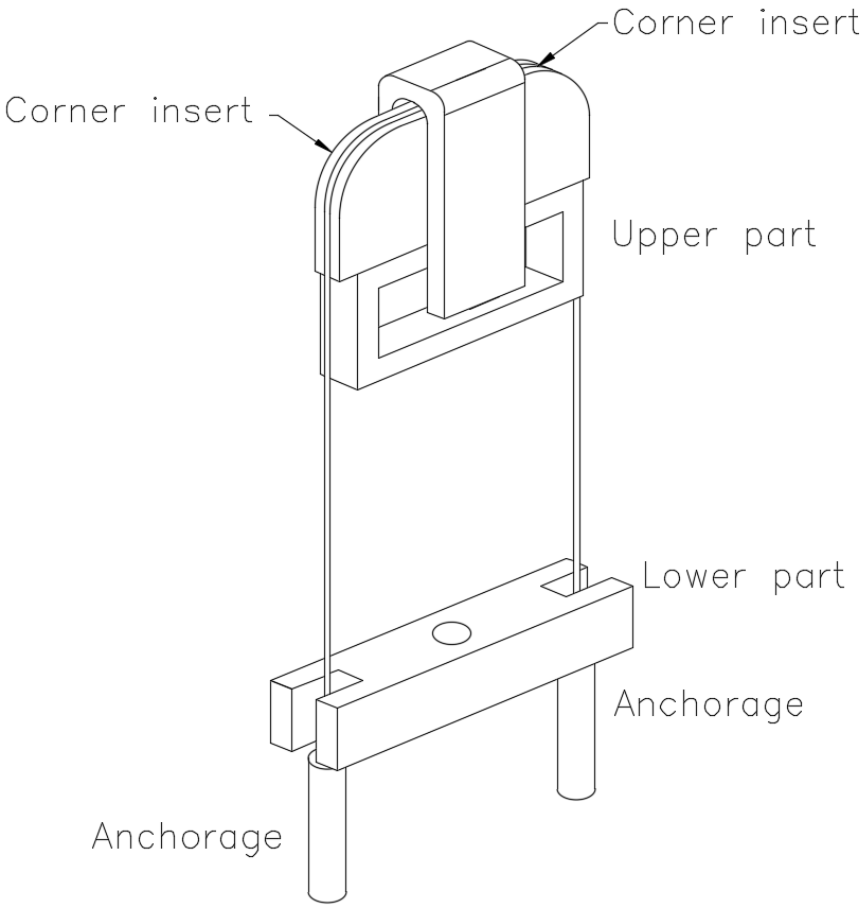

Figure 2.4: ACI B.12 Test Apparatus

Three diameters of GFRP were tested (No. 10, 16, and 19) as well as one CFRP (No. 10). Four specimens were prepared for the B.5 test while five were prepared for the B.12 test. All bent bars were manufactured with $r_b/d = 4$. Additional six specimens were tested according to B.2 to determine the tensile strength of the straight portions.

Results from the B.5 test indicate that the ratio of bend strength to straight portion strength was between 58% and 68%, while tests from the B.12 test show a consistently lower percentage ranging between 35% and 41%. These results are consistent with the prediction given in the equation for predicting the tensile strength of the bend given by ACI guidelines (ACI 440.6-15).

Ahmed et al. (2010) mention that since the results from the B.12 test are consistently lower than the B.5 test, acceptable minimums should be provided for each one. They found that the B.5 test is more representative of the actual behaviour of the bent portion since it is embedded in concrete and works better for bars with surface indentations due to distribution of stresses. It is stated that the B.5 test appears more proper; however, the B.12 test could be used as a preliminary test of the material performance.

2.2 Previous tests on Steel Reinforced Knee Joints

Previous tests on corners were motivated by the inability of details to achieve the designed strength of the adjoining members. Several researchers in the 1960s and 1970s performed tests on steel reinforced joints under both opening and closing moments. The following section reviews tests on steel reinforced joints under closing moments performed by researchers between 1960 and 2001. The effects of reinforcement detail, reinforcement ratio, and joint confinement are reviewed. Different testing configurations are briefly discussed.

2.2.1 Effect of Reinforcement Detail

The Joint Committee on the Detailing of Reinforced Concrete (1970) provided recommendation for detailing of corner bars. The guidelines recommended avoiding the detail shown in Figure 2.5a and suggest better arrangements in Figure 2.5b and Figure 2.5c.

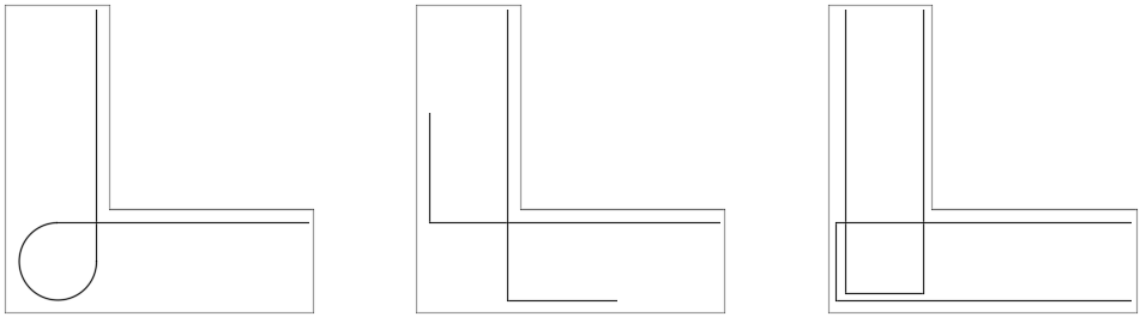

Figure 2.5: Detailing Recommendations for Corner Bars (Reproduced from Joint Committee on the Detailing of Reinforced Concrete, 1970)

Figure 2.5b consists of a compression bar that is routed into the tension face and vice versa, while Figure 2.5c consists of two loop reinforcements meeting at the joint. The former and latter configurations are labelled by the thesis author as “hooked detail” and “loop detail”, respectively. It is obvious that the hooked detail is intended for corners with opening moments. However, previous tests include specimens utilizing this detail with additional continuous tension reinforcement.

Mayfield, Kong, Bennison, & Davies (1971) studied the effect of varying the corner reinforcement configuration on the strength and stiffness of corner joints. Four main reinforcement details were considered by the author under negative moments. Of those, two details consist of continuous longitudinal reinforcement with varying locations of stirrups in adjoining members. The third detail consists of two reinforcement loops meeting at the joint, shown in Figure 2.5c. Also considered was a hooked detail as shown in Figure 2.5b.All details considered are shown in Figure 2.6.

All but one specimen exceeded strength efficiency (experimental/calculated) of 100%. Detail 2 showed a failure load less than calculated (94%). However, another identical specimen was found to have an efficiency of 117%.

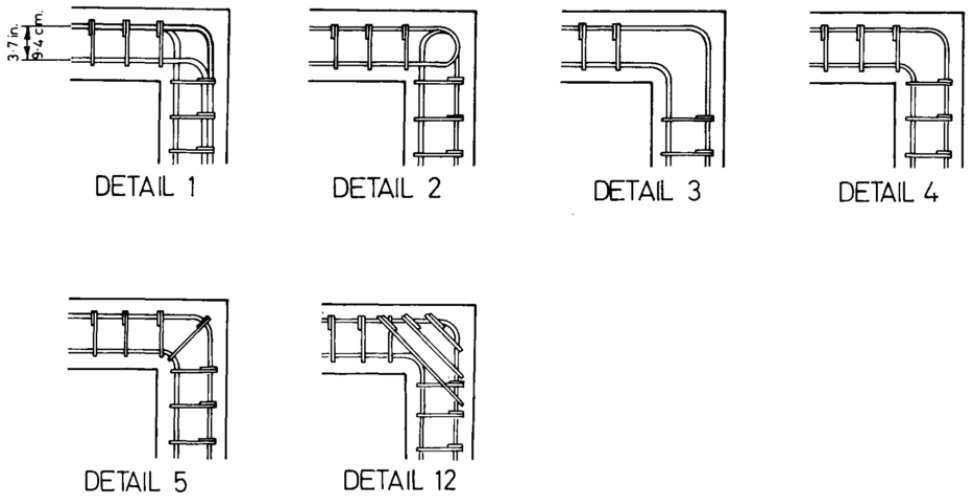

Figure 2.6: Details for Closing Corners (Mayfield et al., 1971)

Detail 1 showed the highest stiffness of all specimens tested, while detail 2 showed the lowest stiffness. Details 3 and 4 exhibited a moderate stiffness relative to the other tested details.

Crack widths measured for detail 1 were the smallest, while details 2 and 3 showed significantly larger crack widths at similar load levels. Detail 4, having only two extra stirrups close to the joint from detail 3, showed less crack width size relative to detail 3. Mayfield et al. (1971) discussed that detailing in corners with negative reinforcement was not important and that focus must be shifted to corners with positive moment.

Swann (1969) discussed the effect of detailing on knee joints. Three detail configurations: hooked bar detail, two loops meeting at the joint, and a looped compression reinforcement bar with additional continuous tension bars (103, 104 and 106 in Figure 2.7). Also considered were two details with continuous longitudinal reinforcement, but with either stirrups or welded bars

parallel to the compression strut. All specimens were designed with a balanced reinforcement ratio (109 and 110 in Figure 2.7).

Only the specimen with the welded bars failed at load larger than calculated with 101% efficiency. The similar detail with stirrups in lieu of welded bars failed at a lower efficiency of 87%. The remaining three specimens tested had efficiencies less than 80%.

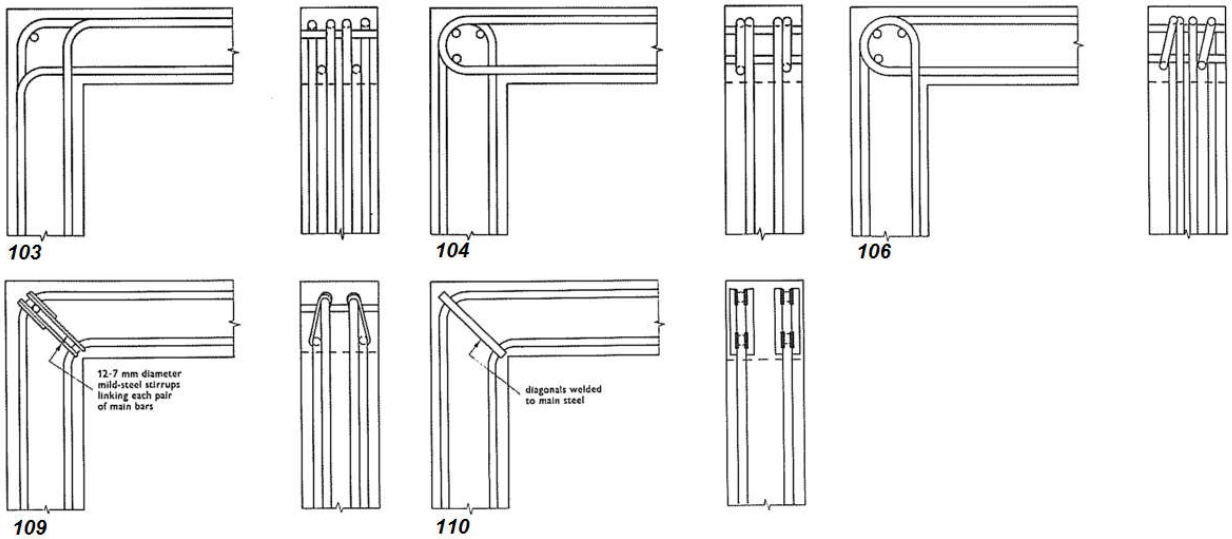

Figure 2.7: Joint Details Tested by Swann (1968)

Swann noted that all specimens failed by crushing of the diagonal concrete strut. Since the specimens were all designed with a balanced reinforcement ratio, this comes as no surprise. The lack of strain readings on the reinforcement prevented the confirmation the simultaneous steel yielding and concrete crushing. Had the reinforcement ratio been designed as under reinforced, there would have been a higher chance of the specimens attaining the full calculated strength. This is especially true given that the diagonal strut, being the source of main joint strength, failed.

The increase in strength exhibited by the stirrups/welded bar specimens can be attributed to the extra diagonal reinforcement, resulting in a reinforced strut. Two legs are provided in the stirrups specimen while four legs are provided for the welded specimen. This is consistent with the

respective strength efficiencies of 87% and 101%. All specimens were found to have similar stiffness, with the exception of the welded bar specimen – which was relatively more stiff and not exceeding 0.03 rad.

Johansson (2001) tested eight specimens to examine a proposed detail compared to the detail suggested by Swedish Shelter regulations. The recommended detail is the hooked bar detail with additional tension bars. Johansson's proposed detail was the use of two loops lap spliced in the corner. Although this detail had been studied in the past, Johansson proposed the same detail for corners subjected to both positive and negative moments.

Six out of eight specimens attained greater than 100% strength efficiency, with two specimens having efficiency less than 90%. Johansson found that despite the concrete spalling off in the latter two specimens, the steel had already yielded in the bar.

Tests done by Mayfield et al. (1971) and Johansson (2001) indicated that reinforcement configuration is not critical as long as reinforcement is provided on the tension face. Although Swann's tests utilized some of the same details used by Mayfield et al. and Johansson, almost all specimens failed prematurely. The major difference between Swann and the other authors is that the reinforcement ratio was chosen as balanced and was likely responsible for these premature failures.

2.2.2 Effect of Reinforcement Ratio

Luo & Bai (1988), Luo, Durrani, Bai, & Yuan (1994) performed tests on 14 full scale concrete frame corner connections to investigate the effect of varying reinforcement ratio, radius of curvature, and compressive strength of the concrete on the joint. The reinforcement layout consisted of a continuous longitudinal tension bar as well as confining stirrups in the corner.

Keeping the radius of bend constant at $R/d_s = 2$ (where R is the radius of bend and d_s is the effective depth), it appears that increasing the reinforcement ratio has a detrimental effect on the strength efficiency of the specimen. Increasing the reinforcement ratio from 0.55% to 1.23%

resulted in a strength efficiency of 143% to 103% respectively. This effect does not appear serious since efficiencies are still larger than 100%. However, when the radius of bend was increased to 7, increasing the reinforcement ratio from 1.25% to 2.09% resulted in strength efficiencies of 117% to 78% respectively.

Luo et. al show that irrespective of radius, high reinforcement ratio specimens resulted in a failure by diagonal strut crushing.

Johansson (2001) also varied the reinforcement ratio in his series of tests. All specimens were designed as under reinforced. Only two specimens failed with sub 100% strength efficiency. These specimens had the highest reinforcement ratio of the loop splice detail (0.88%).

The failure of these specimens by spalling of concrete can be explained by the presence of large bearing stresses in the compression strut. These large stresses in the compression strut are resultant from the higher number of reinforcement used. Johansson states that the risk of brittle behaviour due to spalling is present; however, the risk of brittle failure can be decreased if the corner is laterally restrained or if only a small number of bars are affected. For instance, members with large width similar to a slab-wall connection.

Kemp & Mukherjee (1968) studied the effect of reinforcement ratio of the main tensile reinforcement on the strength of the specimen. L shaped and U shaped specimens were considered in this study. The reinforcement ratio was varied between 0.49, 0.89%, and 1.39%.

Only specimens with low reinforcement ratio possessed strength efficiencies larger than 100%, while specimens with 0.89% and 1.39% had efficiencies as low as 84%. All specimens developed cracks at the beam/joint and column/joint interfaces. The specimens with 0.49% reinforcement ratio failed by yielding of reinforcement at that location – without developing any diagonal cracks in the joint. Specimens reinforced with 0.89% failed in flexure simultaneously with the formation of a diagonal joint crack. A sudden failure was observed in the 1.39% specimens after the diagonal joint formed in the advanced load stages.

A trend can be observed from these modes of failures: At low reinforcement ratios, stresses in the joint do not exceed its capacity before the steel yields in the adjoining member. As the reinforcement ratio was increased, diagonal cracks formed; suggesting that the capacity of the joint, namely the diagonal strut, had been exhausted. With enough increase in reinforcement ratio, the strength of the joint could be exceeded well before the steel yields – resulting in a sudden brittle failure.

The authors noted that the diagonal crack formation was analogous to the behaviour seen in a split tensile test. They obtained an expression for a maximum reinforcement ratio to avoid the splitting failure in the joint. The expression assumes that the formation of the diagonal crack in the joint follows the same mechanism as that of a split cylinder or prism test. The formulation considers diagonal resultant forces occurring from the bars and acting on the joint square core. The expression is given as follows

$$\rho_{km} = k \frac{f'_t}{f'_c} \qquad \textbf{(2-1)}$$

Where k is a factor accounting for the modelling technique (either 1, 1.11 ,or 1.36), f'_t is the tensile strength of concrete, and f'_c is the compressive strength. The authors admit that the forces occurring at the joint are more complex than the assumptions used in the developed expression and state that $k = 1.11$ is a reasonable lower bound. Park & Paulay (1975) used $k = 1.2$.

It is clear that there exists a limit to the maximum reinforcement ratio before crack formation occurs in the joint. Results of tests by Johansson conformed to the observations noted by Kemp & Mukherjee: specimens with reinforcement ratios up to 0.75% attained efficiencies of greater than 100%; however, specimens with reinforcement ratio of 0.88% did not exceed 89%. It is not practical to limit reinforcement ratios to prevent diagonal crack formation in the joint, especially when this limit is usually well below the balanced reinforcement ratio. As such, the formation of

joint cracks is imminent and must be controlled. Providing reinforcement in the joint to control cracks and providing confinement may offer appropriate resistance.

2.2.3 Effect of Confinement

Zouzou & Haldane (1993) performed tests studying the effect of confinement in the joint on strength and ductility. The authors tested two full scale specimens: one with a typical reinforcement detail and one with confinement stirrups and ties in the compression strut. Sufficient stirrups were used perpendicular to the anticipated crack formation, and two ties were placed parallel to the crack formation. The ties were placed just outside the compression strut and their purpose was to force the crack to form outside the strut to preserve the strut and the integrity of the joint. The two specimens are shown in Figure 2.8.

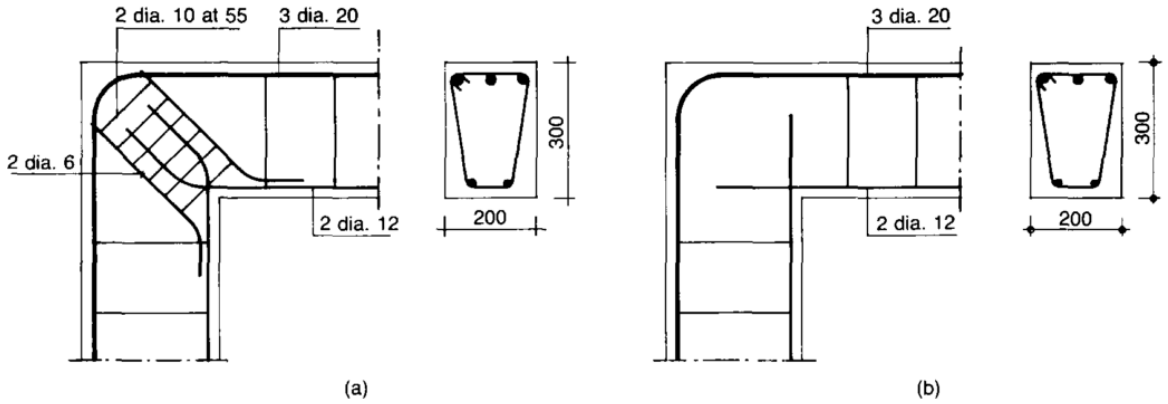

Figure 2.8: Reinforcement Details in Corners Used by Zouzou & Haldane (1993)

Both specimens exceeded the design strength: the unconfined specimen had an efficiency of 114% while the confined specimen attained an efficiency of 120%. Zouzou & Haldane attributed the increase of strength of the unconfined specimen due to strain hardening of steel.

Failure of both specimens occurred in the joint after developing diagonal cracks – which developed at a relatively early load level. The unconfined specimen failed in a brittle manner; immediately after reaching the peak load. On the other hand, the confined specimen displaced by

an extra 50mm after reaching the peak load, showing the added ductility from the confinement of the strut.

Zouzou & Haldane used Equation 2-1 developed by Kemp & Mukherjee (1968) in order to force the premature failure in the joint. Since the specimen exhibited a 114% strength efficiency, Zouzou & Haldane (1993) note that this relationship was developed using specimens that had a small radius of bend in the joint reinforcement – and believed that the high stresses caused from this small radius contributed to early failure.

All specimens tested by Luo et al. (1994) all contained a grid of reinforcement according to ACI 352 guidelines. The author concludes that if large amounts of steel are avoided, the adjoining members should develop the full design capacity.

Stroband & Kolpa (1983) performed tests on 33 portal frames and studied the effect of the quality of concrete, the detailing of reinforcement, additional confinement reinforcement, and the radius of bend. The tests were not full scale models; rather, they were scaled down using a 1:4 scale. Two additional confinement reinforcement configurations were considered: three horizontal 2.8mm "U"-shaped bars, referred to by the authors as hairpins, and a grid of three vertical and three horizontal hairpin reinforcement.

Most of the tested specimens exceeded the calculated strengths. In the case of low radius of bend, the unconfined corner achieved 97% efficiency. Adding the horizontal and grid of hairpins increased the efficiencies to 114% and 115% respectively.

The addition of confining reinforcement showed some increased ductility for all specimens. In the case of low radius of bend, the unconfined corner displaced 10.5mm up to 12mm and 14mm at peak load for the horizontal and grid of hairpins, respectively.

Mayfield et al. (1972) tested one specimen with diagonal stirrups in the corner, placed perpendicular to the anticipated crack in the corner. When compared with the unreinforced joint specimen, the confined corner does not show a larger strength efficiency; albeit both of them

achieved efficiencies greater than 130%. The confined specimen did show higher stiffness and smaller cracks than the unconfined specimen.

2.2.4 Experimental Setups

Previous experiments done on knee joints and portal frame corners were performed using different testing setups. Although the outcome is very similar, there are minor differences with each one.

Swann (1969), Mayfield et al. (1971), and Zouzou & Haldane (1993) performed their tests in the experimental setup shown in Figure 2.9.

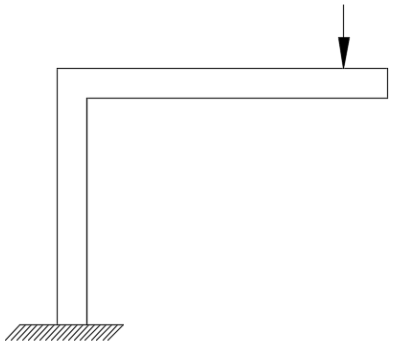

Figure 2.9: Setup with Fixed Base

This setup involved fixing the base of the column while loading the free end of the beam. It is unclear whether the aforementioned authors applied the load while preventing or permitting the sway of the column – that is, if the loading point is either pinned or a roller. In the former case, the lateral sway is prevented which results in a component of axial force parallel to the beam. In the case of a roller loading point, specimen is free to sway and no reaction axial forces are present in the beam. However, depending on the configuration, the may result in a change in moment arm length.

Kemp & Mukherjee (1968) and Luo et al. (1994) opted to test their specimens as shown in Figure 2.10a, while Johansson (2001) used the configuration in Figure 2.10b.

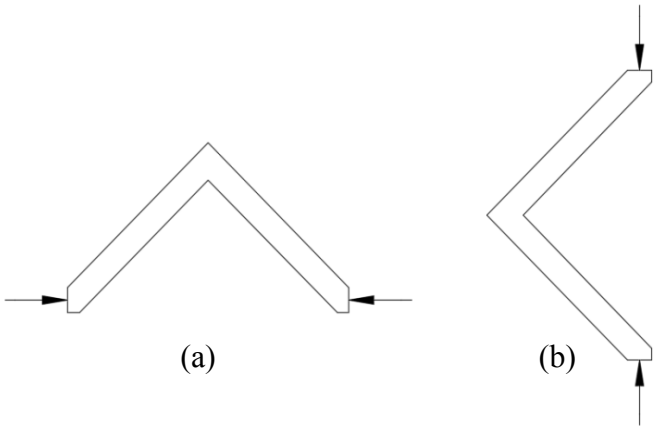

Figure 2.10: Setup with Collinear Loading

The two configurations involve applying the force horizontally or vertically through the edges of the adjoining members. This directly imposes an axial force into the adjoining members; however, the moment arm is kept consistent. In the case of Figure 2.10b, Johannsson required lateral restraint to maintain the stability of the specimen. Kemp & Mukherjee also tested portal frame specimens, and were loaded in a manner similar to Figure Figure 2.10a.

Stroband & Kolpa (1983) tested their specimens according to Figure 2.11. This setup consists of a portal frame with relatively short columns. The specimen was supported using pins at the base of the columns to simulate points of contraflexure.

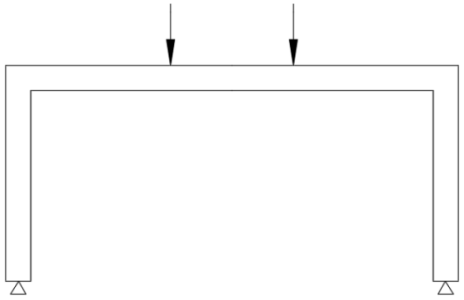

Figure 2.11: Setup used by Stroband & Kolpa

The authors' motivation for using this setup was to mirror the behaviour of a real life structure. When loaded in the centre of the beam, the specimen deforms in a way that is representative of a real structure. The beam would only experience shear and flexure, while the column only experiences flexure and axial compression.

Chapter 3
Experimental Program

3.1 General

A total of eight specimens were fabricated and split into two groups: unconfined and confined corners. Reinforcement ratio was varied as well as the specimen geometry. Six of the specimens were constructed with a 90^{o} corner while two were constructed with an interior corner chamfer – simulating the corner of a box culvert. The details of specimens are shown in Table 3.1.

Table 3.1: Details of Specimens

Joint	Notation	Reinforcement**	Geometry	Reinforcement Ratio	f'_c ǂ
Unconfined	UA-2-4	2 – No. 4	Regular	Over-reinforced*	48
	UA-2-6	2 – No. 6	Regular	Over-reinforced	55
	UA-3-6	3 – No. 6	Regular	Over-reinforced	
	UA-4-6	4 – No. 6	Regular	Over-reinforced	
	UB-3-6	3 – No. 6	Chamfered	Over-reinforced	
Confined	CA-2-6	2 – No. 6	Regular	Over-reinforced	48
	CA-3-6	3 – No. 6	Regular	Over-reinforced	
	CB-3-6	3 – No. 6	Chamfered	Over-reinforced	

* Was initially designed as under-reinforced, details can be found in section 3.3.1.
** Bar information can be found in Table 3.2
ǂ Concrete strength determined on day of testing.

Specimen naming follows the following convention ***XY - # - #:*** *X* specifies if the specimen joint is Unconfined or Confined, *Y* indicates the joint geometry (A and B for regular and chamfered corners, respectively), *the first number* shows the number of reinforcing bars and *the second number* indicates the size of bars used. For example *UA-2-6* is a specimen with unconfined joint, type A geometry, and is reinforced with two No. 6 bars.

3.2 Material Properties

All the specimens were fabricated using concrete supplied from Hogg ready mix. The specimens were poured in two batches on separate days with a specified strength of concrete set at 35 MPa. The average 28 day compressive strength was found to be 48 MPa for the first batch and 42 MPa for the second with slumps of 80 mm and 110 mm, respectively. The difference is attributed to slightly increasing the water content for the second batch due to difficulty of pouring experienced with the first batch. Since the specimens were tested on days beyond the 28th day, the concrete strength was determined the day of the testing as 55 MPa and 48 MPa, respectively. All of the specimens were tested within six months of the pour date.

The GFRP bars used in the specimens was VROD Grade III bent bars supplied by Pultrall Inc. This includes bent bars for use as main longitudinal reinforcement as well as stirrups for shear reinforcement. The mechanical properties were determined by the manufacturer according to CSA S806 test methods and are presented in Table 3.2.

Table 3.2: Mechanical Properties of Reinforcement Bars Provided by Manufacturer

Bar Size Designation	Diameter (mm)	Area (mm^2)	f_u (MPa)	$f_{u,bend}$ (MPa)	Modulus of Elasticity (MPa)*
No. 4	12.70	127	1288	635	53942
No. 5	15.87	198	1413	655	53838
No. 6	19.05	285	1293	655	53808

* Tested moduli of elasticity provided by manufacturer did not specify a minimum, average of five reported tests was used.

The initial specimen design was performed using nominal properties specified by the manufacturer, shown in Table 3.3, but were updated using the properties shown in Table 3.2.

Table 3.3: Nominal Mechanical Properties of Reinforcement Bars

Bar Size Designation	Nominal f_u (MPa)	Nominal $f_{u,bend}$ (MPa)	Nominal Modulus of Elasticity (MPa)
No. 4	1019	459	
No. 5	1001	450	50000
No. 6	1028	463	

3.3 Test Specimens

The design moment resistance of the joint, M_{design}, was taken to be equal to the moment resistance of the adjoining members. This value was used to calculate the strength efficiency by comparing it with the tested moment capacity, M_{test}(to be discussed in Chapter 4).

The design of members reinforced with FRPs is similar to that of steel reinforced concrete, and can fail with an over-reinforced, under-reinforced, or balanced failure. Typically, steel reinforced structures are designed with an under-reinforced section due to the plastic behaviour of steel, utilizing the ductile behaviour. Since FRPs do not exhibit the yield plateau shown by steel, the design philosophy is to achieve an over-reinforced failure. Tests show that that concrete crushing failure is more desirable since the flexural members show some plastic behaviour prior to failing (ACI Committee 440, 2015).

The balanced reinforcement ratio marks the point where the simultaneous reinforcement-rupture and concrete crushing occur. For over-reinforced and under-reinforced reinforcement ratios, the failure is marked only by concrete crushing and bar rupture, respectively. The balanced reinforcement ratio, $\rho_{frp,b}$, can be calculated by considering strain compatibility and equilibrium of forces across a beam section, outlined by Equation 3-1.

$$\rho_{frp,b} = \alpha_1 \beta_1 \frac{\phi_c}{\phi_{frp}} \left(\frac{\varepsilon_{cu}}{\varepsilon_{cu} + \varepsilon_{frp,u}} \right) \frac{f'_c}{f_{frp,u}} \quad (3\text{-}1)$$

This expression is valid provided that reinforcement is placed only in one layer. Failure will occur by concrete crushing when this value is exceeded and by bar rupture when the reinforcement ratio is below $\rho_{frp,b}$. Here,

$f_{frp,u}$: Ultimate tensile strength of FRP bar, MPa

α_1: Ratio of average stress in rectangular compression block to specified concrete strength

β_1: Ratio of depth of rectangular compression block to depth of neutral axis

ε_{cu}: Maximum usable strain at extreme compression fibre = 0.0035

$\varepsilon_{frp,u}$: Ultimate tensile strain of FRP bar

$\rho_{frp,b}$: FRP balanced reinforcement ratio, %

ϕ_c: Concrete material resistance factor

ϕ_{frp}: FRP bar resistance factor

As seen in Figure 3.1 for a concrete crushing failure, crushing occurs at the top fibre, while the tensile stress in the bars is less than ultimate.

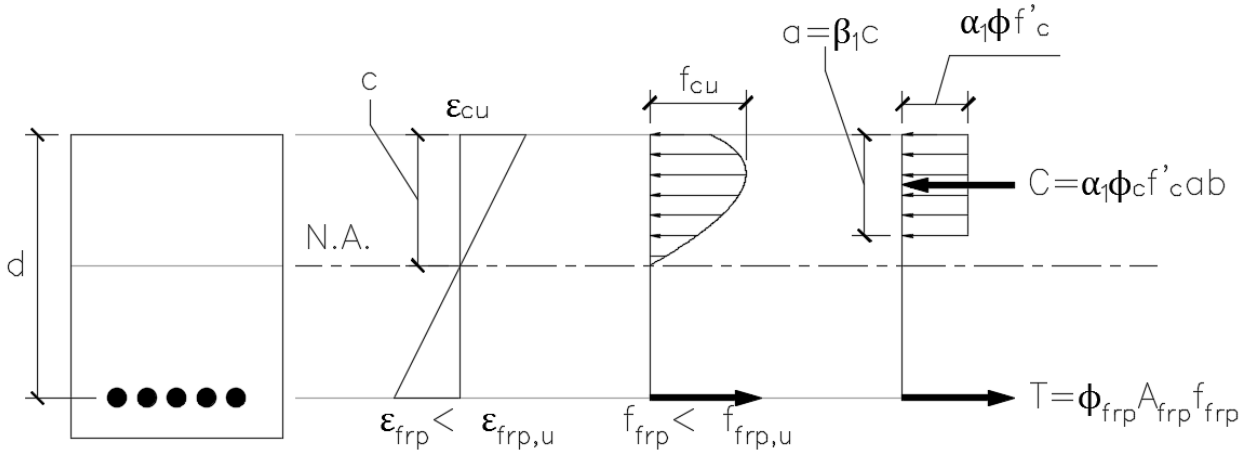

Figure 3.1: Strain Profile of an Over-reinforced Beam

Here,

a: Depth of equivalent rectangular stress block, mm

c: Distance from extreme compression fibre to neutral axis, mm.

d: Distance from extreme compression fibre to centroid of tensile force, mm

A_{frp}: Area of FRP reinforcement

The moment resistance can be calculated as the tension force resultant, T, multiplied by the distance between the compression and tension force resultants, z.

$$M_{design} = T\ z = \phi_{frp}\ A_{frp}\ f_{frp}\ \left(d - \frac{a}{2}\right) \qquad \textbf{(3-2)}$$

Since bars do not rupture, f_{frp} is not known and can be determined from strain compatibility. f_{frp} is a function of ε_{frp} and E_{frp}. ε_{frp} is also unknown, and is a function of c and ε_{cu}. A quadratic equation to solve for a (which depends on c) can be developed by equating the tension and compression force resultants, T and C; as seen in equation 3-5.

$$\boldsymbol{C = T} \qquad \textbf{(3-3)}$$

$$\alpha_1\,\phi_c\,f'_c\,a\,b = \phi_{frp}\,A_{frp}\underbrace{E_{frp}\overbrace{\left(\frac{\beta_1\,d}{a}-1\right)}^{\varepsilon_{frp}}\varepsilon_{cu}}_{f_{frp}} \qquad \textbf{(3-4)}$$

$$\left(\alpha_1\,\phi_c\,f'_c\,b\right)\boldsymbol{a^2} + \left(\phi_{frp}\,A_{frp}\,E_{frp}\,\varepsilon_{cu}\right)\boldsymbol{a} - \phi_{frp}\,A_{frp}\,E_{frp}\,\varepsilon_{cu}\,\beta_1\,d = 0 \qquad \textbf{(3-5)}$$

3.3.1 Design of Adjoining Members

The beam and column portions of the specimen were designed according to the *Canadian Highway Bridge Design Code (CHBDC)*, CSA S6-12. The reinforcement ratio was varied by changing the number of reinforcement bars. All specimens but UA-2-4 utilized No. 6 GFRP bars.

One main consideration in the specimen design was the tensile stress per bar. Given that the strength of the bent portion was approximately 50% of the straight portion as reported by the manufacturer, there was a risk of bar rupture within the joint despite the adjoining members being designed as over-reinforced.

The baseline specimen was chosen with three reinforcing bars. This had a reinforcement ratio much larger than $\rho_{frp,b}$. The stress in each bar was slightly larger than the bend tensile strength. Given the large material variability, this had a chance of failing by either bar rupture or concrete crushing.

In order to guarantee a bar rupture case with $\rho > \rho_{frp,b}$, a specimen was chosen with two No. 6 bars. The stress was well above the strength of bend and had high probability of rupture at the bend. To completely prevent the bar rupture, a specimen was chosen with four No. 6 bars. This

guaranteed the stress would be well below the strength of the bend. Specimen UA-2-4 was designed with two No. 4 bars in order to achieve an under reinforced ratio.

It must be noted that the initial design was performed using minimum guaranteed properties as specified by the manufacturer in Table 3.3. The designs were updated using values reported the manufacturer's tests on the reinforcement batch received, Table 3.2. The higher strengths resulted in the reinforcement ratio of specimen UA-2-4 to be over-reinforced.

The specimen width was chosen as 270 mm to accommodate the number of reinforcing bars and also to ensure enough cover on each side. The beam height was taken as 300 mm. The beam height was to not be too large in order to have a larger a_o/d ratio. The length of the beam was chosen as 1700 mm to prevent the possibility of shear failure, while the column height was chosen as 1000 mm to avoid slenderness effects as well as minimize lateral sway.

Specimen with geometry type B contains an interior chamfer with side length equal to the beam and column height with a 1:1 slope.

All specimens contained continuous longitudinal tension reinforcement that ran from the beam, into the joint, and through the column. Stirrups were spaced at 110 mm in the beam while the column tie spacing varied between 100 mm in the base of the column and 150mm near the joint. The first stirrup was placed at 55 mm away from the beam/joint and column/joint interfaces. Two continuous No. 5 bent reinforcement bars were placed in the compression side of the beam to provide an anchor point for stirrups and ties. Following the CHBDC provisions, the added strength of the compression bars was neglected. Clear cover at all sides was chosen as 30 mm.

In addition to the longitudinal tensile and compression bars, two No. 5 U-bars were provided in the interior chamfer region. These bars run longitudinally from the adjoining members and are bent such that they are parallel to the face of the interior chamfer. Although the interior chamfer is in the compression region, these bars were added to eliminate the risk of the concrete spalling off.

The spacing of stirrups and ties used in type A specimens was also adopted for type B specimens. Differences in the stirrup layout are shown in Figure 3.3 to Figure 3.6and are discussed in section 3.3.2. The details of all reinforcing bars is shown in Figure 3.2.

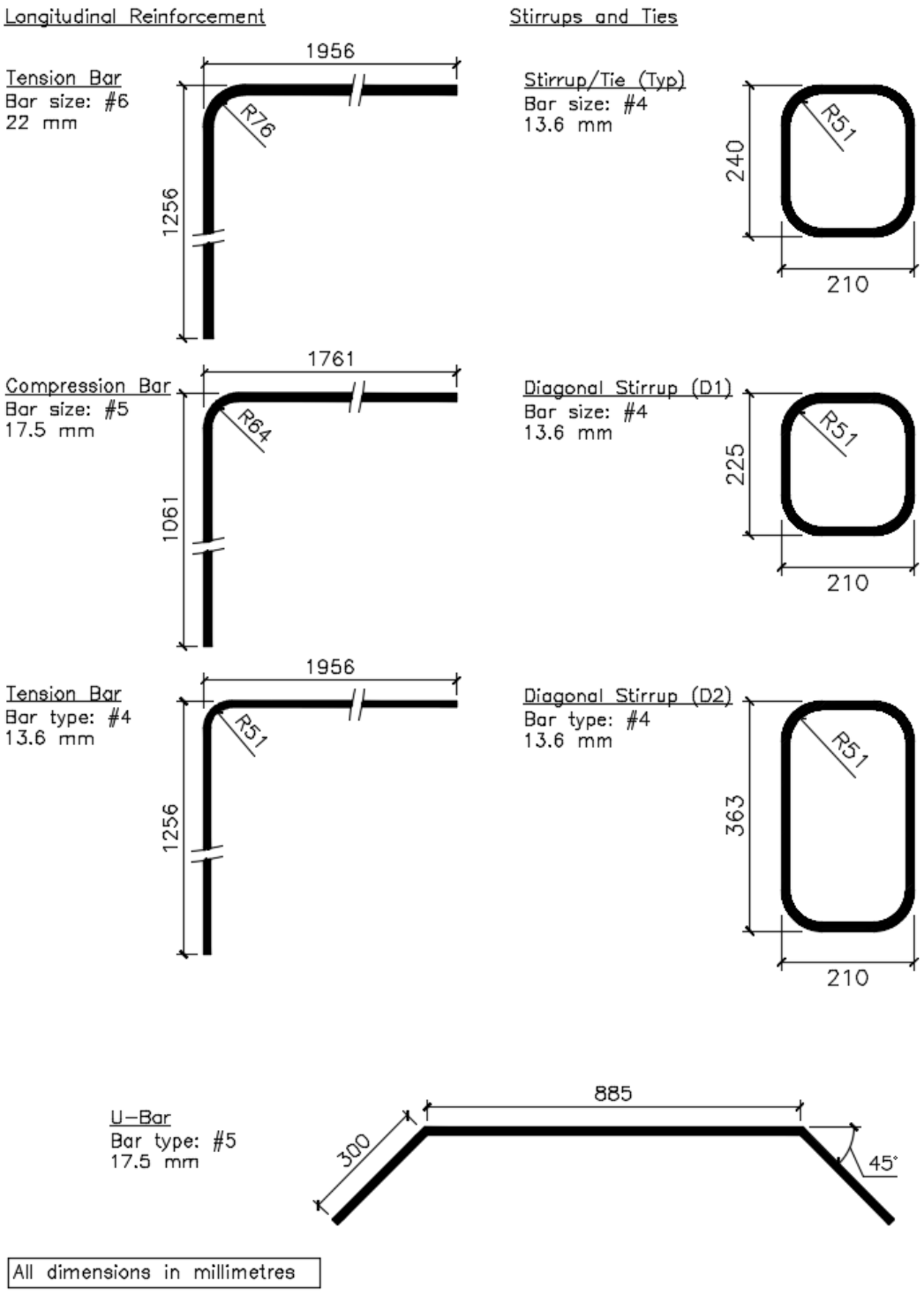

Figure 3.2: Reinforcing Bar Dimensions

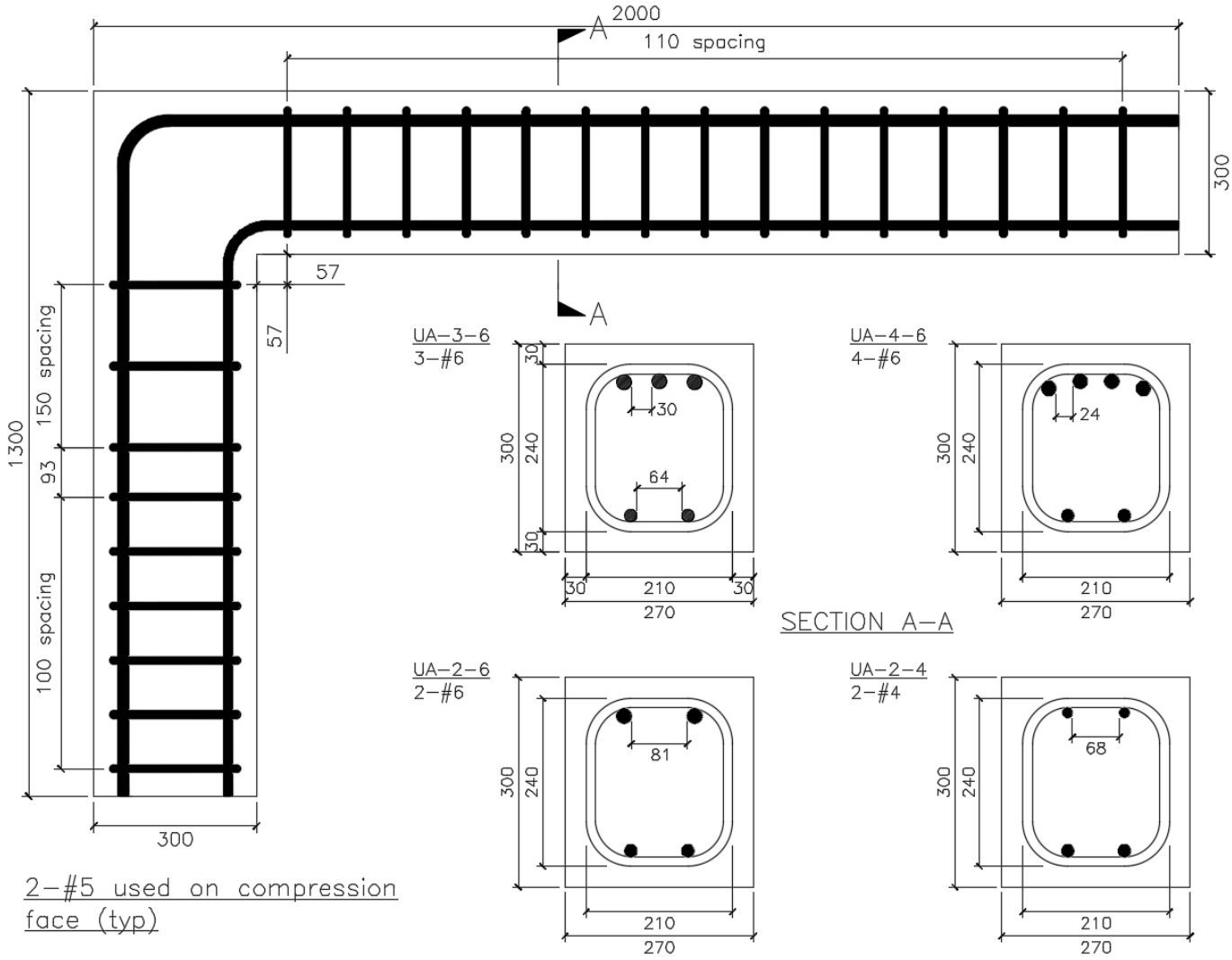

Figure 3.3: Reinforcement Details for Unconfined Joint Series (Type A)

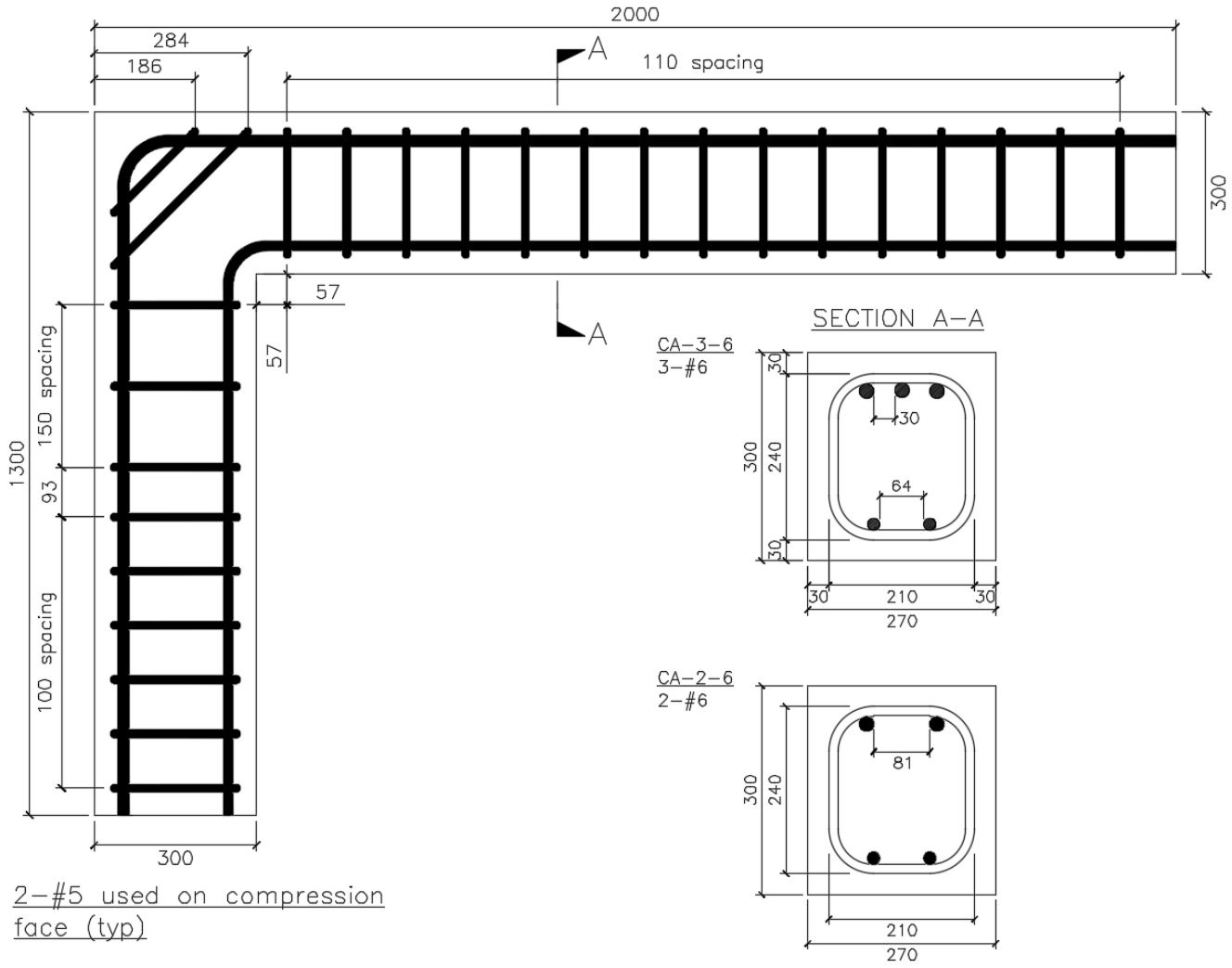

Figure 3.4: Reinforcement Details for Confined Joint Series (Type A)

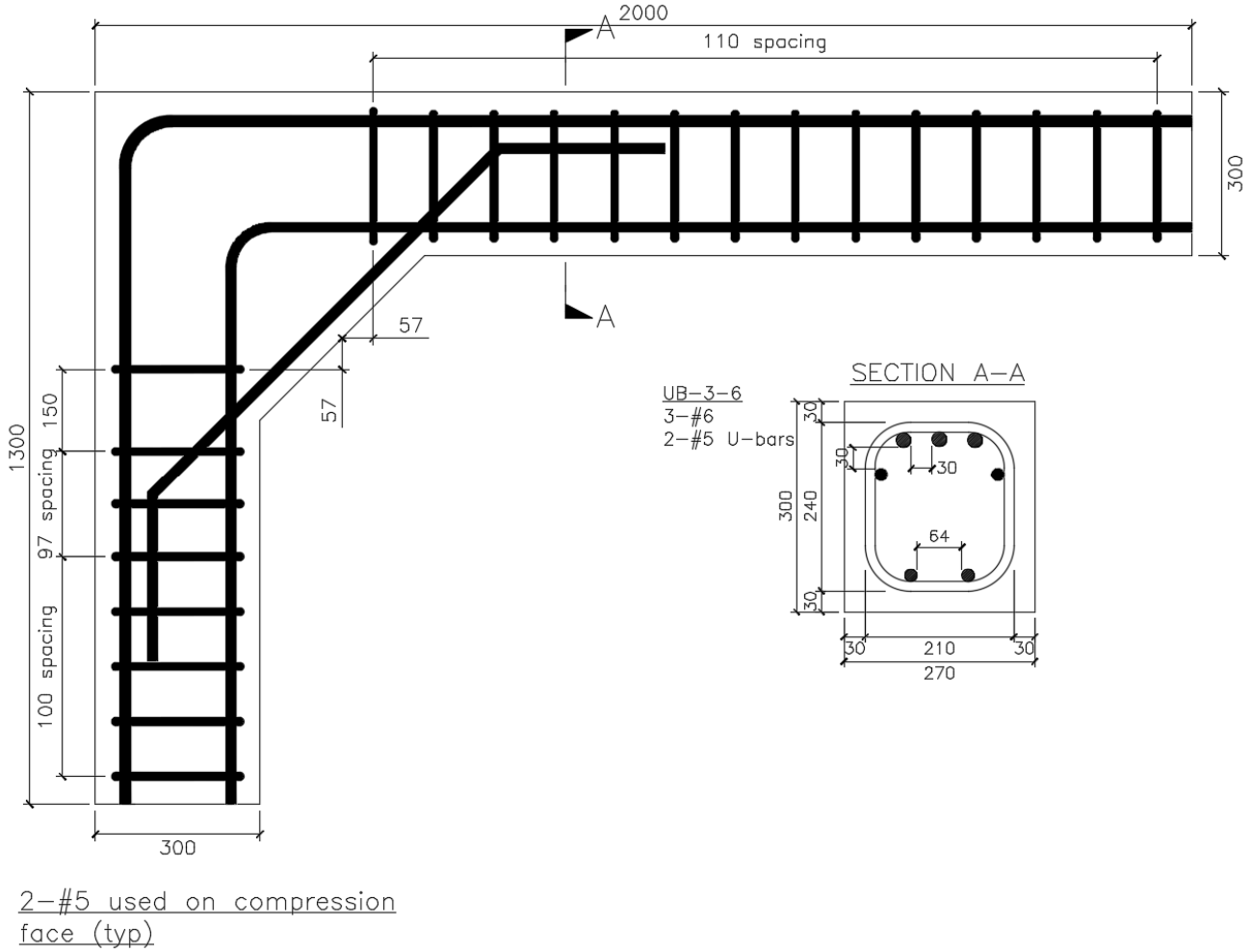

Figure 3.5: Reinforcement Details for Unconfined Joint (Type B)

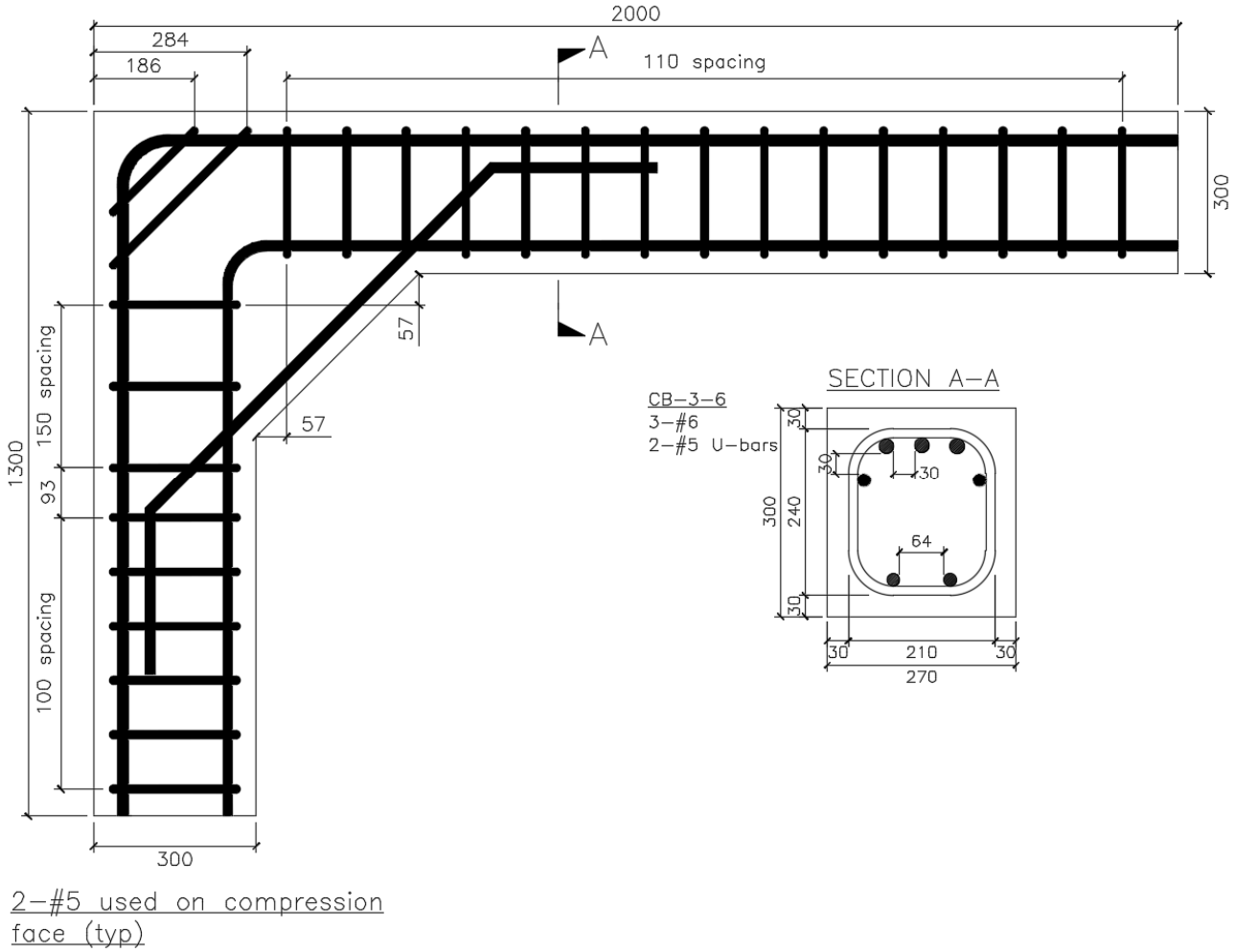

Figure 3.6: Reinforcement Details for Confined Joint (Type B)

3.3.2 Design of Joint

Previous literature on steel reinforced specimens showed that detailing is not critical for negative moments causing closing. In order to check these observations with GFRP reinforced specimens, two main types of joints were considered: unconfined and confined joints.

The joints with unconfined detailing scheme will comprise of only the longitudinal tension bars running through. This was done to observe the behaviour of the bent bars when no additional reinforcement was present.

The joints with confined detailing scheme comprise of longitudinal bent bars running through the joint in addition to two No. 4 diagonal stirrups. The purpose of the diagonal stirrups is two-fold: First, the stirrups will confine the concrete in that region and provide some extra stiffness. Secondly, the stirrups will intercept the major cracks that may form within the joint caused by flexure. ACI 352R (Joint ACI-ASCE Committee 352, 2002) recommends a grid of reinforcement (e.g. vertical and horizontal stirrups) in steel reinforced joints. This configuration is difficult to construct using GFRP – especially considering that reinforcement must be manufactured pre-bent. The difficulty of construction is also rationale for using the diagonal stirrups – which offer much more ease of construction in comparison.

The unconfined joint region for type B specimens is not as obvious as that of type A. The stirrups and ties for type A specimen were placed 55 mm from the joint interface. In order to mimic a similar unconfined specimen while keeping the specimen safe from shear failure, the joint/adjoining member interface was taken to start at the centre point of the chamfer. As such, the stirrups were placed at 55 mm from that location, shown in Figure 3.5.

3.3.3 Base of Column

Four one-inch diameter steel tubes were cast in the base of the column as part of the fixed support assembly. The location of the tubes was placed in a way such that it does not interfere with the longitudinal bars or the ties present in the column.

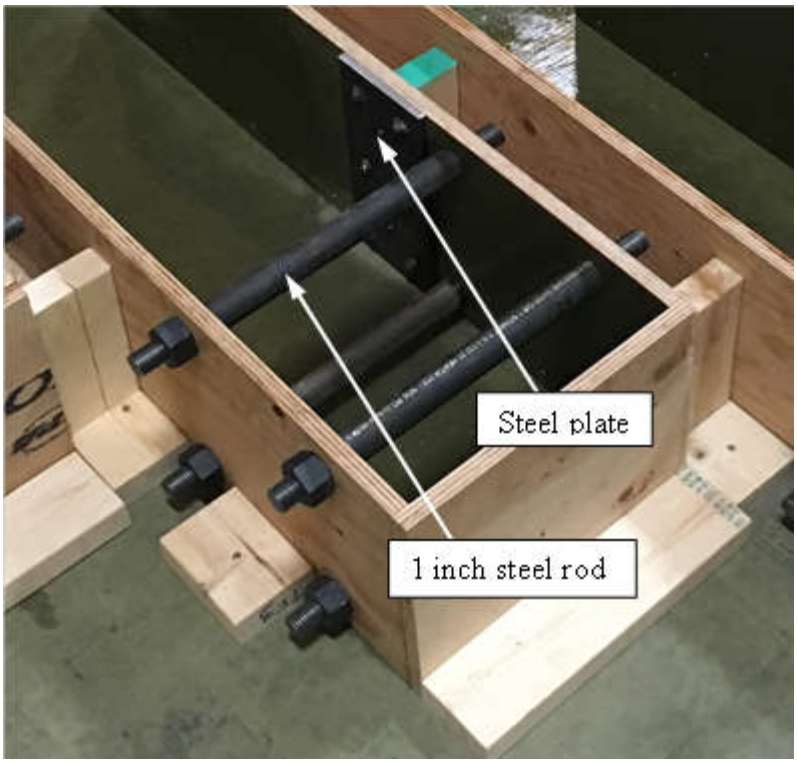

Figure 3.7: Steel Rods and Bearing Plate in Column Base

Additionally, a 19 x 130 x 270mm steel bearing plate was included in the compression side of the column to prevent a possibility of local bearing failure due to contact with the steel support assembly.

3.4 Specimen Fabrication

This section describes the formwork construction and design, the process of caging, and concrete casting.

3.4.1 Formwork

Formwork was constructed out of lumber and plywood in the University of Waterloo Structures Laboratory. The formwork was designed to be modular and consisted of separate pieces that fit together in a repeating fashion. The formwork assembly was built to fabricate three type A specimens and one of type B. Considering the unconventional shape of specimen, the formwork

was built such that the specimens are nested in one another in order to reduce space and materials.

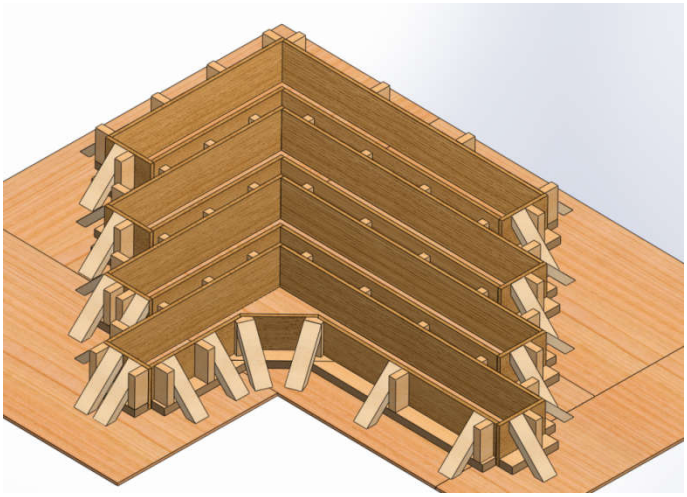

(a) Formwork design

(b) Reinforcement Cage in Assembled Formwork

Figure 3.8: Formwork and Reinforcement Cage

In order to ensure proper location of the steel tubes in the column base, four one inch holes were drilled in the correct locations on the plywood pieces. One inch threaded rods were routed into the holes to hold the steel tubes in place. The threaded rods were tightened using nuts on each side to preserve the geometry and prevent the forms from bowing during casting.

Diagonal pieces of 2x4 were placed on the outside of the formwork to add some stiffness to the overall assembly.

3.4.2 Caging

Reinforcement cages were assembled on two stands supporting the tensile reinforcement (Figure 3.9). Four jigs were constructed in order to maintain the proper spacing of bars and also to hold the reinforcement in place. Jigs were placed at the start and end of the adjoining members, shown in Figure 3.10.

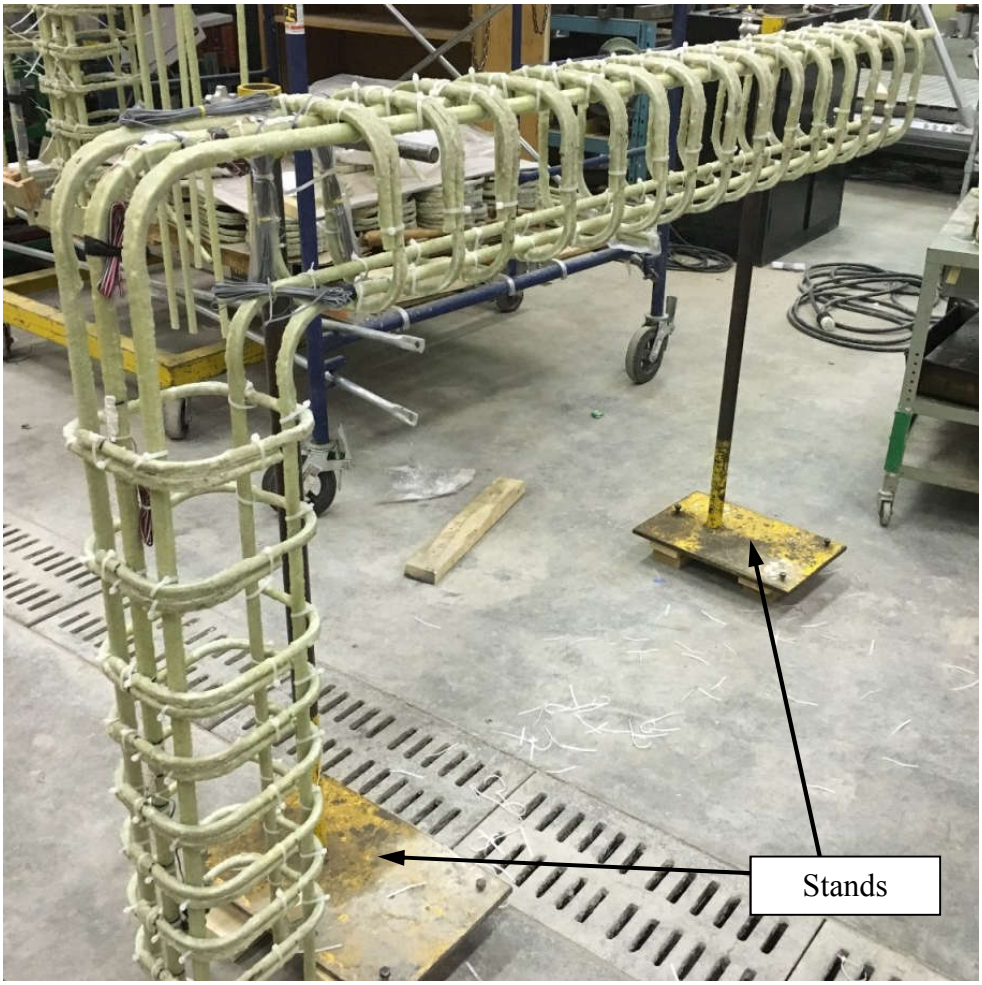

Figure 3.9: Reinforcement Cage Suspended by Stands

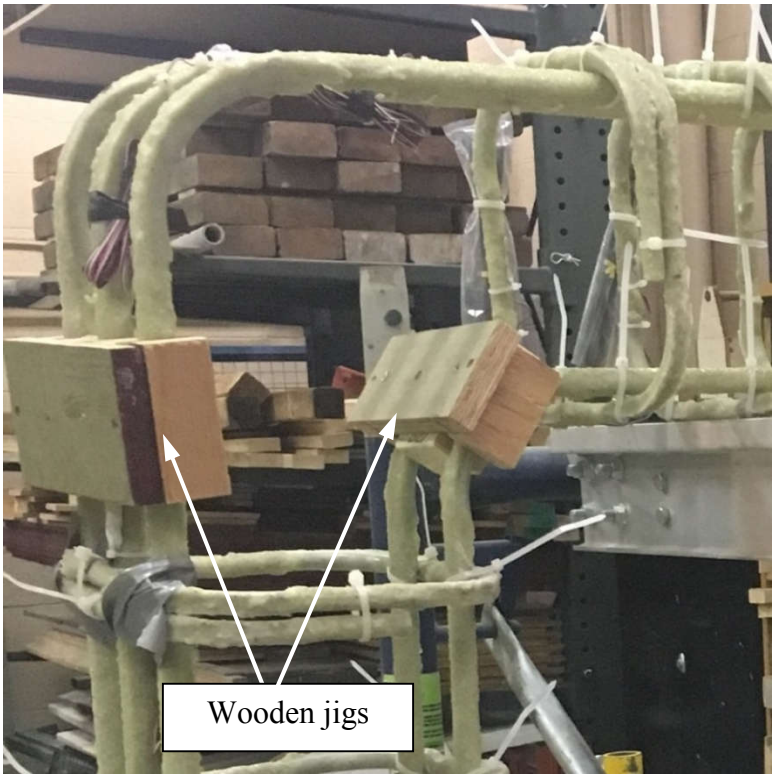

Figure 3.10: Separating Reinforcement Bars Using Wooden Jigs

Stirrups were placed on the specified locations on the beam and tied using heavy duty plastic zip ties. The seven inch zip ties provided adequate length to wrap around the reinforcement. The compression longitudinal bars were placed after the stirrups were secured. Similar jigs were constructed to maintain the compression bar spacing. The column ties were affixed after the compression bars were secured to the beam stirrups.

3.4.3 Casting

The casting of specimens was done in two batches. To control the placement of the fresh concrete, the concrete was transported from the concrete truck to the formwork using wheelbarrows and shovels. The concrete was poured in two layers and was thoroughly consolidated using rod vibrators. Steel anchors were placed in the beam and column to facilitate the relocation of the specimens. Plastic chairs were affixed to the reinforcement cages to maintain adequate cover on the specimen sides. Similarly, thin strips of plywood were wedged

between the formwork sides and the stirrups to limit the movement of the cage as well as ensuring the cover.

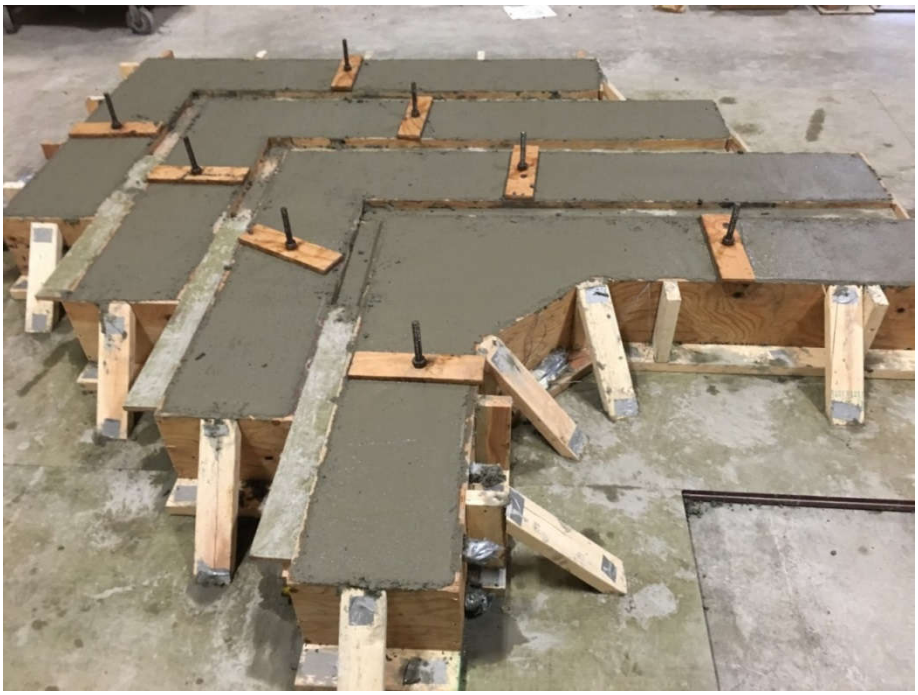

Figure 3.11: Poured Specimens with Anchors Installed

Twenty 100 mm x 200 mm cylinders were prepared for each batch for compression and split tensile testing.

3.5 Test Setup

3.5.1 Fixed Support Connection

The specimen support consist of two 400mm x 400mm steel angles that are clamped to the column base. Four high-strength B7 threaded rods are routed through the four tubes that were cast inside the column base. The steel angles are attached to a steel beam with holes matching the laboratory floor.

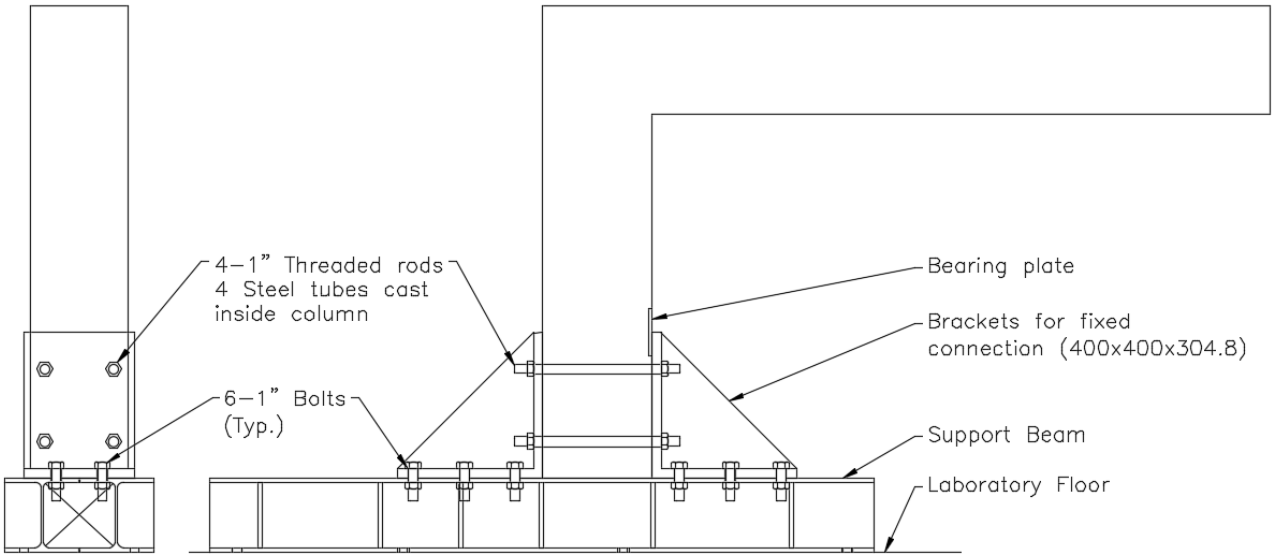

Figure 3.12: Fixed Support Details, North Face (left) and West Face (right)

The stiffened angles consisted of two 400 mm leg lengths and are 304.8 mm (12 in) wide. Two 19 mm (¾ in) stiffeners were placed on each in lieu of typically one stiffener. This was to prevent the angle from deforming and provide extra torsional resistance.

The support beam consists of two W200x46 sections that have been welded together along the top and bottom flanges. Adequate stiffeners are welded at the necessary locations to provide extra resistance against web crippling and flange bending. Eight bolt holes were positioned such that the beam is compatible with the laboratory bolt holes.

3.5.2 Loading Configuration

All specimens were loaded at the far beam end using the hydraulic load actuator. A relatively large moment arm of 1470 mm was chosen to remove the risk of failure by shear. The moment arm was taken as the distance between the beam/joint interface and 230 mm from the free end of the beam. This was taken to be the location of the centre of load application.

A structural testing frame with a capacity of 2500 kN was chosen for the series of tests. Although the full capacity of this frame will not be utilized, it was chosen in order to accommodate the

large anticipated displacements occurring at the beam end. Given the size of the frame, the size of the actuator head was similarly as large, with a length of 610 mm (24 inches) and width of 452 mm (18 inches). A 254 x 254 x 304.8 mm (10 x 10 x 12 inch) spacer was attached to the actuator head to avoid the risk of the actuator edge touching the beam at a location other than the bearing plate.

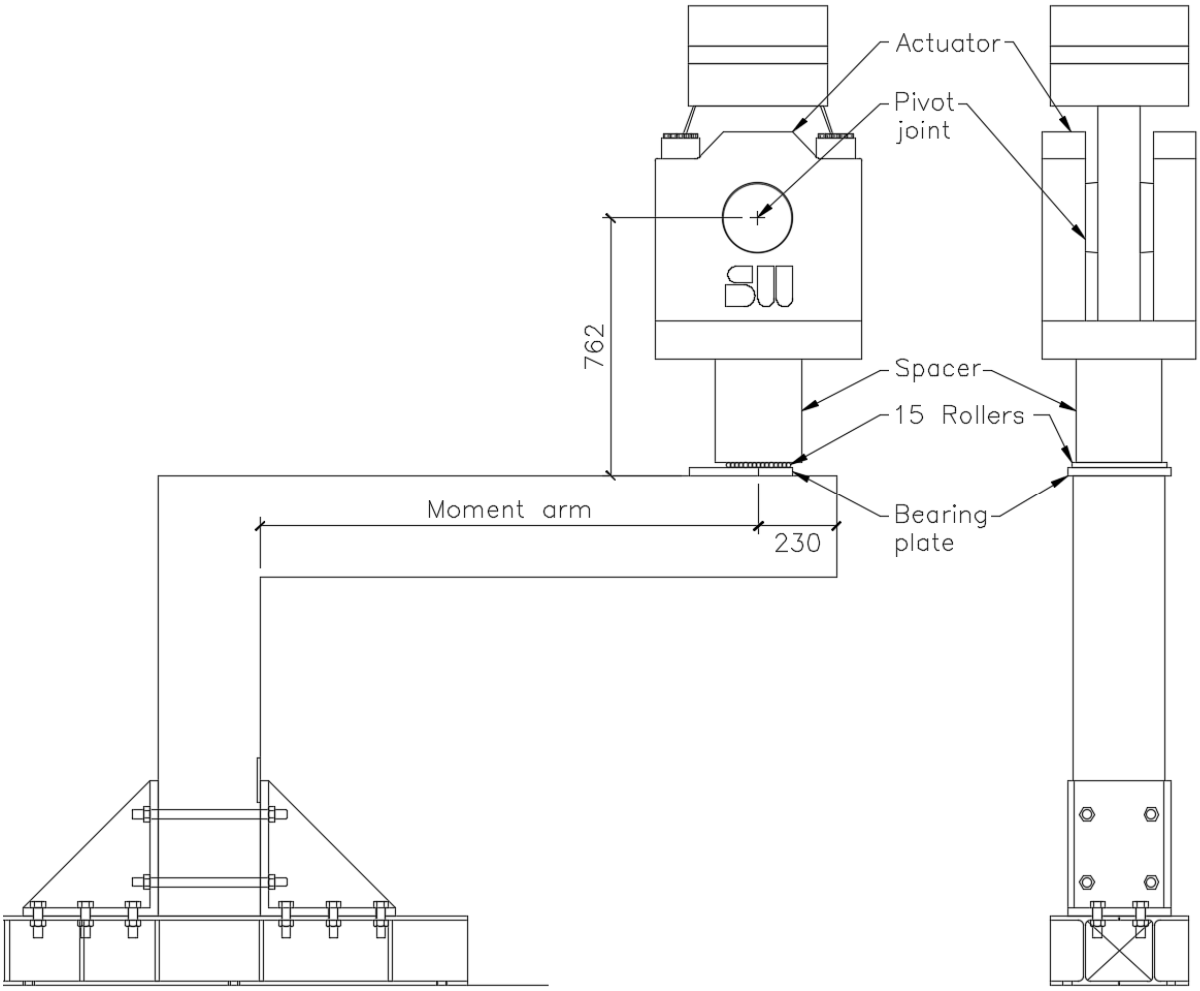

Figure 3.13: Loading Configuration for All Specimens, West Face (left) and North Face (right)

The loading configuration was developed to avoid the application of axial force along the length of the beam. The choice of using a roller support in lieu of a pin support eliminated this axial

force from occurring. Another requirement of the loading configuration was to apply the load perpendicular to the surface of the beam at all times. Since relatively large displacements and rotations were expected to occur at the beam end, a series of 15 rollers were placed between the actuator head and a bearing plate on the specimen. This ensured that the beam is not restrained horizontally while the beam end experiences displacements and rotations.

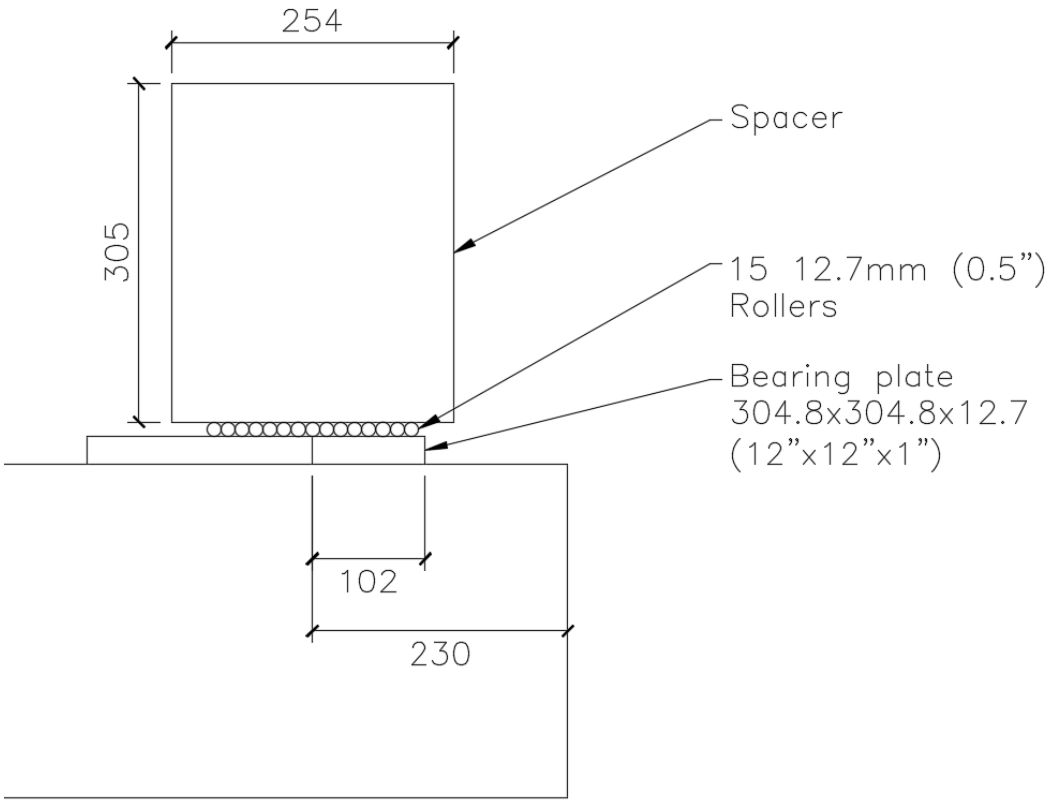

Figure 3.14: Pure Roller Load Application

A consequence of this configuration is the change in moment arm length. As the beam end displaces and rotates, the actuator head rotates to maintain perpendicularity – causing a decrease in the moment arm. This effect is compensated for by referencing displacement measurements and is discussed in more detail in Chapter 4.

3.6 Instrumentation

3.6.1 Strain Gauges

Each specimen was instrumented with at least nine strain gauges: five 5mm gauges installed on the longitudinal tension reinforcement, two 5 mm gauges installed on the first two stirrups in the beam, one 5 mm gauge on the longitudinal compression reinforcement, and one 60 mm gauge placed on the compression surface of the concrete adjacent to the joint. Specimens with confinement contained one additional 5 mm gauge on each diagonal bar. Also, specimens with type B geometry contained an additional two 5 mm gauges on the U-bar reinforcement.

Figure 3.15: Installed Strain Gauge

Of the five gauges installed on the longitudinal bars, one was placed in the beam, one was placed at the beam/joint and column/joint interfaces respectively, one was placed at the onset of

bending, and one was placed in the column. The number of gauges affixed in the joint region was kept at a minimum to preserve the bond between the bar and concrete. The detailed locations of all strain gauges are shown in Figure 3.16 and Figure 3.17.

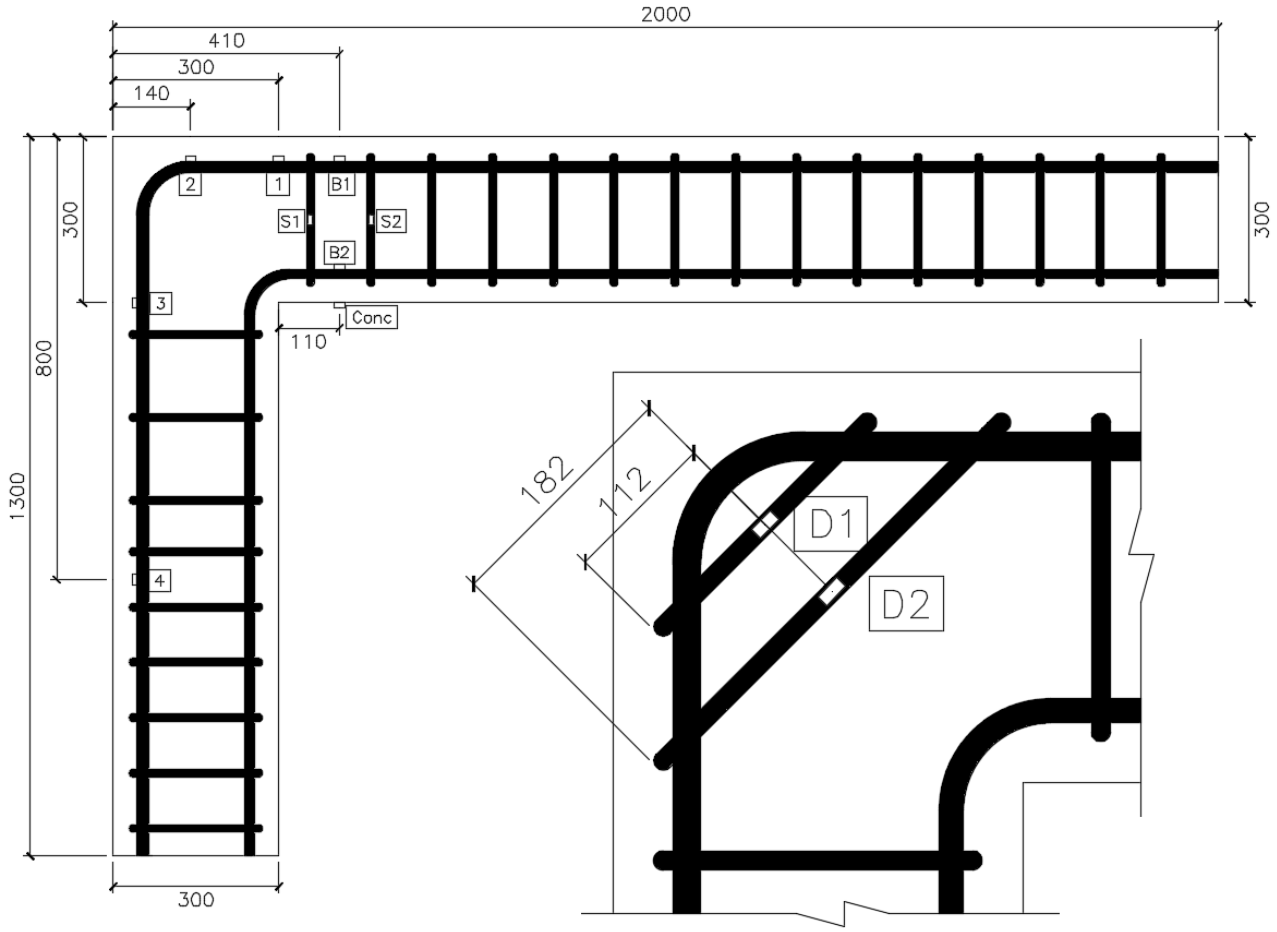

Figure 3.16: Strain Gauge Locations of Type A Specimens

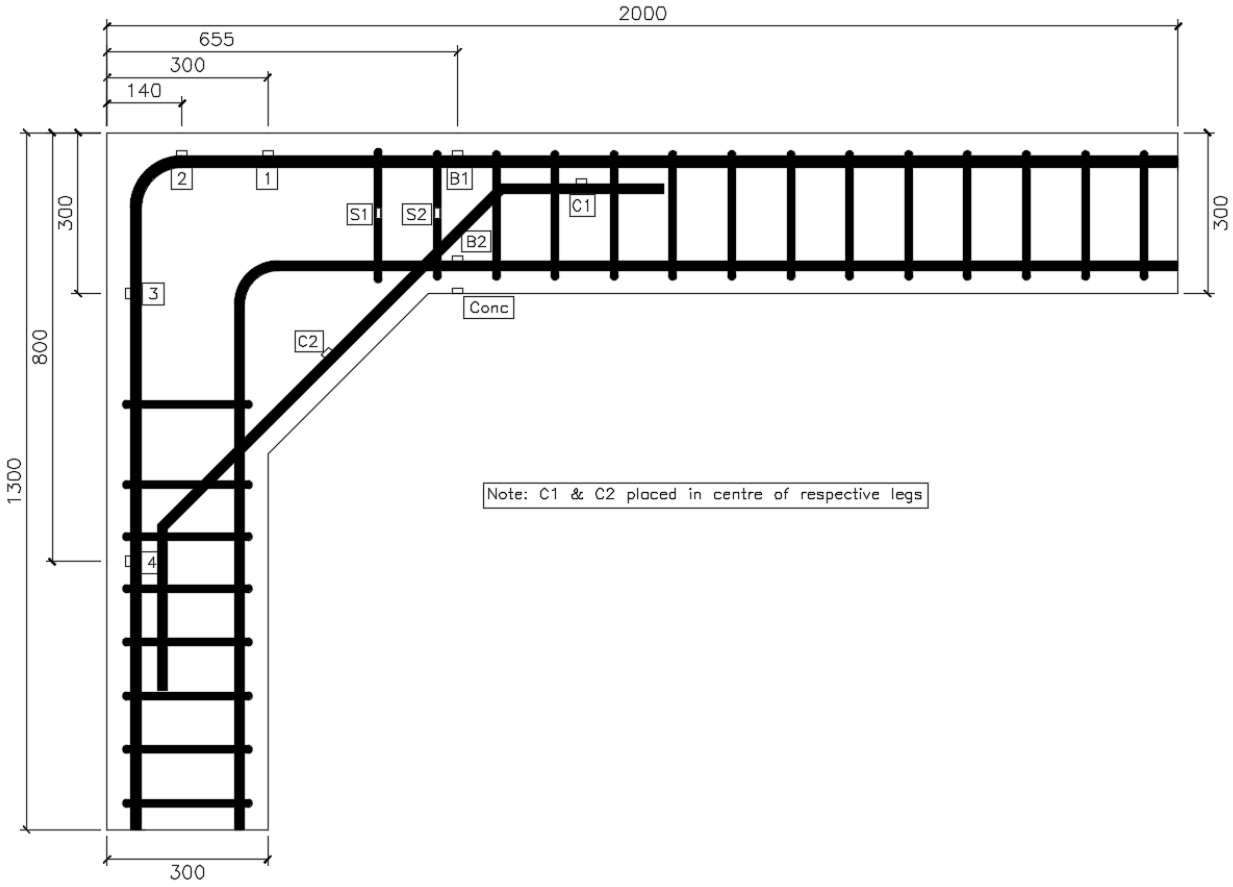

Figure 3.17: Strain Gauge Locations of Type B Specimens

3.6.2 String Potentiometers and LVDTs

A total of six string potentiometers (string-pot) and one linear variable displacement transducer (LVDT) were installed for testing. The sway and rotations occurring in the specimen make the use of LVDTs more difficult due to the way the specimen is expected to deform. For that reason, string-pots were used instead of LVDTs in most locations.

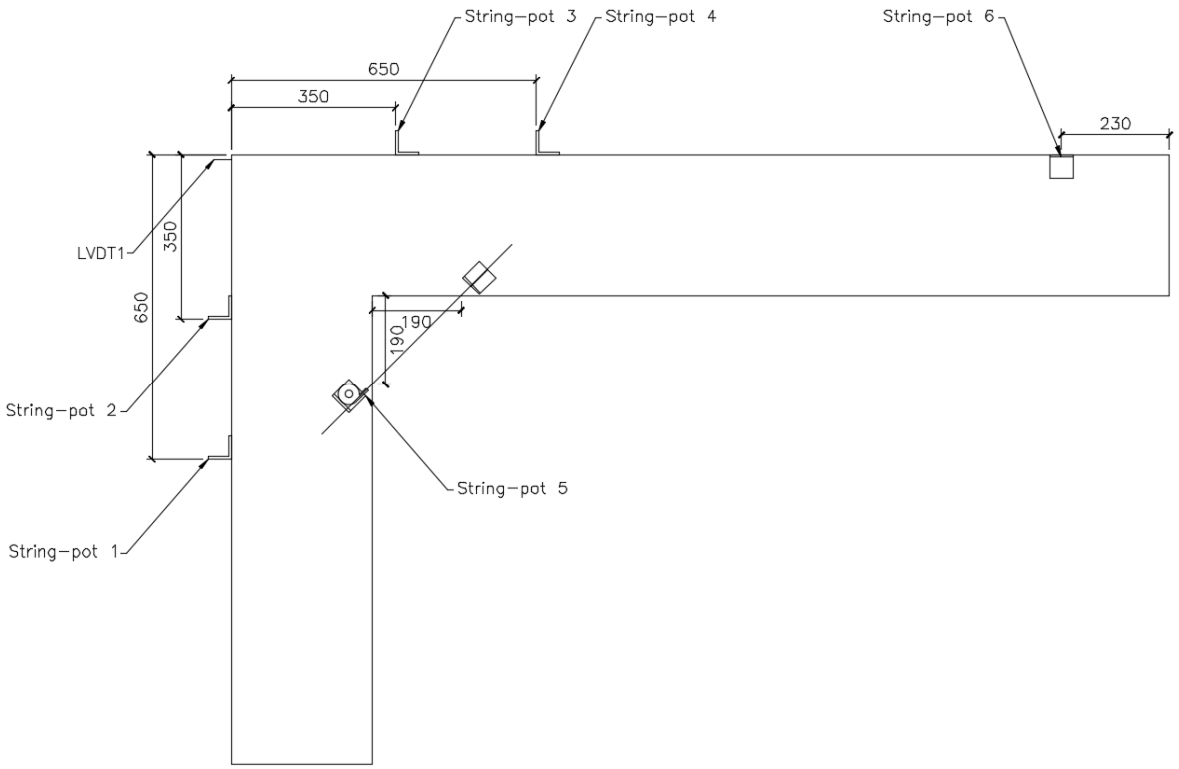

Figure 3.18: Location of String-pots and LVDT

One string pot is placed right under the point of load application to measure the total vertical deflection. Two string-pots were placed on the surfaces of the beam and column and spaced at 300mm in order to calculate the change in angles the beam and column are experiencing. The remaining string-pot is placed between the column and beam to measure the change in angle of the joint. This was placed at an equal distance of 190 mm from the interior corner between the beam and column. For the specimens with type B geometry, this string-pot was placed at a distance of 50 mm from the chamfer/adjoining member interface. The only LVDT was placed at the tip of the column to measure the lateral sway. All string pots and LVDT were attached to a stationary reference frame, shown in Figure 3.19.

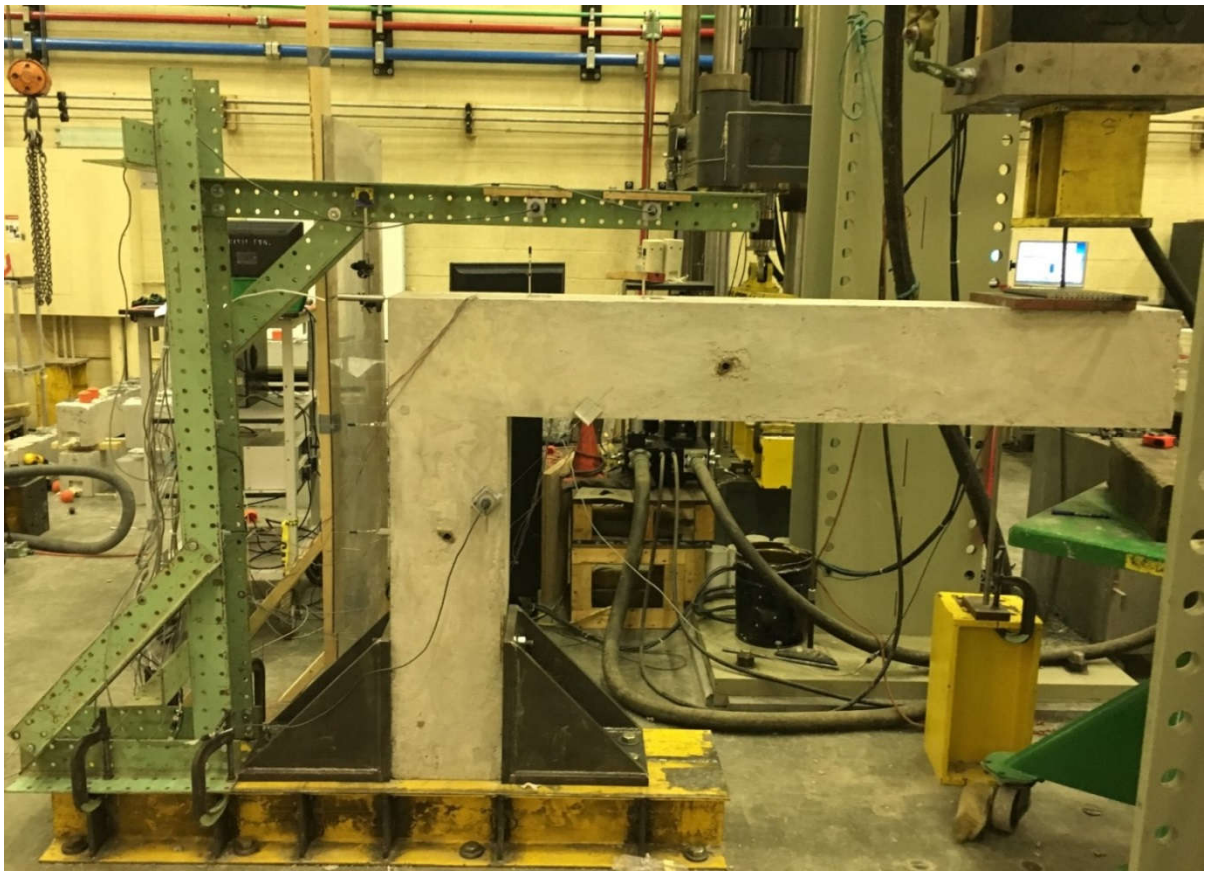

Figure 3.19: Specimen Ready for Testing

Chapter 4
Experimental Results

4.1 Testing Procedure

All specimens were loaded under vertical loads, 230 mm away from the free end of the beam. The chosen load application method ensures the force is constantly perpendicular to the beam surface. All specimens were loaded using displacement control. Initially, the loading rate was taken as 0.010 mm/second. This rate was increased to 0.017 mm/second after loading up to 25 kN.

Tests were paused for a maximum of five minutes at 10 kN increments to record the crack widths at each increment. Measurements were taken with a crack comparator card and flashlight in order to properly view the crack widths. Crack measurement was stopped when the specimen was deemed close to failure and plexiglass barriers were erected.

Crack formation and propagation was tracked by closely monitoring the specimen through the test duration. When a new crack was noticed, the corresponding load was noted and the outline of the crack is drawn on the specimen using a permanent marker pen. Gridlines drawn on the specimen aided in tracking cracks and reproducing the crack locations onto crack tracking sheets. Locations of anticipated concrete crushing were also watched during the test

4.2 Calculations

4.2.1 Moment Arm Change

The loading configuration involves the use of rollers between the actuator head and the bearing plate. This allows the specimen to sway while avoiding any applied axial loads on to the beam, while also maintaining the applied force to be normal to the beam surface. Keeping the loading point unrestrained means that the moment arm is not constant throughout the test. The change in moment arm length must be accounted for.

Two components make up the change in moment arm. First, the total deflection of the beam forces the rotation of the actuator head to maintain perpendicularity with the bearing plate. This makes up the majority of the moment arm reduction, Δ_1. Second, the sway of the column causes a horizontal shift, reducing the moment arm by that amount Δ_2. These components are shown in Figure 4.1.

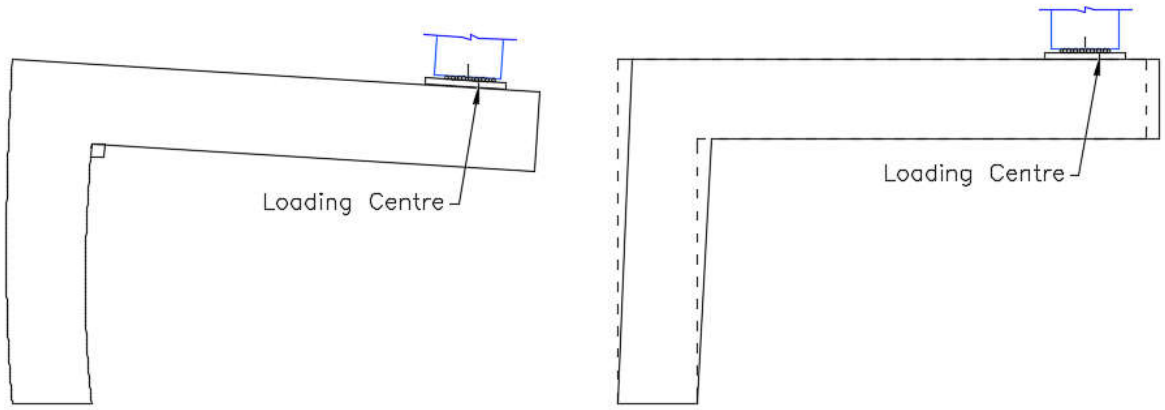

Figure 4.1: Change in Moment Arm Length Caused by End Deflection, Δ_1 (left) and Sway, Δ_2 (right)

Δ_1 depends on the original moment arm length, h, the distance between the actuator pivot point to the specimen surface, L, as well as the angle the surface of the beam makes with the horizontal, θ. This angle is also equal to the angle of the centreline of actuator head relative to the vertical.

Calculating Δ_1 was done using basic geometry. A schematic is shown in Figure 4.2.

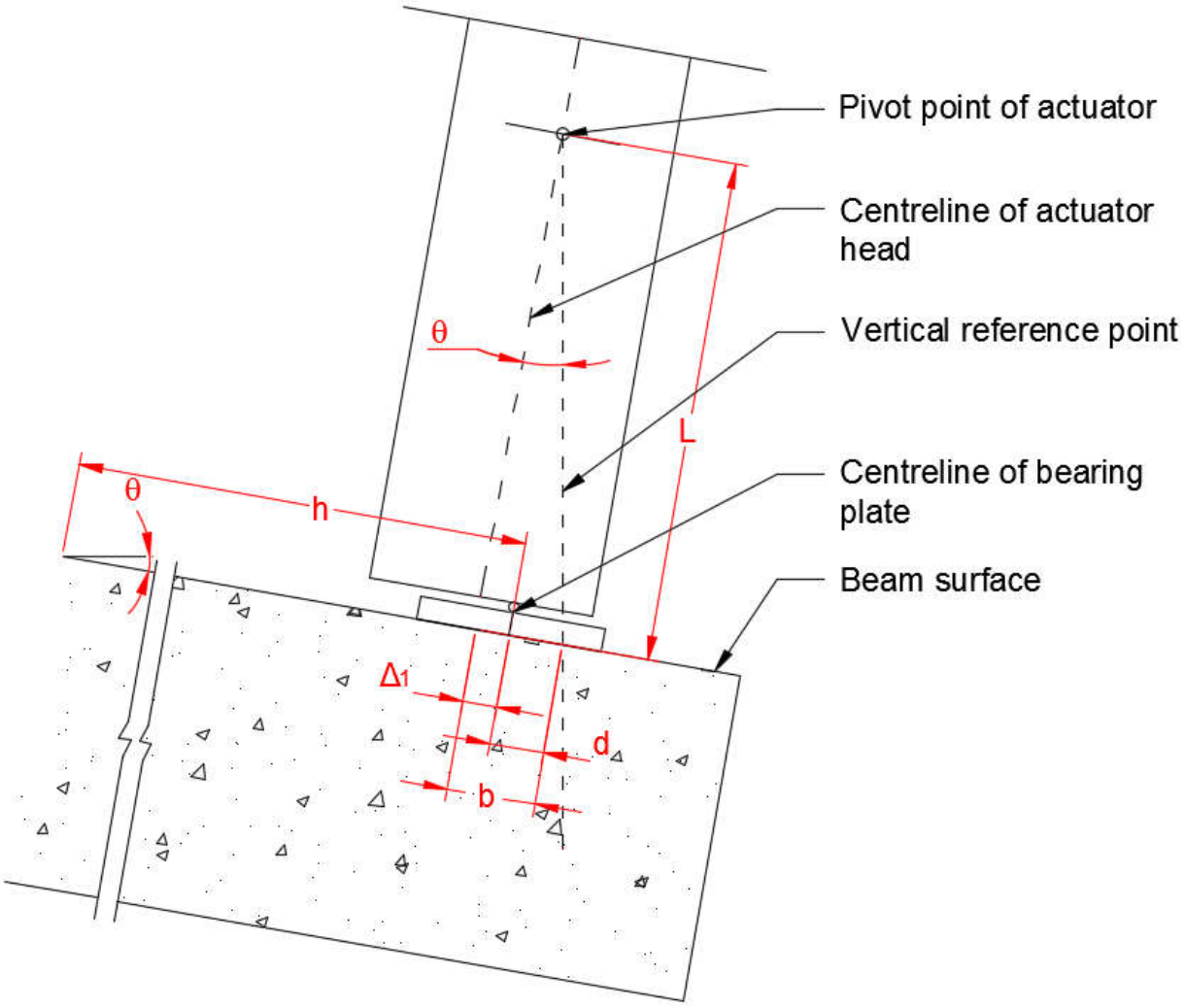

Figure 4.2: Calculation of Δ_1 using Geometry

$$\Delta_1 = b - d \qquad \textbf{(4-1)}$$

Where,

$$b = L \tan\theta \qquad \textbf{(4-2)}$$

d considers the change in location of the centreline of the bearing plate relative to the original location. This change is calculated as follows

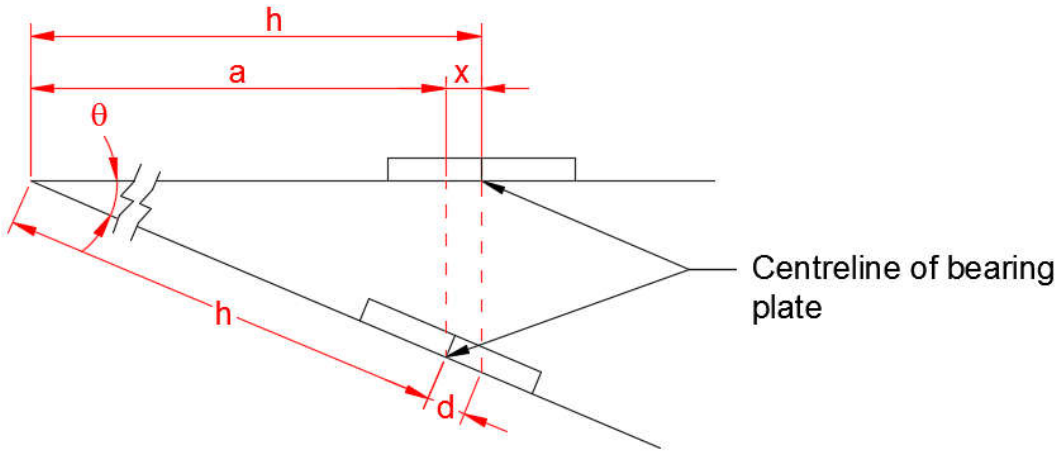

Figure 4.3: Calculating the *X*-component of Relative Displacement Due to Rotation, *d*

$$d = \frac{x}{\cos\theta} \qquad \textbf{(4-3)}$$

Where,

$$x = h - a \qquad \textbf{(4-4)}$$

and

$$a = h\cos\theta \qquad \textbf{(4-5)}$$

Therefore,

$$d = \frac{h\,(1-\cos\theta)}{\cos\theta} = h\,(\sec\theta - 1) \qquad \textbf{(4-6)}$$

Finally,

$$\Delta_1 = L\tan\theta - h\,(\sec\theta - 1) \qquad \textbf{(4-7)}$$

The reduction in moment arm accounting for sway, Δ_2, can also be calculated using geometry. When $\theta = 0$ (i.e. the beam is horizontal), Δ_2 can be taken as the total sway. However, as θ increases, the component parallel to the beam surface must be considered. Simply, it can be calculated as follows

$$\Delta_2 = \frac{\delta_{LVDT1}}{\cos\theta} \quad \textbf{(4-8)}$$

Where δ_{LVDT1} is the displacement reading of LVDT1, positioned at the top of the column.

4.2.1.1 Moment Arm Length

The bending moment, M_{test}, is taken as the applied load multiplied by the moment arm. The strength efficiency, M_{test}/M_{design}, compares the experimental strength with the strength of the adjoining member, M_{design}, as calculated in section 3.3. Using a moment arm measured from the centre of load to the joint/adjoining member interface was found to be reasonable for this comparison. This moment arm was kept consistent for both geometry types and is shown in Figure 4.4.

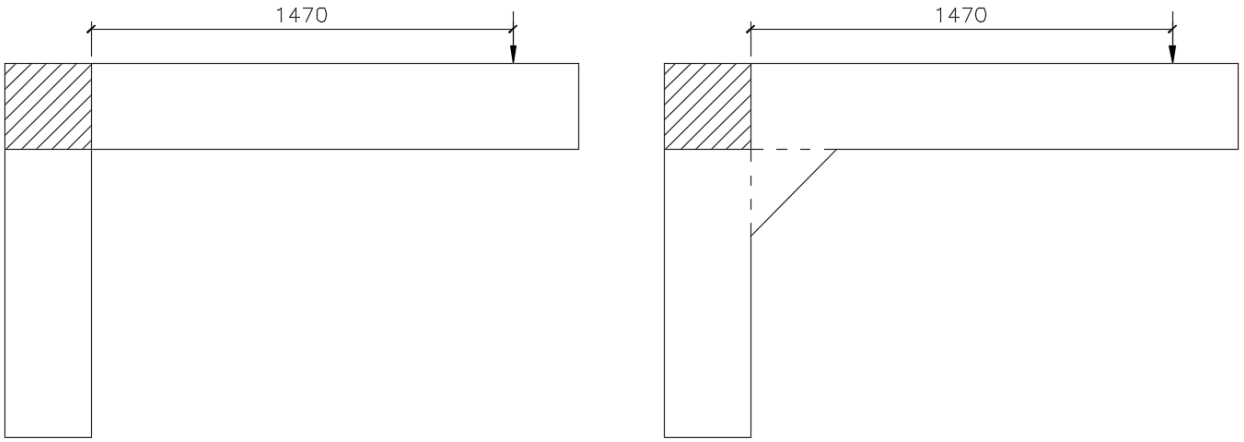

Figure 4.4: Measuring Moment Arm for Type A and B Geometries

4.2.2 Calculation of Theta

The angle θ is calculated using the difference in string-pot readings as well as the distance between them, as shown in Figure 4.5. Although the beam deformed shape is nonlinear assuming the deformed shape as being linear, for the purposes of calculating θ, yields an almost equal result as the former case. Equation 4-9 shows this calculation.

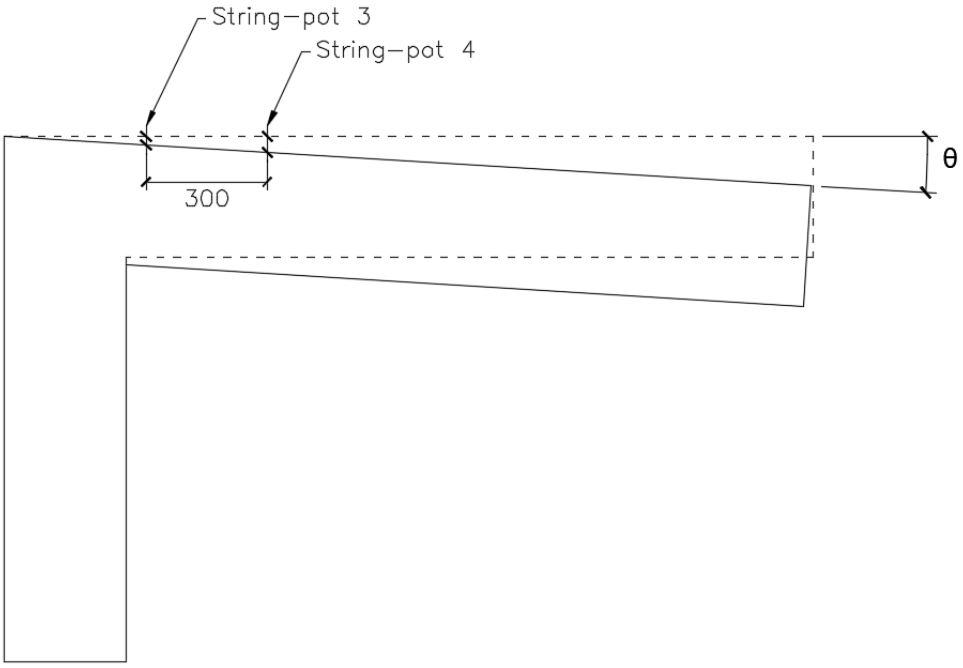

Figure 4.5: Calculation of θ using String-pot Readings

$$\theta = Tan^{-1}\left(\frac{\delta_{SP4} - \delta_{SP3}}{300}\right) \quad \textbf{(4-9)}$$

Where δ_{SP} is the measurement taken by the respective string-pot.

4.2.3 Change in Interior Angle

String-pot 5 measured change in the hypotenuse length of the interior corner "triangle" (shown in red), as seen in Figure 4.6. This measurement can be used to calculate the change in the corner angle for each corresponding load. Triangle leg lengths of type A and B specimens were 190 mm and 350 mm respectively.

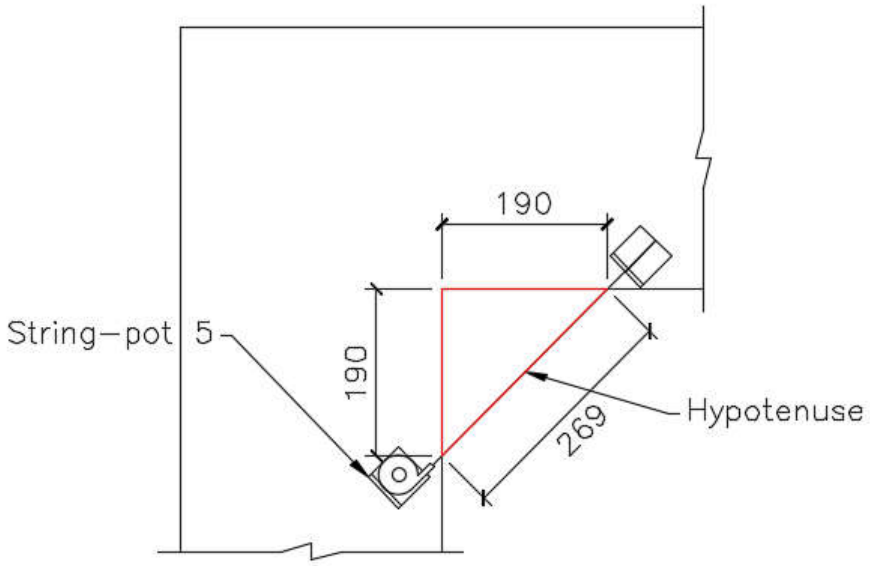

Figure 4.6: Calculation of Interior Angle Change

4.3 Test Observations

This section presents the test observations of all eight specimens. Test observations are discussed in order of testing.

4.3.1 General Observations

4.3.1.1 Cracking

Cracks were formed throughout the specimens during testing. The first cracks occurred at the beam/joint and column/joint junctions. This is consistent with the location of maximum bending moment. Cracks along the column also formed at the same time, following the constant moment distribution in the member. As loads were increased, cracking occurred along the beam with cracks forming towards the load application point with increasing load.

Formation of cracks within the joint occurred in all specimens. Due to the varying behaviour of these cracks, they are discussed in more detail in the next section. Appendix A shows additional cracking details.

4.3.1.2 Longitudinal Strains

Strain gauges placed on the tension longitudinal bar length show the strain distribution along its length. Typical strain distribution of specimens with type A geometry showed increasing strains approaching the adjoining member/joint junctions as well as a peak in bend strain after cracking in the joint occurs. Type B geometry specimens showed an increase of strains similar to that of type A; however, after diagonal cracks formed in the joints, large strains were exhibited by the column strain gauges.

4.3.2 Specimen UA-2-6

UA-2-6 was reinforced with two No. 6 tension bars with no confinement stirrups in the joint having a reinforcement ratio to balanced reinforcement ratio $\rho/\rho_b = 2.64$. The geometry of the corner was type A. Failure of this specimen occurred by rupture of both GFRP bars at the onset of the bend near the beam side. Failure occurred within the joint and can be seen in Figure 4.7.

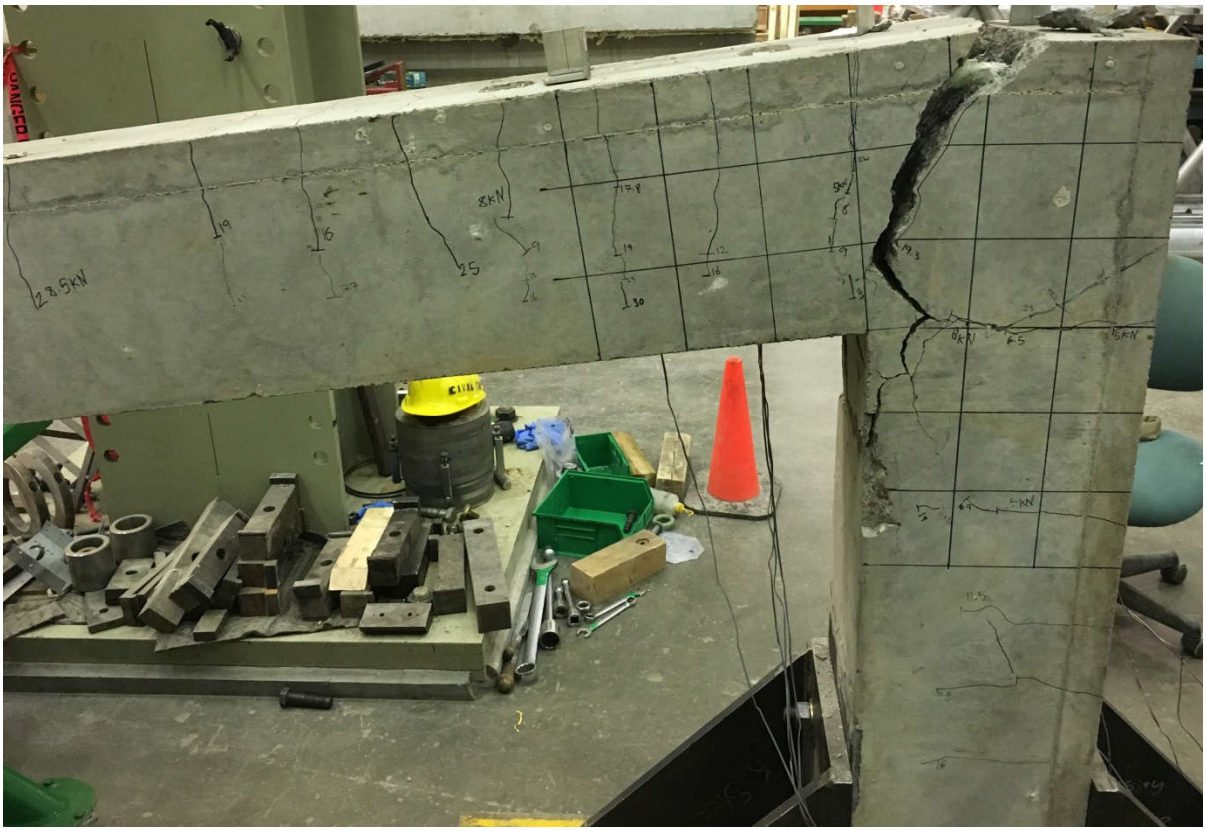

Figure 4.7: Crack Patterns on East Face, UA-2-6

Peak bending moment occurred at 62.1 kN.m with a deflection of 120.67 mm and maximum change in corner angle of 2°.

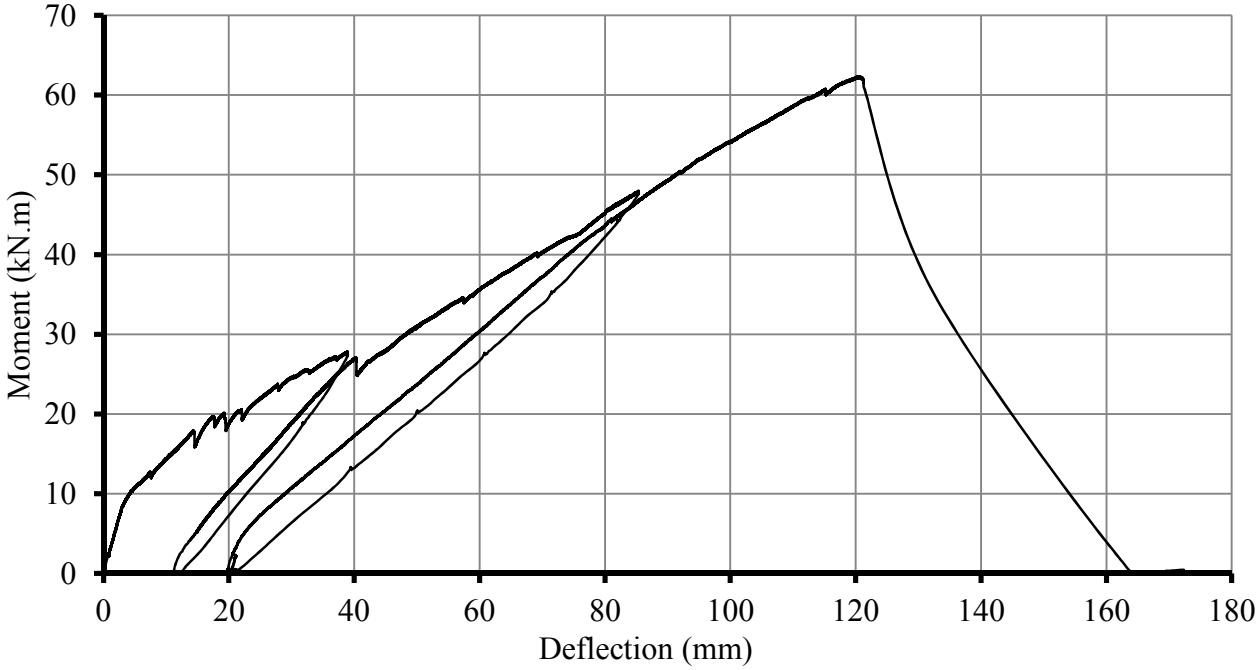

Figure 4.8: Moment-Deflection Response of Specimen UA-2-6

The specimen had to be unloaded twice in order to reposition the bearing plate at the load application point. This occurred at 27.5 kN.m and 47 kN.m.

Test setup was performed a day in advance of the testing day. At the time of test set up, anchors for holding the heavy actuator head were not yet installed. The actuator pump was required to be switched off at the end of the work day, which means the actuator head will fully protract given its inability to suspend its self-weight. As a result, the actuator head had to rest on top of the beam free end overnight. Supports were placed under the beam end in line with the actuator head to prevent the loading of the specimen. There is a risk that the specimen was preloaded, albeit negligibly due to the supports directly underneath the actuator head.

The first cracks formed at the beam/joint and column/joint junction. This occurred at a relatively low load and is believed to have occurred due to the actuator resting on the specimen overnight as mentioned earlier. At approximately 19 kN, a diagonal crack was observed in the joint on the beam side. No shear cracks were observed throughout the test, signalling that the strength of

concrete in shear was not exhausted. This was confirmed by strain readings on two stirrups in the beam which didn't increase significantly.

As loads were increased, crack widths in and around the joint also increased. As the test progressed the width of the diagonal in the joint rapidly started increasing. Since the position of this crack was coincidental with strain gage 2, the strain reading was also rapidly increasing. Eventually, the crack became extremely wide and both longitudinal bars ruptured at that location. Peak recorded load was 45 kN.

The behaviour of the specimen can be seen in Figure 4.8. The load was increasing at a steady rate until about 10 kN.m where the stiffness dropped due to cracking. This was quite less than the calculated cracking moment of 18 kN.m.

4.3.3 Specimen UA-4-6

UA-4-6 was reinforced with four No. 6 tension bars with no confinement stirrups in the joint with $\rho/\rho_b = 5.30$. The geometry of the corner was type A. Failure of UA-4-6 occurred by tensile failure of the concrete diagonal strut. The failure was sudden and occurred within the joint and can be seen in Figure 4.9. This failure was characterized by the lateral ejection of cover concrete.

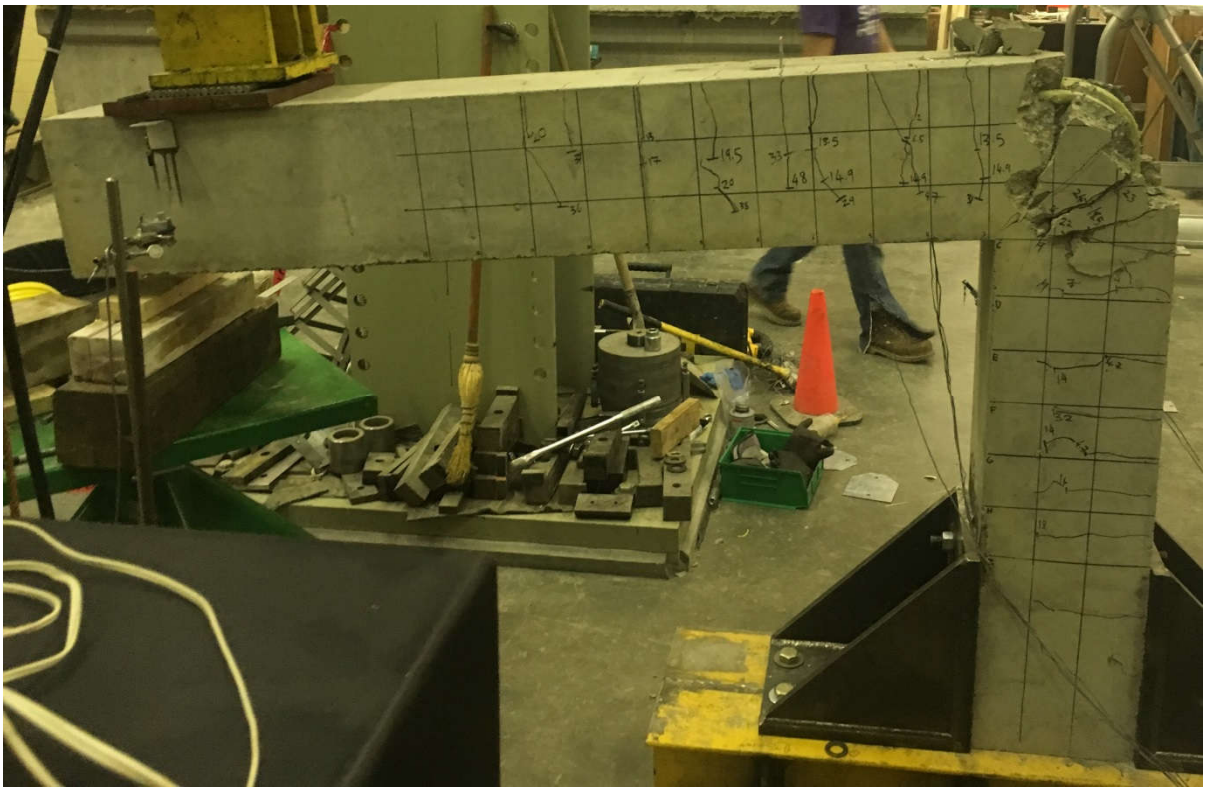

Figure 4.9: Crack Patterns on East Face, UA-4-6

Peak bending moment occurred at 98.6 kN.m with a deflection of 119.7 mm and maximum change in corner angle of 2.3^{o}.

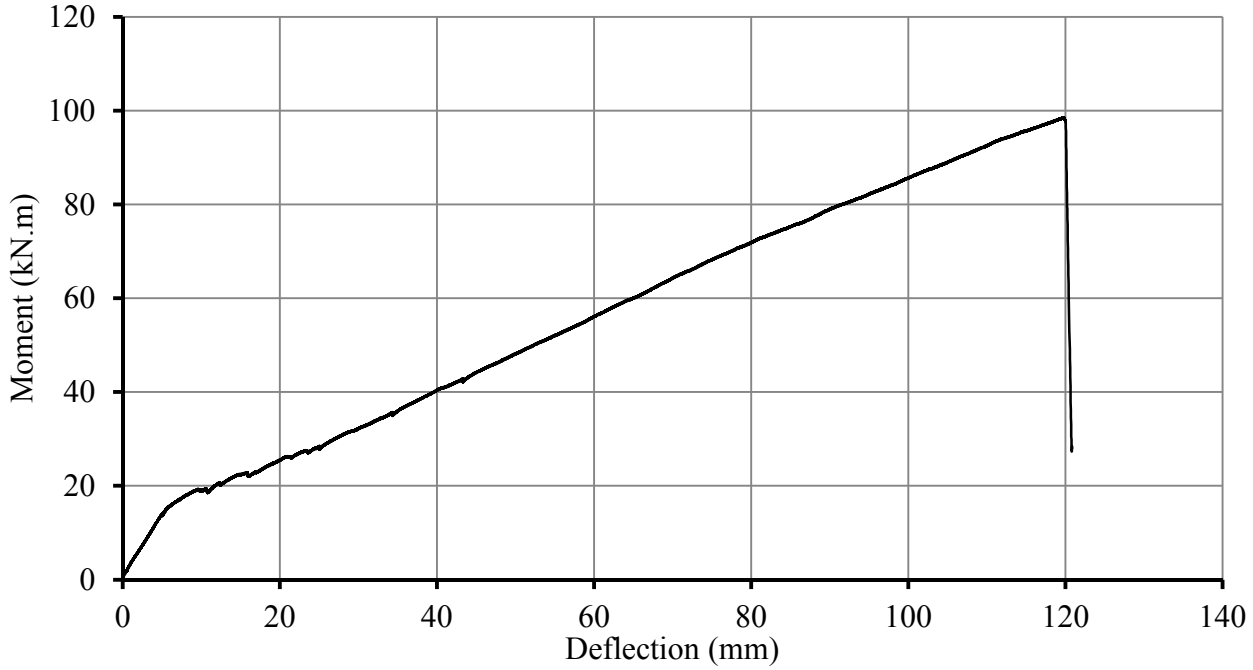

Figure 4.10: Moment-Deflection Response for Specimen UA-4-6

The formation of flexural cracks was typical in the beam and column. Similar to UA-2-6,first cracks occurred at relatively low loads due to the actuator resting on the specimen overnight. A diagonal crack formed soon after the specimen was loaded. At approximately 23 kN cracks had formed around the diagonal strut while the strut itself remained uncracked. At 62 kN, a crack formed at the centre of the diagonal strut.

The behaviour of the specimen can be seen in Figure 4.10. The load was increasing at a steady rate until about 16 kN.m where the stiffness dropped due to cracking. This was less than the calculated cracking moment of 18 kN.m, but larger than that of UA-2-6.

After the load was increased to a peak of 70.9 kN, the specimen suddenly failed after the joint exploded. A video recording of the test indicated that the failure initiated underneath the bend. Concrete pieces were ejected from all directions (the back face of joint, top face of the joint, and laterally on both sides of the joint).

No rupture occurred for any of the longitudinal bars or stirrups. The longitudinal bars experienced some damage: Cracks formed directly on the centre of bend at the inner face. Kinking/bending of the fibres was observed at some locations in the bend. Furthermore, some of the sand coating appeared to be sheared off at the straight portion of the beam side.

Strain gages 1 and 3, at the entrance and exit of the joint respectively, showed almost equal readings. While strain gage 2 consistently exhibited larger strains than 1 and 3 at equal load levels. All three strain gauges displayed equal readings until the cracking of specimen. Strain gage S1, attached to the first stirrup, showed very low strains; indicating that stirrups were mostly unengaged. This was confirmed by the presence of no shear cracks.

4.3.4 Specimen UA-3-6

UA-3-6 was reinforced with three No. 6 tension bars with $\rho/\rho_b = 5.30$. No confinement stirrups in the joint and the corner geometry was type A. Similar to UA-4-6, failure of this specimen occurred by tensile failure of the concrete diagonal strut. The failure was sudden and occurred within the joint as shown in Figure 4.11. This failure was characterized by the lateral ejection of cover concrete.

Figure 4.11: Cracking Patterns on East Face, UA-3-6

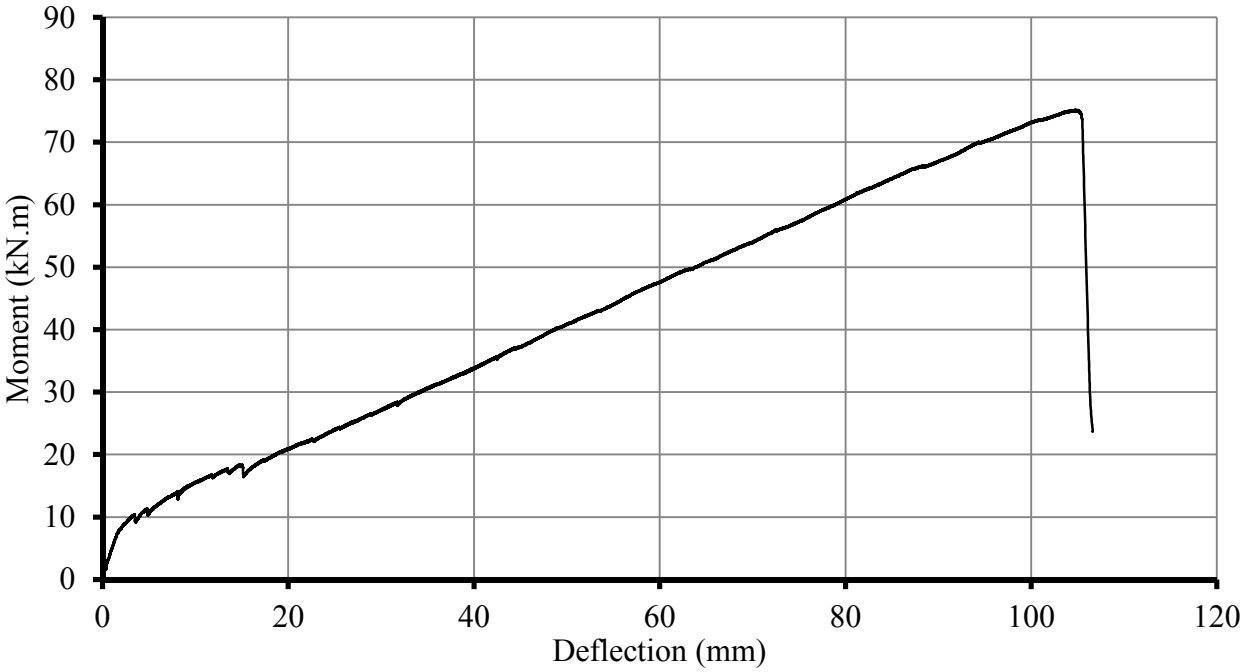

Figure 4.12: Moment-Deflection Response of Specimen UA-3-6

Peak bending moment occurred at 75.2 kN.m with a deflection of 104.7 mm and maximum change in corner angle of 2.1^{o}.

The formation of flexural cracks was typical in the adjoining members. Anchors for the actuator head were installed following the testing of UA-4-6, preventing any loading of the specimen prior to the actual testing. This resulted in the formation of cracks at a later stage relative to UA-2-6 and UA-4-6 – which did experience some preloading. After a load of approximately 13 kN, diagonal cracks formed in the joint around the diagonal strut, with the strut itself uncracked. At 35 kN, a crack formed directly in the centre of the diagonal strut.

The general behaviour can be seen in Figure 4.12. After reaching approximately 8.5 kN.m, the slope decreases , showing less stiffness and signalling that cracking had occurred. This was lower than the calculated cracking moment of 18 kN.m.

After the load was increased to the peak of 53.7 kN, the load dropped by 1.5 kN before sudden failure of the specimen occurred. The concrete in the joint exploded without warning. It was

observed from test recordings that the failure started underneath the bend. Concrete was ejected from all directions.

Similar to UA-4-6, no rupture occurred for any of the longitudinal bars or stirrups. The longitudinal bars experienced some damage: Cracks formed directly on the centre of bend at the inner face. Kinking/bending of the fibres was observed at some locations in the bend. Furthermore, some of the sand coating appeared to be sheared off at the straight portion of the beam side.

Prior to cracking, strain gauges 1, 2, and 3 were showing similar readings. After about 20 kN.m, strain gauge 2, located at the onset of bend, began to register strains at higher rates. Strain gauges 1 and 3 showed almost equal readings. Strain gauges affixed to stirrups showed relatively low strains throughout the test, however, strain gauge S2 reached a peak strain of 0.0017, equivalent to 85 MPa. No shear cracks were observed throughout the test.

4.3.5 Specimen UB-3-6

UB-3-6 was reinforced with three No. 6 tension bars with $\rho/\rho_b = 5.30$. No confinement stirrups were installed in the joint and the corner geometry was type B. Failure of this specimen occurred by crushing of concrete on the compression face of the column/chamfer interface, as shown in Figure 4.13.

Figure 4.13: Crack Patterns on East Face, UB-3-6

Peak bending moment occurred at 76.2 kN.m with a deflection of 91.5 mm and maximum change in corner angle of 0.42°.

Cracking in the adjoining members was typical. Initial cracks occurred at the joint/adjoining members at relatively larger loads. The joint region remained uncracked until 20 kN. At 35 kN, diagonal cracks around the diagonal strut appeared. The diagonal cracks were extended at 60 kN.

As loads were increased, the width of the diagonal crack on the column side also increased, reaching a width of 5 mm in some locations.

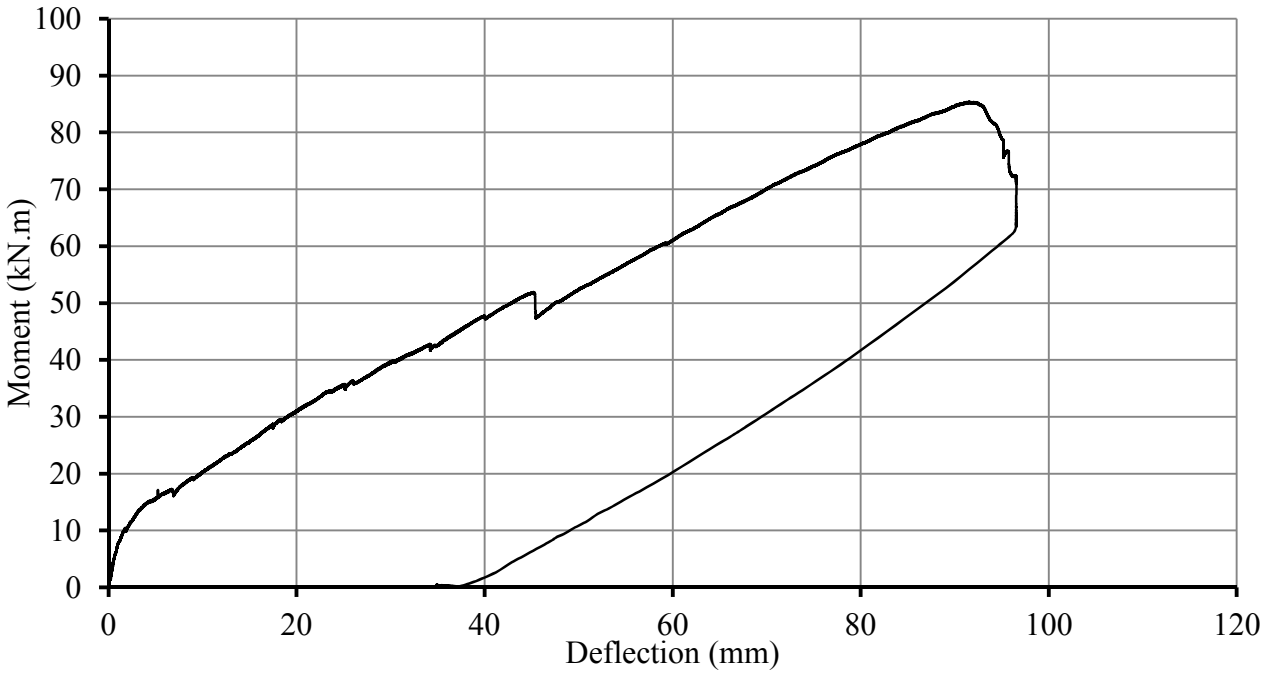

Figure 4.14: Moment-Deflection Response of Specimen UB-3-6

The general behaviour can be seen in Figure 4.14. After about 15 kN.m, the stiffness of the member decreases. At 51 kN.m (load = 36 kN), there is a visible drop in in load to 47 kN.m (load = 33.6 kN). This directly corresponds with the formation of the diagonal cracks around the diagonal strut.

Failure of this specimen was generally unremarkable. Concrete crushing was observed at the column/chamfer interface at a load of 60 kN. After reaching a peak of 61 kN, the load began to steadily drop. The specimen was unloaded in order to preserve the bars for specimen autopsies.

Strain gauge 3 reading was consistently higher than strain gauge 1. This is due to the crack formation and widening around strain gauge 3. The visible drop seen in Figure 4.15 marked the engagement of strain gauge 2. This is consistent with the proximity of the diagonal crack formed at the respective load drop to the location of strain gauge 2. Stirrup strain gauge readings were explicably low given the lack of shear cracks.

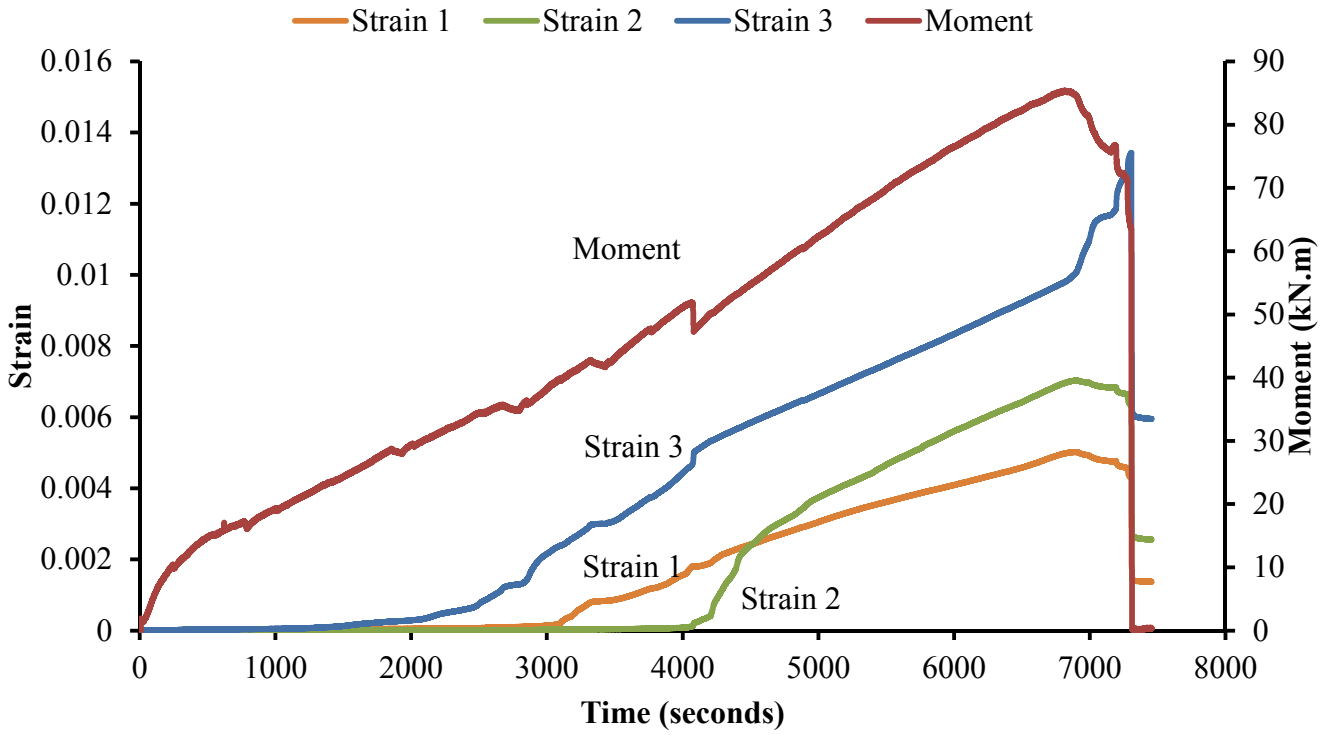

Figure 4.15: Strain and Moment Overlayed Versus Time, UB-3-4

4.3.6 Specimen CA-2-6

Specimen CA-2-6 was reinforced with two No. 6 tension bars with confinement stirrups in the joint. The reinforcement ratio to balanced reinforcement ratio $\rho/\rho_b = 2.93$. The geometry of the corner was type A. Failure of specimen CA-2-6 occurred by anchorage debonding at the base of the column. The joint at failure can be seen in Figure 4.16.

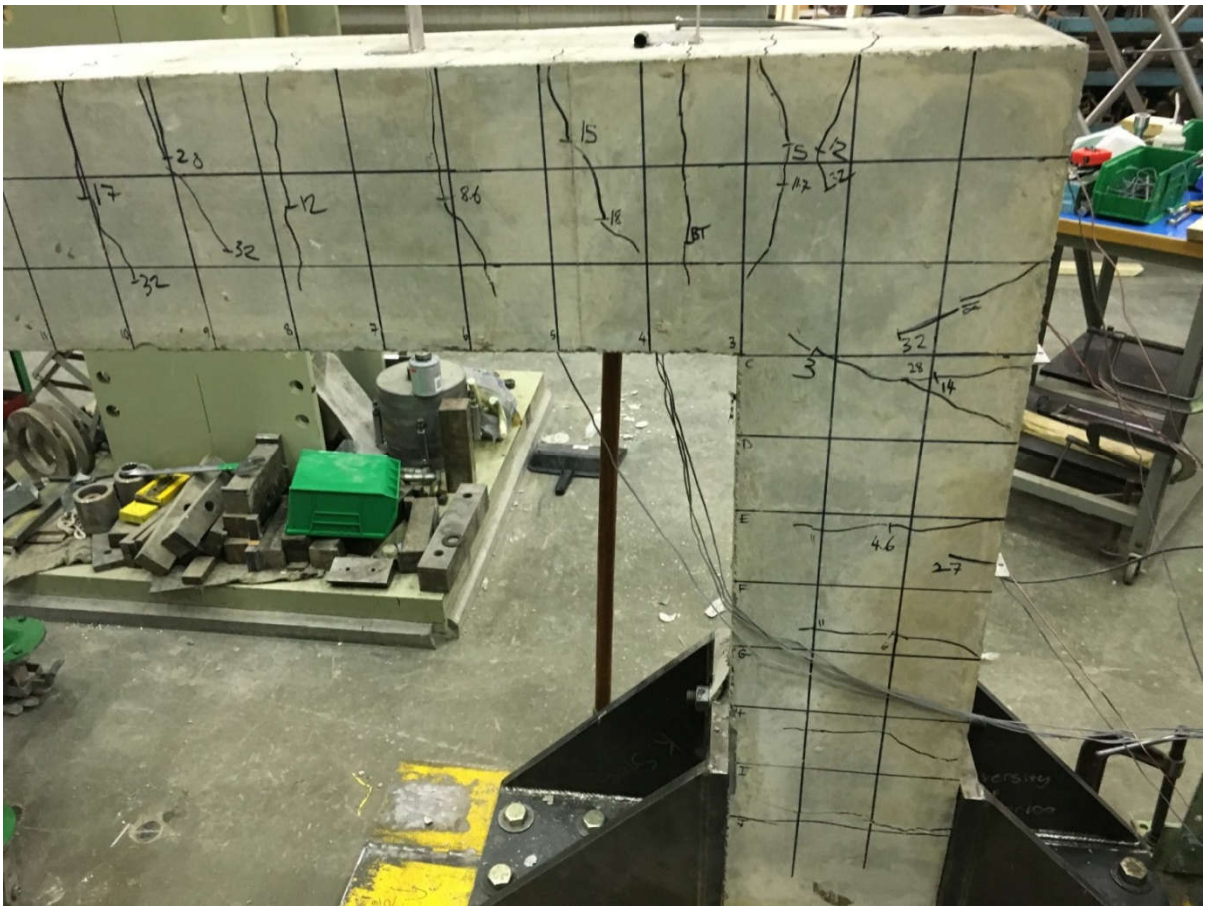

Figure 4.16: Crack Patterns on East Face, CA-2-6

Specimen CA-2-6 was reinforced with two No. 6 tension bars with confinement stirrups in the joint. The reinforcement ratio to balanced reinforcement ratio $\rho/\rho_b = 2.93$. The geometry of the corner was type A. Failure of specimen CA-2-6 occurred by anchorage debonding at the base of the column.

Peak bending moment occurred at 75 kN.m with a deflection of 153.2 mm and maximum change in corner angle of 2.86^{o}.

Cracking in adjoining members was typical. The formation of the cracks initiated at the locations where the diagonal stirrups was tied to the tension bars. At higher loads, the aforementioned cracks propagated slightly. No new cracks were observed after 32 kN load level. Throughout the test, the diagonal strut remained uncracked, similar to specimen UA-2-6.

The general behaviour can be seen in Figure 4.17. It is noted that this specimen did not experience a large pre-cracked behaviour that was observed in other specimens: The stiffness was constant throughout the entire test.

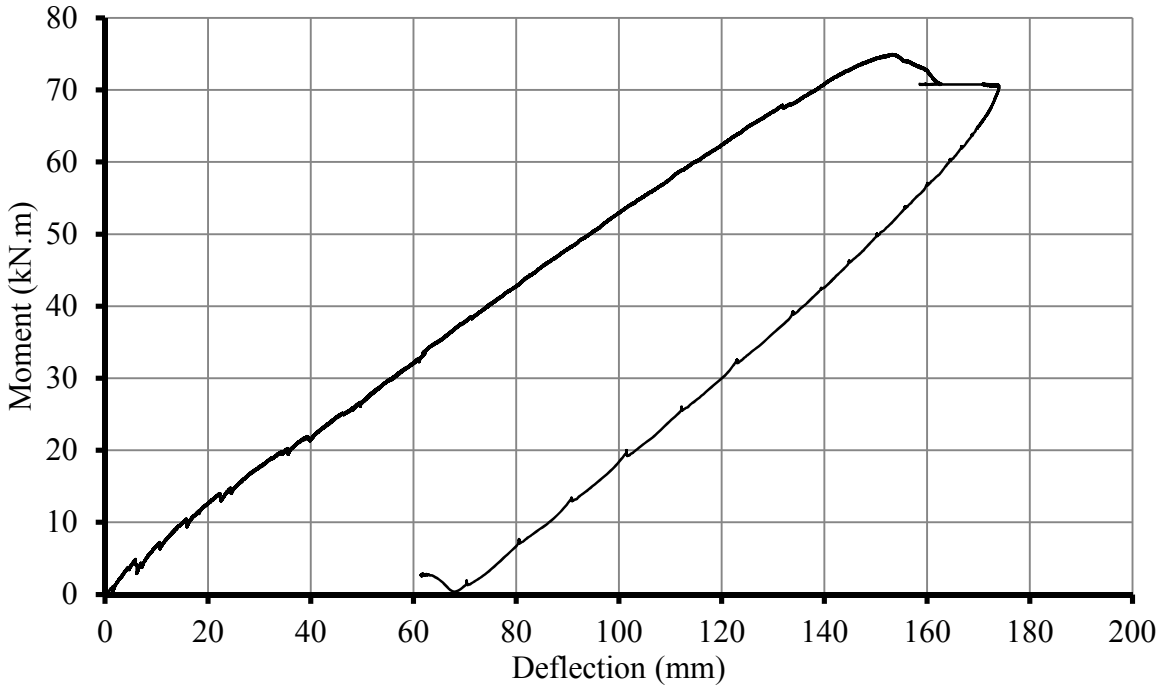

Figure 4.17: Moment-Deflection Response of Specimen CA-2-6

After reaching a peak load of 55 kN, the load slowly decreased and was eventually unloaded. A crack at the column base was observed at failure, with a significantly larger crack widths than other crack formations. The drop in load was accompanied with an increase in displacements

increase in the column base crack. This indicates an anchorage failure due to the bars slowly pulling out with increasing crack width.

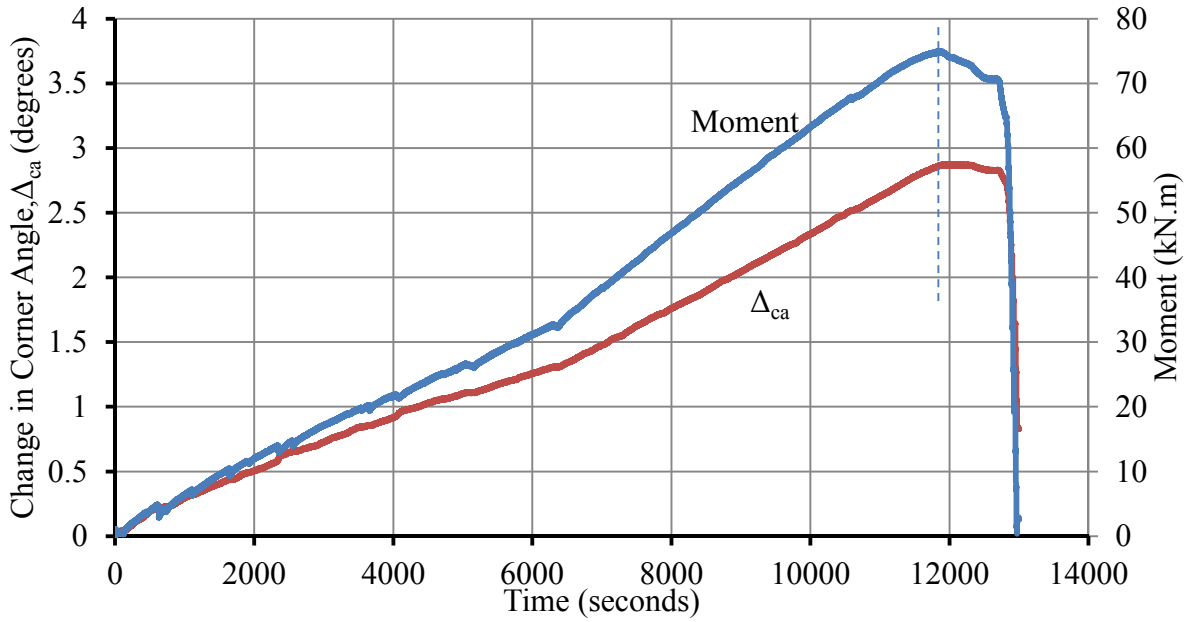

Figure 4.18: Change in Corner Angle and Moment Versus Time, CA-2-6

Figure 4.18 shows the decrease in corner angle and moment versus time. As it is loaded, both the moment and the change in corner angle increased. Δ_{ca} became constant at peak load, indicating that the displacement at the beam end post peak load was due to the widening of the crack.

4.3.7 Specimen CA-3-6

CA-3-6 was reinforced with three No. 6 tension bars with $\rho/\rho_b = 4.39$. Confinement stirrups were installed in the joint and the corner geometry was type A. The failure of this specimen initiated through crushing of concrete in the interior corner; however, final failure occurred suddenly in the joint and was characterized by ejection of concrete. The specimen at failure can be seen in Figure 4.19.

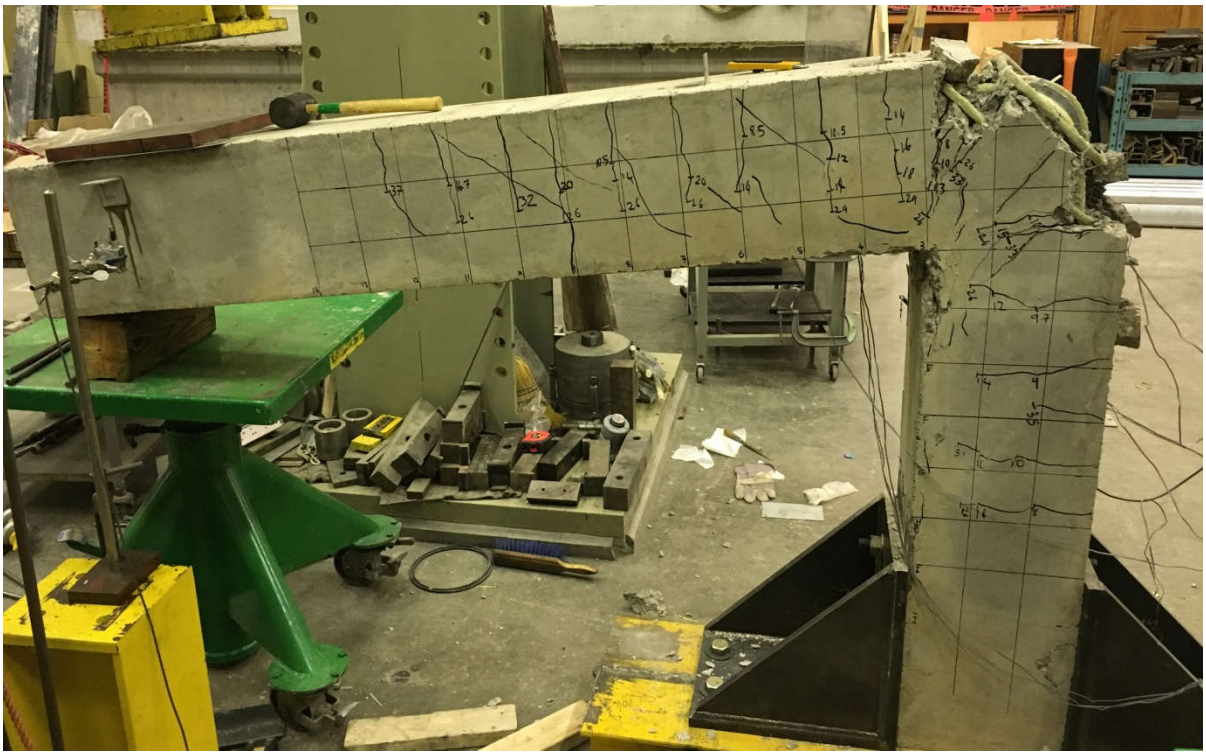

Figure 4.19: Crack Patterns on East Face, CA-3-6

Peak bending moment occurred at 115.2 kN.m with a deflection of 182.1 mm and maximum change in corner angle of 3.85^o.

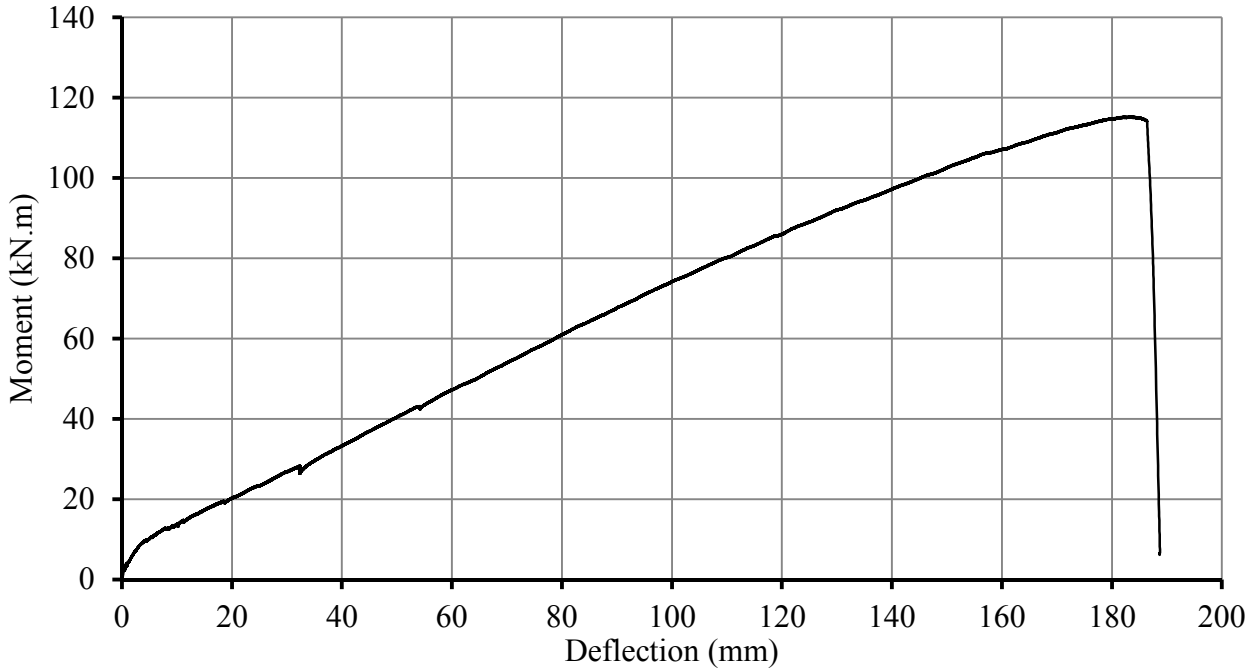

Figure 4.20: Moment-Deflection Response of Specimen CA-3-6

Cracking in adjoining members was typical. At relatively low loads, flexural cracks formed in the joint near the joint/adjoining member interface. The formation of the cracks initiated at the locations where the diagonal stirrups was tied to the tension bars. At higher loads, cracks parallel to the aforementioned cracks formed. However, unlike previous specimens, these cracks were not directly adjacent to the diagonal strut. No new cracks formed in the joint after 40 kN load level. Throughout the test, the diagonal strut remained uncracked.

The general behaviour can be seen in Figure 4.20. After reaching approximately 10 kN.m, the slope decreases, showing less stiffness and signaling that cracking had occurred. This was lower than the calculated cracking moment of 16.8 kN.m.

After attaining a load of 74 kN, early signs of concrete crushing were observed in the interior corner. At 80 kN, obvious signs of crushing were seen – the mortar was pulverized and small pieces were falling off. After reaching a peak of 85 kN, the load steadily dropped to 84 kN before suddenly failing. Pieces of concrete were ejected from the back and top faces of the joint.

No lateral ejection of concrete was observed. At failure, it was noticed that the diagonal strut was held by the confining stirrups. A crack parallel to the diagonal strut was detected after failure.

Rupture of the middle tension bar occurred at failure. Typical kinking/bending of fibres within the bends was seen in all tension bars. Lateral displacement of the bars at the bend occurred, which is described in section 5.3. Unruptured bars appear to be pulled inwards towards the adjoining members, shown in Figure 4.21.

Figure 4.21: Slip of Longitudinal Bars towards Adjoining Members, CA-3-6

Readings of strain gauge 1 and 3 were consistent throughout the test, and only slightly varied towards the end of test. Strain gauge 2 was engaged at a later stage but showed a higher rate of strain than gages 1 and 3.

4.3.8 Specimen UA-2-4

UA-2-4 was reinforced with two No. 4 tension bars with no confinement stirrups in the joint having a reinforcement ratio to balanced reinforcement ratio $\rho/\rho_b = 1.27$. The geometry of the corner was type A. Failure of this specimen occurred by rupture of both GFRP bars at the onset of the bend near the beam side. Failure occurred within the joint as shown in Figure 4.22.

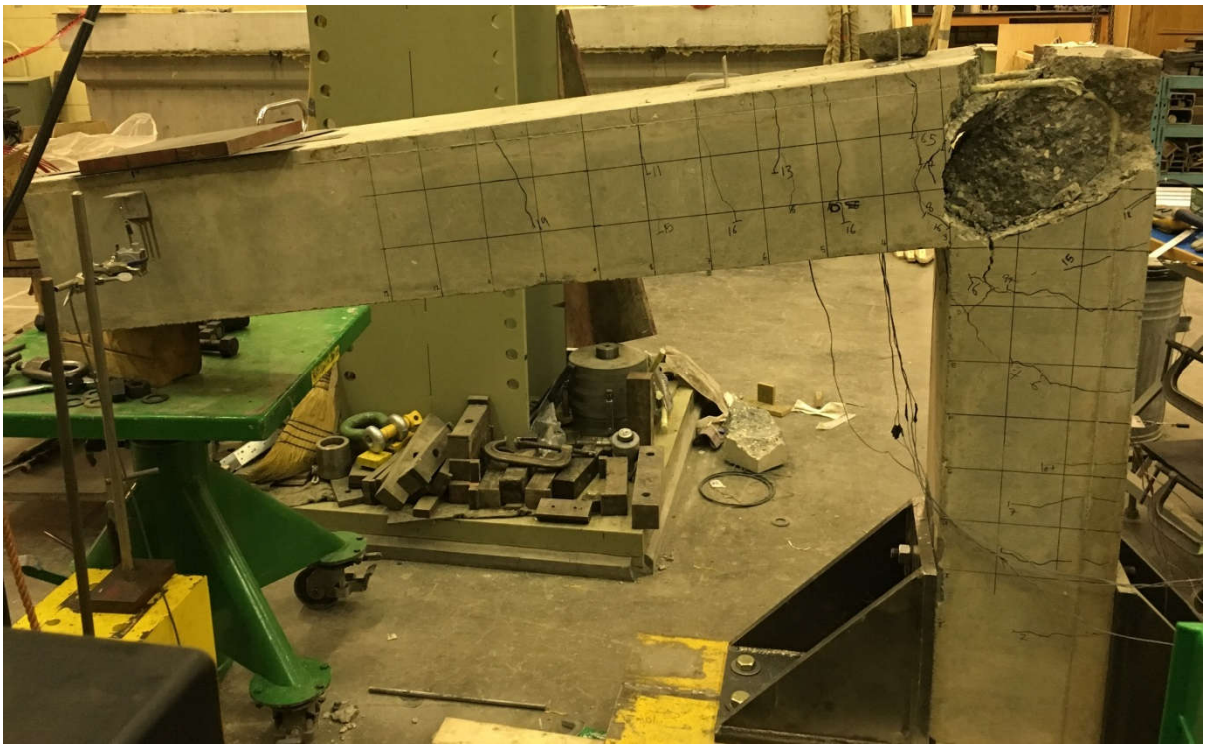

Figure 4.22: Crack Patterns on East Face, UA-2-4

Peak bending moment occurred at 39.2 kN.m with a deflection of 140.26 mm and maximum change in corner angle of 2.47^o.

Cracking was typical in the adjoining members. At 12 kN and 18 kN, cracks formed in the joint at the beam and column side respectively. These cracks were aligned with the diagonal strut, but did not form directly adjacent to it. No further cracks were observed beyond this load level.

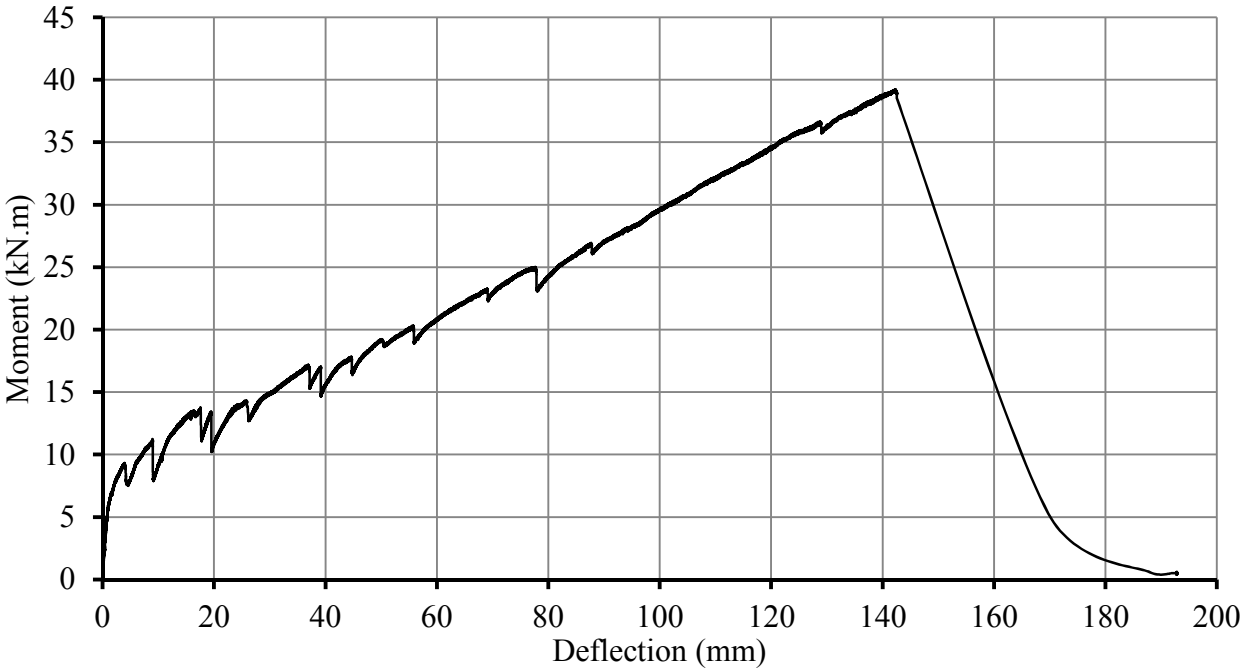

Figure 4.23: Moment-Deflection Response of Specimen UA-2-4

The moment-displacement response can be seen in Figure 4.23. The sudden drops in the moment-defection curve can be observed. Since the reinforcement size is small, the beam derives more stiffness from the tensile strength of concrete – relative to other specimens. This may explain the sudden drops in stiffness as the cracking of the specimen occurs. At later stages, no drops occur since the specimen is fully cracked. This behaviour does not appear in the higher reinforced specimens, such as UA-3-6 and UA-4-6.

Compared to UA-2-6, no excessive widening of cracks occurred within the joint. Soon after the peak load was reached (28.5 kN), the specimen failed suddenly by rupture of both bars. The left half of the joint spalled off, exposing the inner bars. No cracks formed within the diagonal strut; however, most of the aggregate fractured. The sand coating on straight portion of the bar adjacent to the bend was completely sheared off.

Readings of strain gauges 1 and 3 showed close values, albeit the latter gage was engaged at a later load level. Strain gauge 2 was unengaged until a load of approximately 11 kN, which is

consistent with the formation of the crack intercepting this gauge. At 83% of peak load, strain gauge 2 failed.

4.3.9 Specimen CB-3-6

CB-3-6 was reinforced with three No. 6 tension bars with $\rho/\rho_b = 4.39$. Confinement stirrups in the joint were used and the corner geometry was type B. Failure of specimen 8 occurred by crushing of concrete on the compression face of the column/chamfer interface, and can be seen in Figure 4.24.

Figure 4.24: Crack Patterns on East Face, CB-3-6

Peak bending moment occurred at 119.88 kN.m with a deflection of 186.8 mm and maximum change in corner angle of 0.83^{o}.

Crack formation was typical in the adjoining members. First cracks within the joint region occurred at approximately 12 kN. These cracks occurred on both sides of adjoining members and were located closer to the respective member than the joint. The diagonal strut remained uncracked until 55 kN where a crack formed adjacent to the strut. This crack coincided with the

location of strain gauge 2. At increasing loads, the column-side diagonal crack width steadily increased.

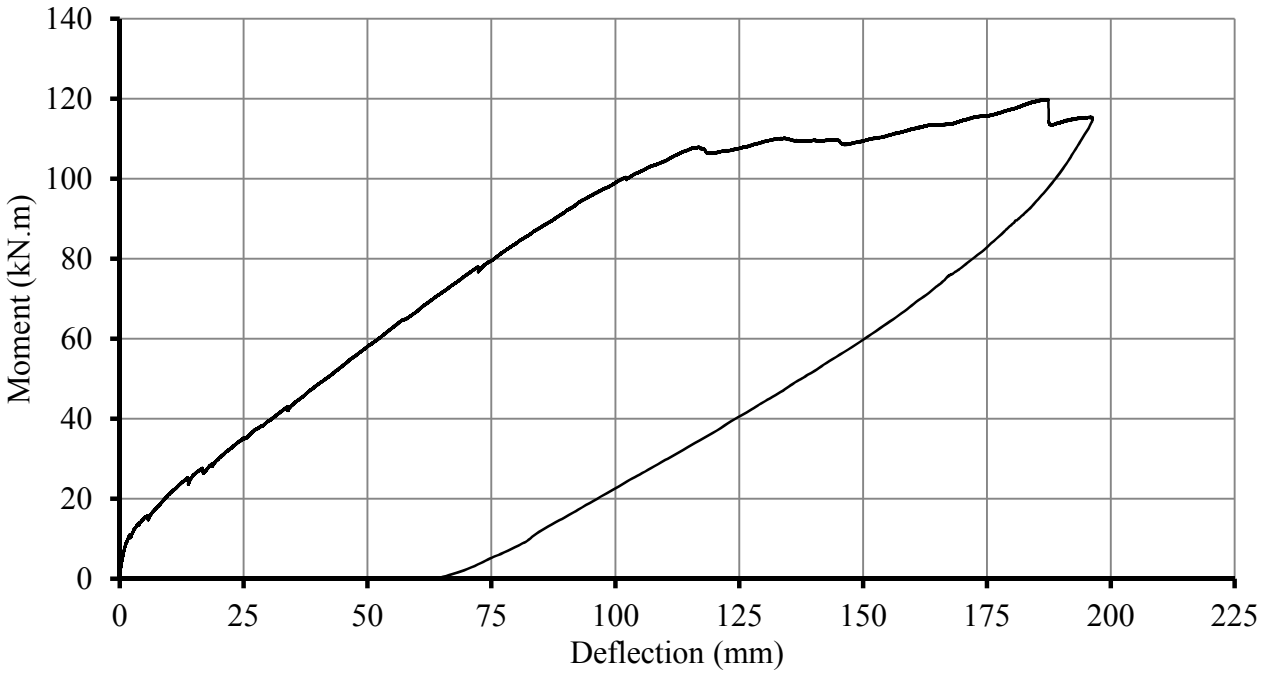

Figure 4.25: Moment-Deflection Response of Specimen CB-3-6

General behaviour can be seen in Figure 4.25. At 64 kN, early signs of crushing appeared at the compression face of the column/chamfer interface. At 70 kN, it became obvious that crushing had taken place. The load was increased until approximately 78 kN until the load suddenly dropped to 76 kN. Loading was increased until it plateaued at 80 kN while displacement at the beam end continued to increase. The peak load of 88 kN was accompanied by a loud noise and formation of crack which seemed in line with the tensile reinforcement. Despite the resulting 2 kN load drop, the load continued to increase with increasing displacement. The test was stopped after excessive deflections were observed (196mm). At the end of test, the severity of concrete crushing was noted.

Readings of Strain gauge 1 and 3 showed similar strains throughout the first part of the test. After the crack widening near the column initiated, strain gauge 3 displayed larger strains –

despite the load levelling off at some point. The formation of the 55 kN crack engaged strain gauge 2. At failure, strain gauges 1 and 2 had similar readings, while strain gauge 3 was significantly larger.

Chapter 5
Discussion of Experimental Results

5.1 General

All specimens without confinement stirrups failed with strength efficiencies less than 100%. For the specimens using confinement stirrups, two specimens attained strength efficiencies greater than 100% while the third failed prematurely (CA-2-6). The following section discusses the effects of reinforcement ratio, confinement stirrups, and geometry type on the behaviour of the joint. A summary of all test results is shown in Table 5.1.

Table 5.1: Summary of Predicted and Actual Capacities

Specimen	ρ	Peak Load (kN)	Peak Moment, M_{test} (kN.m)	$\frac{M_{test}}{M_{design}}$	Mode of failure
UA-2-4	0.38%	28.5	39.2	58.8%	Bar rupture
UA-2-6	0.86%	45.0	62.1	64.3%	Bar rupture
UA-3-6	1.29%	53.7	75.2	66.2%	Diagonal strut failure
UA-4-6	1.72%	70.9	98.6	77.7%	Diagonal strut failure
UB-3-6	1.29%	61.0	85.4	72.4%	Crushing of interior corner
CA-2-6	0.86%	55.0	75.0	80.8%	Column bar anchorage
CA-3-6	1.29%	84.9	115.2	106.8%	Crushing of interior corner*
CB-3-6	1.29%	88.8	119.9	110%	Crushing of interior corner

* Specimen CA-3-6 indicated crushing of interior corner; however, combined strut failure and middle-bar rupture occurred at ultimate.

5.2 Effect of Reinforcement Ratio

The moment deflection response of the unconfined specimens of type A geometry is shown in Figure 5.1. The variable studied was the effect of reinforcement ratio on the behaviour of the specimen. Reinforcement ratio was changed between 0.38% and 1.72%.

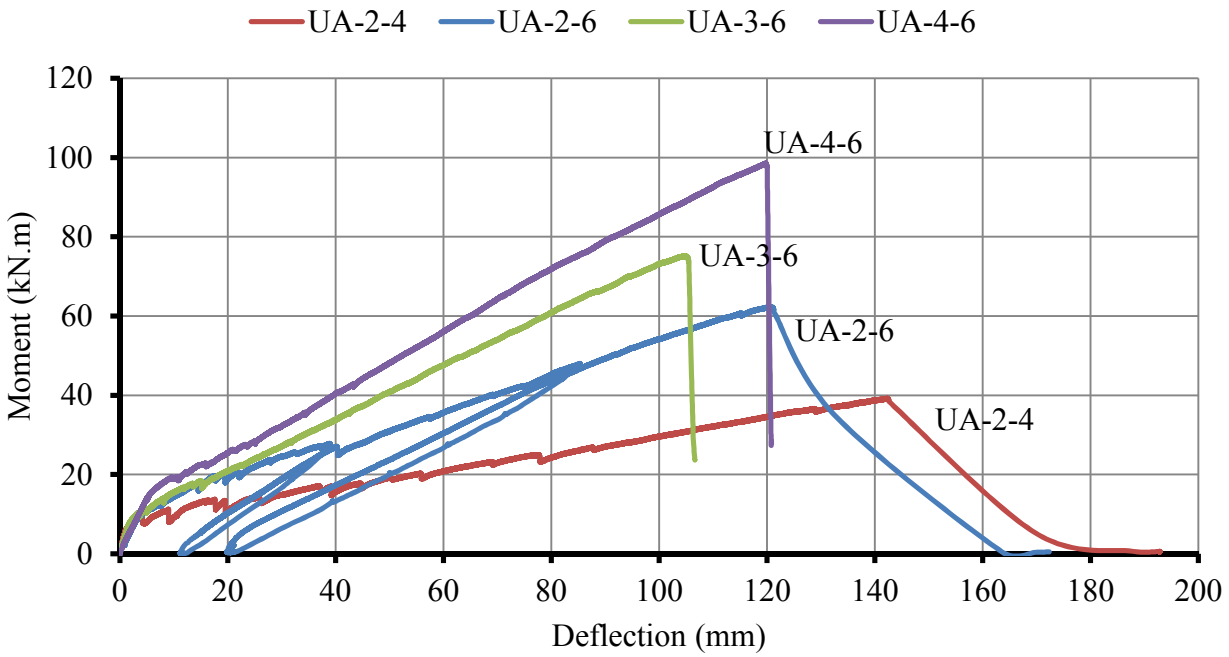

Figure 5.1: Moment-Deflection Response of Specimens Without Confinement With Variable Reinforcement Ratios

As the reinforcement ratio is increased, it can be seen that both the peak load and the stiffness of the member increase. This is obvious since extra reinforcement provides additional stiffness to the member. The additional bars also decrease the amount of stress carried per bar, allowing an overall increase in member capacity, and lead to the prevention of bar rupture.

Another apparent observation is the decrease in maximum deflection at failure with increasing reinforcement ratio. An increase in maximum deflection can be observed from specimen UA-3-6 to UA-4-6. Since more bars are present in the corner, bearing stress on the concrete per bar is less. Furthermore, the extra bars provide extra confinement in the joint; however, this effect may be negligible.

All specimens tested contained a reinforcement ratio larger than balanced. Specimen UA-2-4 was initially designed as under-reinforced using nominal manufacturer specified strengths.

However, actual tested values resulted in the specimen becoming over-reinforced, despite the rather small ratio of 0.38%.

Two main failure modes dominated: bar rupture and failure of the diagonal strut. Specimens UA-2-4 and UA-2-6 experienced failure by bar rupture at the onset of bend. This occurred despite the adjoining members being designed as over-reinforced. The bend, being the weakest point in the bar, failed first.

Table 5.2: Comparing Actual Strain at Rupture with Calculated, Bent portion

Specimen	Failure Strain	Bend Strength* (MPa)	Modulus of Elasticity*† (MPa)	Calculated Failure Strain
UA-2-4	0.020046	634	53942	0.011753
UA-2-6	0.018975	655	53808	0.012173

* Tested by manufacturer

† Average value of tests used – manufacturer did not specify a minimum.

Table 5.2 presents the failure strains prior to rupture in the respective specimens. Specimen UA-2-6, being reinforced with larger bars, shows a consistent increase in strain relative to the calculated. However, both calculated failure strains were greatly underestimated. The bend strength used in this calculation was obtained using CAN/CSA S806 Annex D (equivalent to ACI B.5 test method); which, while conservative, may not accurately predict the bend strength. The state of stress in the specimen is more complex than this test method – which involves unbonded regions of bar as well as loading through pure tension. The greater actual failure strain is advantageous since the actual material behaves better than predicted.

When the bend tensile strength is not exceeded, failure of the diagonal strut can be anticipated. Specimens UA-3-6 and UA-4-6 both failed in this manner. Cracks forming in the centre of the diagonal strut were observed at 67% and 87% of peak load, respectively. The formation of the diagonal crack within the diagonal strut signals that the tensile strength of the concrete was exhausted. This can be seen in figure Figure 5.2.

(a) (b)

Figure 5.2: Cracks Along Diagonal of Specimens UA-3-6 and UA-4-6

Upon close inspection of the joints after failure, it was noticed that the specimens that failed in bar rupture showed no cracks along the diagonal strut, as shown in Figure 5.3. Whereas the specimens that failed through failure of diagonal strut showed obvious cracking within the strut. It is clear that there is a threshold when failure switches from bar rupture to failure of strut and appears directly related to reinforcement ratio.

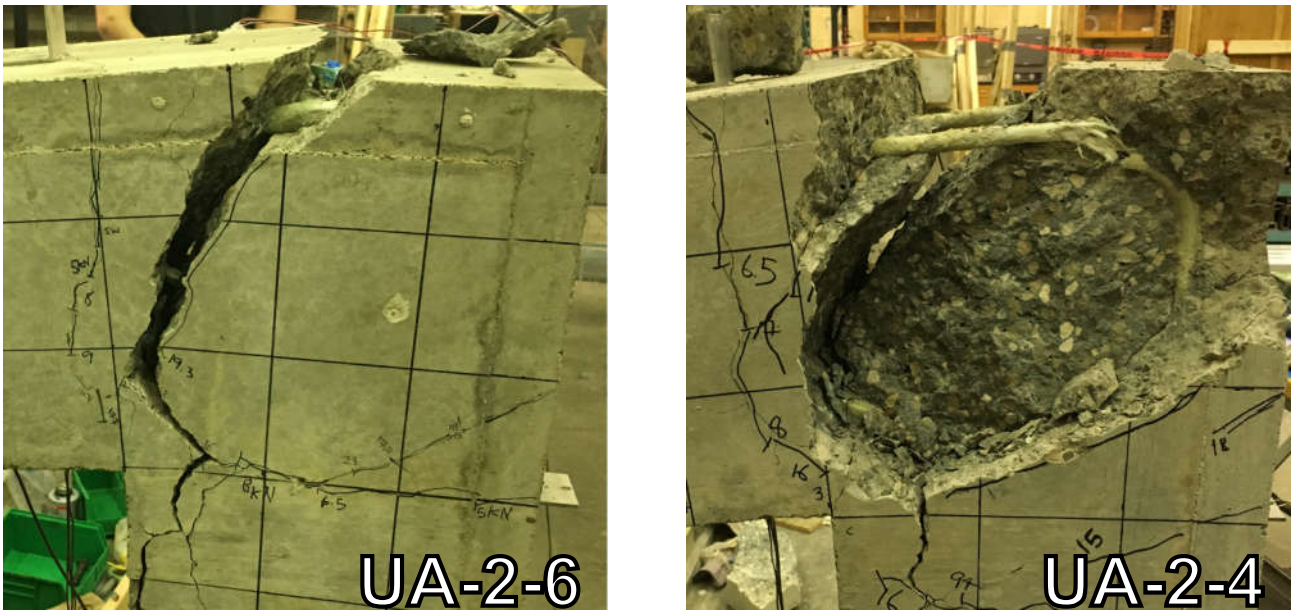

(a) (b)

Figure 5.3: Lack of Crack Along Diagonal Strut in Specimens Failing in Bar Rupture

Kemp and Mukherjee (1968) discusses this phenomena and notes that the formation of the diagonal crack is analogous to the formation of cracks in split tensile tests, as shown in Figure 5.4.

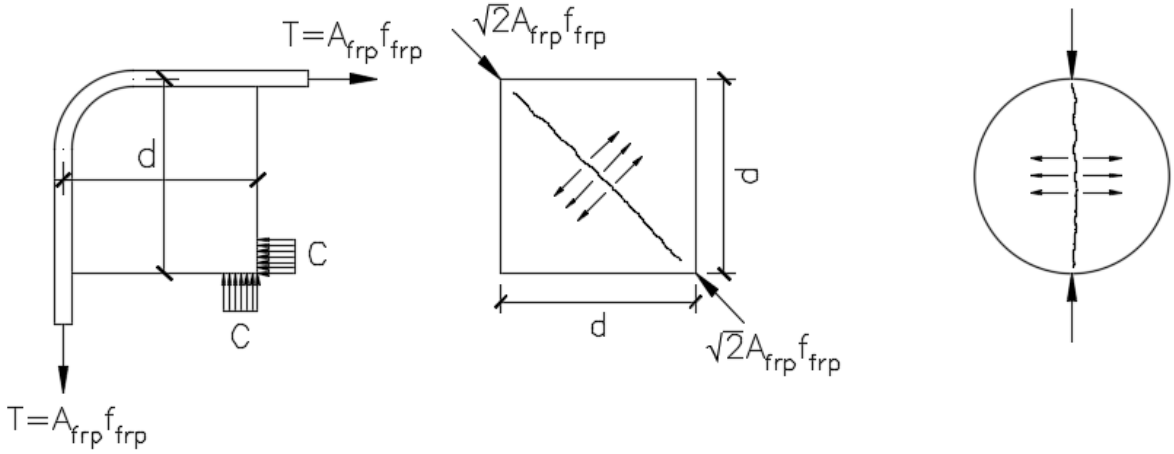

Figure 5.4: Visualizing the Stresses in the Joint Region (left & centre) as Analogous to Split Tensile Test (Reproduced from Kemp & Mukherjee, 1968) (right)

The formulation recommended by Park and Paulay (1975) is based on that research and is shown in equation 5-1. This relationship provides a limiting reinforcement ratio in order to avoid the formation of a crack in the diagonal strut.

$$\rho_{KM} \leq 1.2 \frac{f'_t}{f_y} \quad \textbf{(5-1)}$$

This formulation depends on the yield stress of steel. For over reinforced FRP beams, the denominator, f_{frp}, should be taken as the stress in the bar at failure. Table 5.3 shows the application of Equation 5-1on the GFRP reinforced specimens.

Table 5.3: Applying ρ_{KM} on Unconfined GFRP Specimens

Specimen	Reinforcement Ratio	Failure Mode	Limiting Reinforcement Ratio, ρ_{KM} **
UA-2-4	0.38%	Bar rupture	0.449%
UA-2-6	0.86%	Bar rupture	0.476%
UA-3-6	1.29%	Diagonal strut failure	0.532%
UA-4-6	1.72%	Diagonal strut failure	0.580%

* Specimen CA-3-6 indicated crushing of interior corner; however, combined strut failure and middle-bar rupture occurred at ultimate.

** ρ_{KM} was calculated using the determined $f'_t = 4.05MPa$; and f_{frp} was found by multiplying the strain in the bar by elastic modulus.

It can be seen that the formulation developed by Kemp & Mukherjee does not show meaningful results for GFRP reinforced specimens. Furthermore, it is not practical to calculate f_{frp} from a design perspective since it is not directly known. Contrary to steel, where the denominator,f_y, is a fixed and known quantity.

5.3 Effect of Confinement

The moment deflection response of unconfined versus confined specimens from geometry type A and B are shown in Figure 5.5, Figure 5.8, and Figure 5.9. The specimens had a constant reinforcement ratio, with a slight variation in concrete strength due to casting of specimens on different days.$f'_c = 55MPa$ and 48 MPa for the unconfined and confined specimens, respectively. Dashed lines show the capacity of adjoining members according to design calculations.

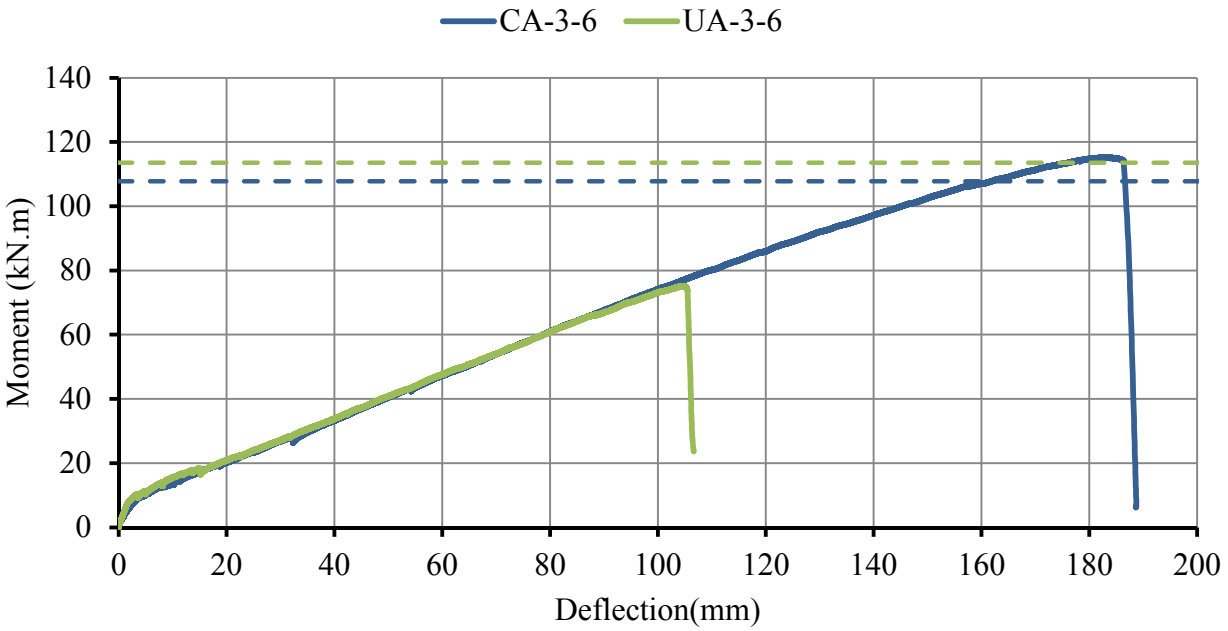

Figure 5.5: Moment-Deflection Response of Confined and Unconfined Specimens of Type A, three No. 6

The use of confinement stirrups shows a 150% increase in capacity of the specimen. This moment at failure exceeded design capacities of the two concrete strengths used. A 170% increase in peak deflection was also observed. These increases occurred despite the use of slightly weaker concrete. An interesting response is the unaffected stiffness of the specimen. The addition of the confinement stirrups allowed the joint to achieve full potential without premature failure.

As discussed previously, the failure of specimen UA-3-6 was due to the failure of the diagonal strut. Specimen CA-3-6 failed by crushing of concrete in the interior corner, followed by an explosive simultaneous bar rupture and failure of strut.

During the test duration, no diagonal cracks were observed along the diagonal in the confined specimen. However, the strut crack formation was observed after failure.

When reviewing the strain readings in strain gauges D1 and D2 (installed on the diagonal stirrups), sudden jumps in strain appear simultaneously in both strain gauges in two instances, as shown in Figure 5.6. It is believed that the first blip signifies the interior formation of the crack- which, due to the diagonal stirrups, did not emerge to the surface. The second blip may indicate the further widening of this crack. The stirrups being perpendicular to the cracks provide the most resistance relative to controlling the crack.

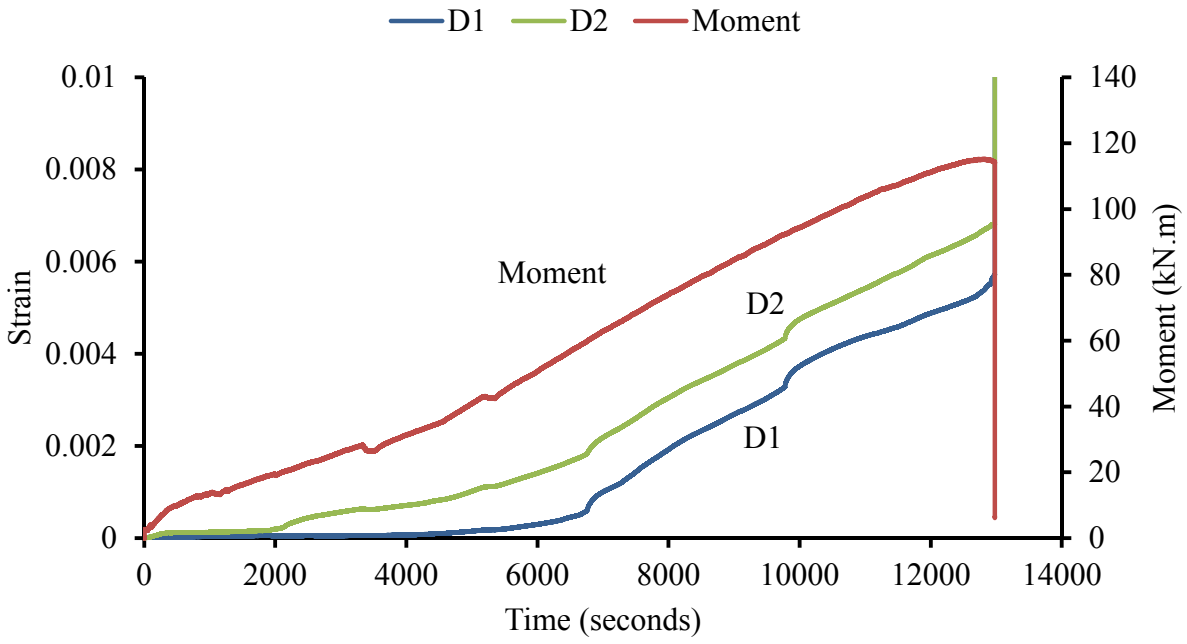

Figure 5.6: Strain Gauge Readings of D1 and D2 Relative to Moment, CA-3-6

Lateral ejection of concrete observed in specimens UA-3-6 and UA-4-6 was prevented with the addition of the diagonal stirrups. It appears that the bearing stresses from the bend caused

splitting of concrete in the plane of the bars. Combined with the failure of the strut, concrete splitting from the bars contributes to the explosive and sudden failure. The diagonal struts provided no improvement with regards to ejection of concrete on the top and back faces of the joint.

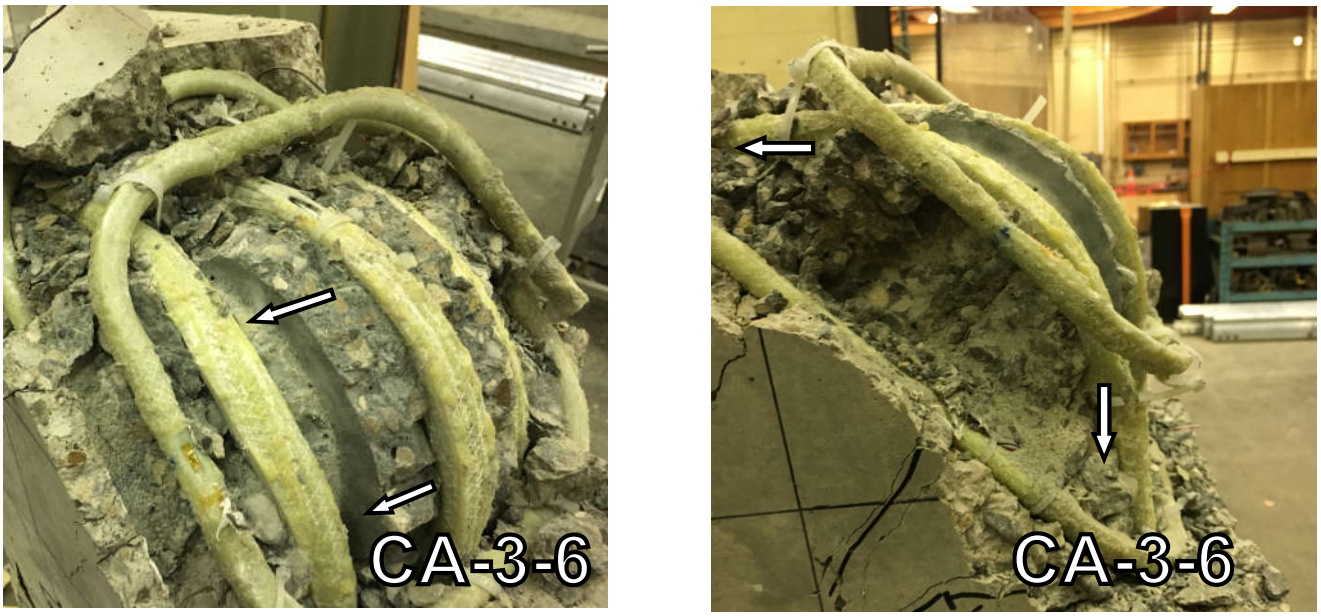

(a) (b)

Figure 5.7: (a) Lateral Movement and (b) Slip of Longitudinal Bar

The outside two bars in CA-3-6 appear to have slipped towards the adjoining members, shown in Figure 5.7. Similar behaviour was observed by Bai & Luo (1988), where relative slip occurred between the bars at the bend and surrounding concrete due to deformation of concrete under the bend. In the case of CA-3-6, this relative slip can be explained by the significant lateral dislocation of the bars caused by lateral resultant stresses in the joint. The perfectly smooth surfaces of the sides and underside of the bend may have contributed to the slip.

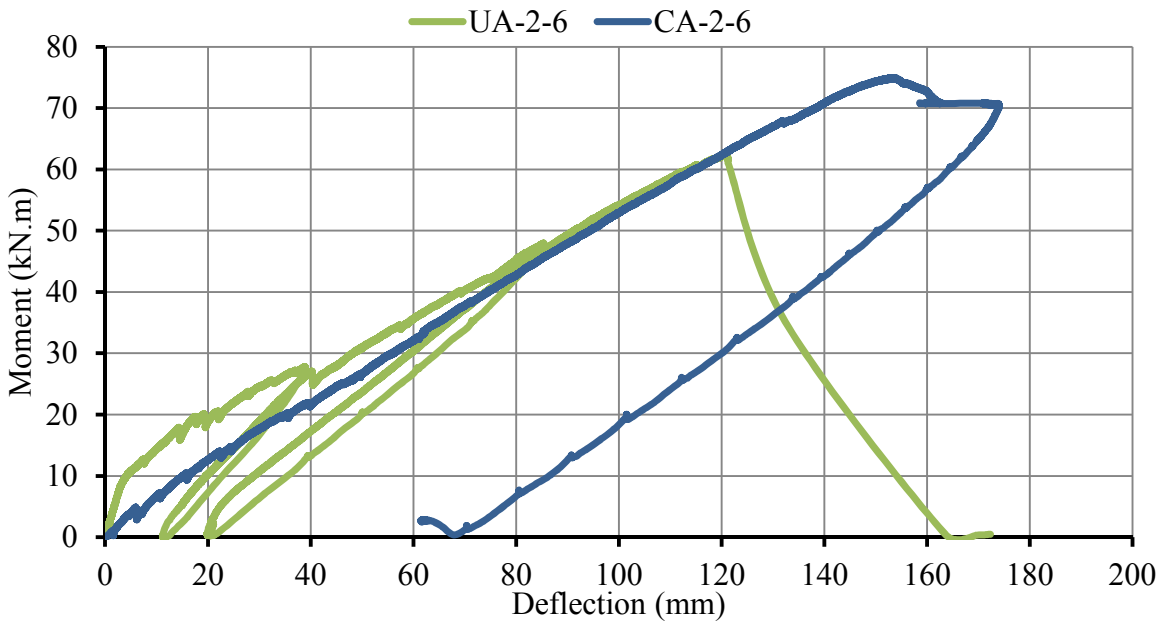

Figure 5.8: Moment-Deflection Response of Confined and Unconfined Specimens of Type A, Two No. 6

The effect of confinement was considered for the specimens reinforced with two No. 6 bars. CA-2-6 displayed a 26% increase in ultimate strength relative to UA-2-6, as shown in Figure 5.8. The stiffness of the unconfined is comparable to the unconfined specimen; however, the respective behaviour is different initially.

The addition of confinement stirrups had a significant effect on the ultimate strength. The concrete in the joint was contained and the diagonal crack widening was prevented. The specimen had potential for higher load capacity; however, this was not attained due to the anchorage failure. Due to the premature failure, the effect of confinement stirrups on the lower reinforcement specimen cannot be determined.

The effect of confinement was also considered for corners of geometry type B. It can be seen in Figure 5.9 that the specimen with confinement displayed a significant increase in capacity (40%) as well as a 100% increase in deflection. Similar to the specimens with geometry type A, member stiffness of UB-3-6 and CB-3-6 was almost identical.

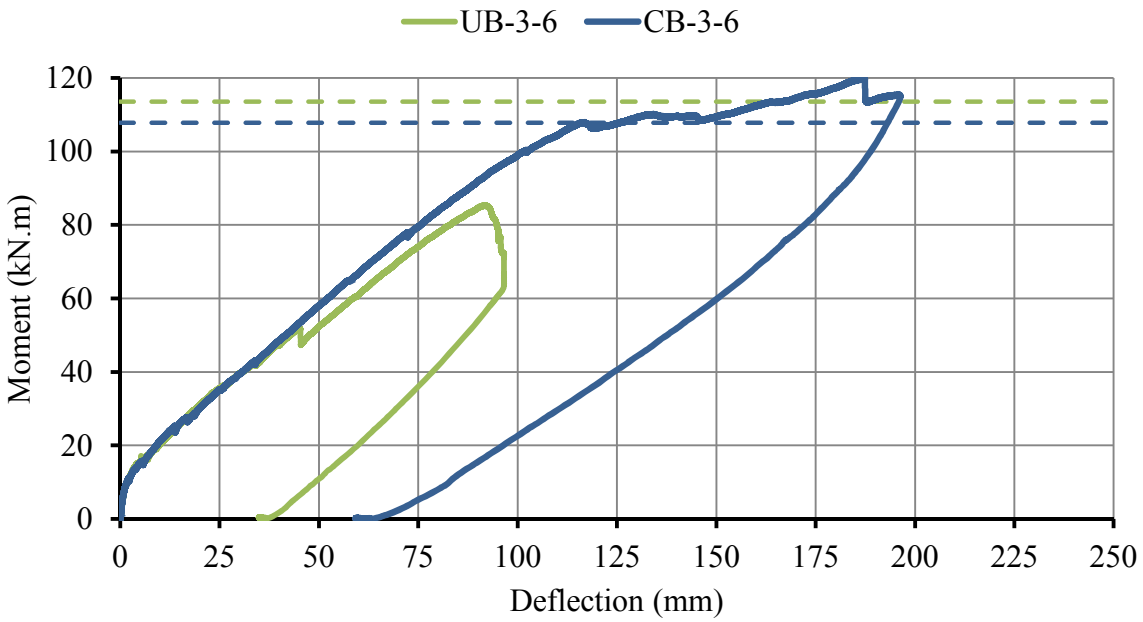

Figure 5.9: Moment-Deflection Response of Confined and Unconfined Specimens of Type B

One important observation in test CB-3-6 is the increase in deflection with little to no increase in load. Upon reaching the first peak, the loads increased by 11% and totaling 70 mm increase of deflection from that point. At some locations, the moment deflection curve appears to be completely flat.

The increase in crack widths within the joint in UB-3-6 prevented the specimen from reaching full capacity. After utilizing the confinement stirrups, cracks were intercepted and contained the surrounding concrete. It is thought that providing one or two extra diagonal stirrups will have a higher chance of intercepting more cracks, given the larger joint region, and will result in a further increase in capacity.

Comparing the strain readings of gauges D1 and D2 in CB-3-6 shows that the bars themselves were not engaged to the same extent as CA-3-6. Type B geometry does not experience the same risk of strut failure as type A. This suggests that while the stirrups helped maintain the integrity of the joint in type A, they do provide some confining benefits of the surrounding concrete.

The addition of confining stirrups controlled the formation of the diagonal crack, and prevented the premature failure of the strut. Lateral ejection was also improved due to the stirrups. This allowed the joint to reach full strength and resulted in larger displacements.

5.4 Effect of Geometry

The moment deflection response of specimens designed with geometry type A and B are shown in Figure 5.10. The reinforcement ratio and concrete strengths were kept constant in this group of tests.

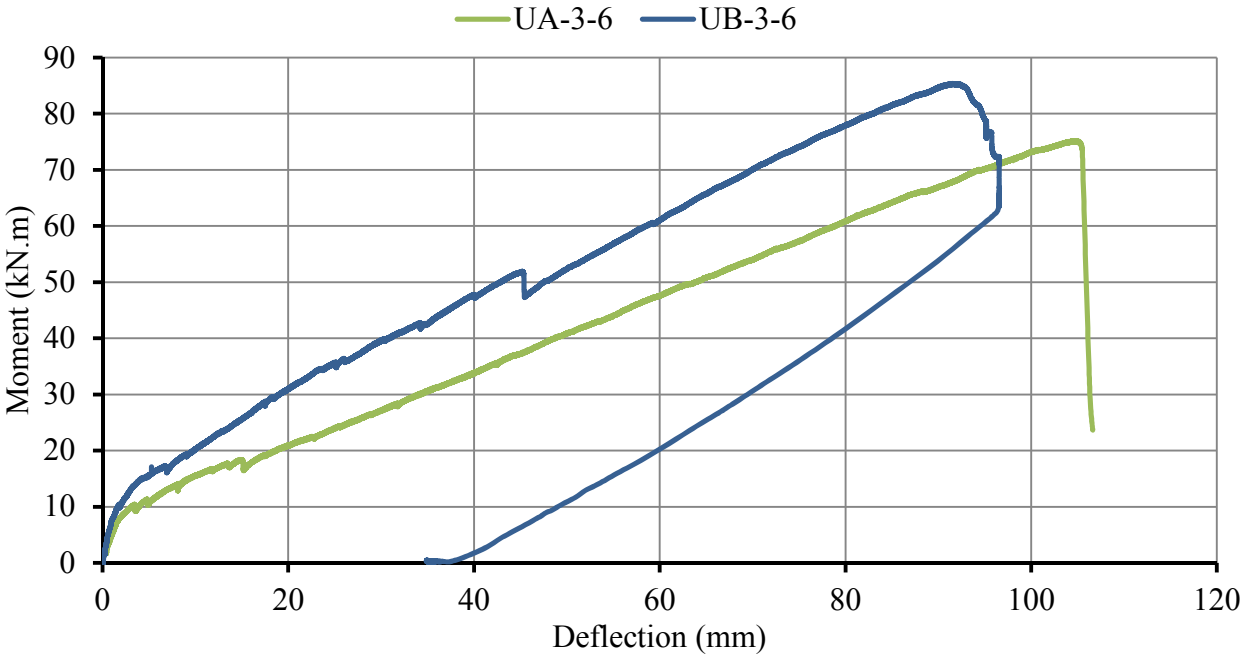

Figure 5.10: Moment-Deflection Response of Type A and B Specimens with No Confinement in the Joint

The capacity of the specimen with type B geometry was 13.5 % larger than the specimen with type A geometry. The former specimen displayed lower displacements at ultimate load: Specimen UB-3-6 failed with a peak deflection of 91 mm while UA-3-6 failed at 104 mm. An increase in stiffness can be seen in specimen UB-3-6, an understandable effect of the extra corner concrete.

As discussed previously, the failure of specimen UA-3-6 was due to the failure of the diagonal strut. Specimen UB-3-6 failed by crushing of concrete at the column/chamfer interface. This failure occurred gradually, starting off with early signs of crushing and progressing into debris falling off – which is unlike the sudden failure of geometry type A. This test was stopped after loads were found to drop and only experienced a plastic deformation of 37 mm after unloading. A simple strut-and-tie model can be created for this joint. It can be seen that two diagonal struts transfer the loads from the bend to the compression region. As a result, the stresses carried in each strut are greatly reduced, and the risk of strut failure is lowered. Despite that, capacity of this specimen was low considering the large crack widths that developed.

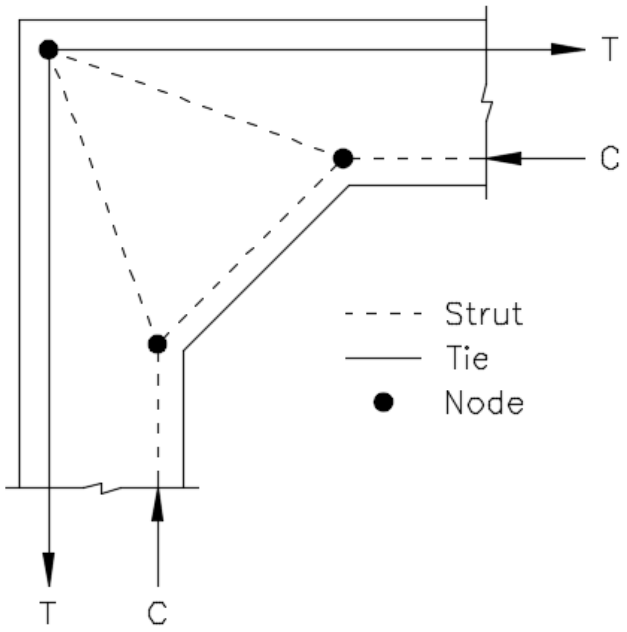

Figure 5.11: Strut-and-Tie Model for Type B Geometry

The effect of geometry type was also considered for the confined corners. Specimen with type B geometry displays a higher overall stiffness than type A. Specimen CB-3-6 showed a slight

decrease in capacity relative to CA-3-6; however, it displayed some significant “pseudo-ductility”.

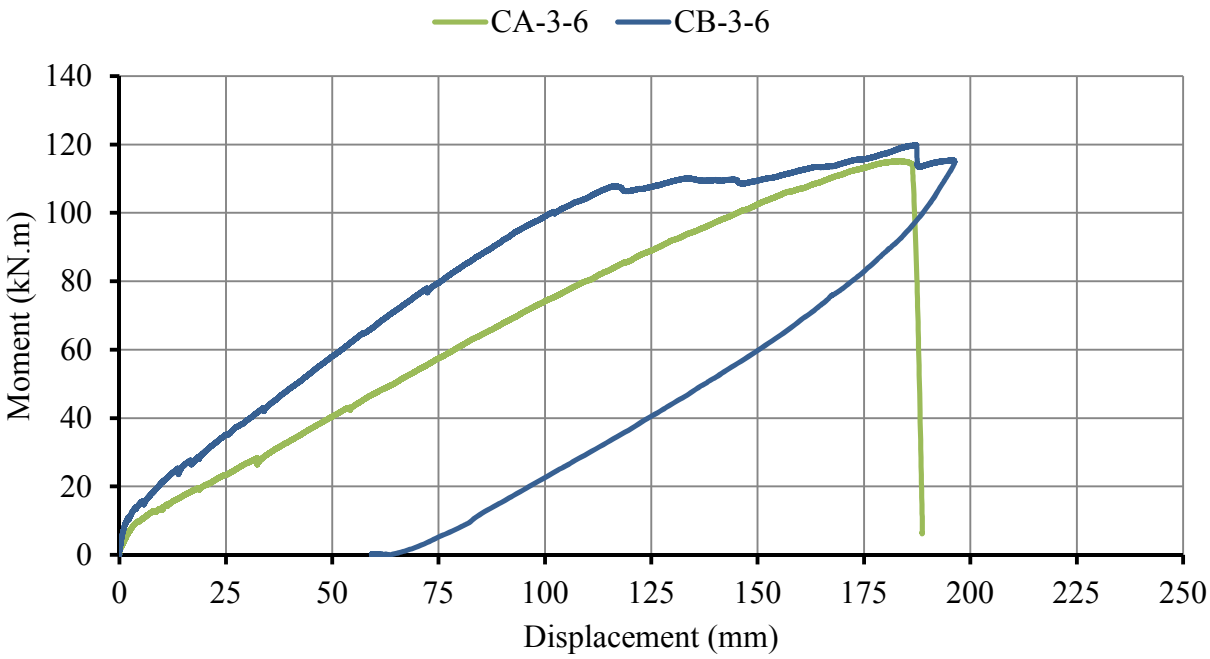

Figure 5.12: Moment-Deflection Response of Type A and B Specimens with Confinement in the Joint

The effect of changing joint geometry was also considered for confined joints. This response is shown in Figure 5.12. Specimen CB-3-6 shows larger stiffness relative to CA-3-6. Specimen CB-3-6 shows increased strength efficiency as well as the nonexplosive failure combined with the apparent pseudo-ductility, making it an overall superior specimen.

5.5 Strains in Reinforcement

A summary of strain gauges installed on the tensile longitudinal bars is presented in Table 5.4. Two rupture strains are calculated based on the straight and bend tensile strengths as well as the modulus of elasticity. The specimens experiencing bar rupture are indicated with an "^{R}" superscript.

Table 5.4: Summary of Longitudinal Strain Gauge Readings

Specimen	Strain Gauge					Rupture Strain	
	B1	1	2	3	4	Straight	Bend
UA-2-4^{R}	0.009579	0.012927	0.020036*	0.013916	0.011675	0.024030	0.012173
UA-2-6^{R}	0.006878	0.104212ǂ	0.018965**	0.010760	0.010114		
UA-3-6	0.006168	0.008008	0.016948	0.008022	0.009068		
UA-4-6	0.006827	0.008096	0.015566	0.008671	0.009375		
UB -3-6	0.005584	0.004982	0.006963	0.009796	0.009241		
CA-2-6	0.010309	0.012354	-	0.012823	0.012918		
CA-3-6^{R}	0.104050ǂ	0.012279	0.022608	0.01446	0.104316ǂ		
CB-3-6	0.007816	0.008325	0.007716	0.013001	0.015840		

^{R} Specimens experiencing bar rupture
* Maximum strain before strain gauge failed, at 85% of max load
** Maximum strain before strain gauge failed, at 97% of max load
ǂ Failed strain gauge

Only the readings from strain gauge 2, which are installed on the bent portion, are compared with the bend rupture strain. It can be seen that gauge 2 readings always exceeded the calculated bend rupture strain for type A specimens. The least strain at which rupture was observed was in UA-2-6 at 0.018965, approximately 56% larger than the calculated. The material behaves stronger than is predicted by test methods. It also indicates that the actual bend strength in this type of joint is between the tested bend and straight tensile strengths. While the CAN/CSA S806 Annex D test results are conservative, they do not accurately represent the stresses in the tested specimens' reinforcement bars .

Chapter 6
Conclusions and Recommendations

6.1 Conclusions

The goal of the experimental program was to investigate the behaviour of GFRP reinforced knee joints under closing moments. There is a lack of reported research in literature regarding knee-joints reinforced with FRPs.

The experimental program consisted of eight full-scale knee-joint specimens. The test variables considered were: the reinforcement ratio by varying the amount of reinforcement, the addition of confinement stirrups in the joint, and the corner geometry type (type A, 90^o, versus type B, interior chamfer). The tests were conducted by applying a monotonic load at the free end of the beam while fixing the column base. Analysis of the test results was conducted based on the modes of failure, crack patterns, strain readings, and moment-deflection curves. From the experimental work discussed in this thesis, the following conclusions can be drawn:

1. **The ultimate strength of the joints was increased as influenced by:**

   - Reinforcement ratio

   - Confinement in the joint

   a) Increasing the reinforcement ratio saw an overall increase in strength as well as strength efficiencies.
   b) Introducing confinement stirrups in the joint allowed the joint to achieve its full potential. The strength efficiency was 107% for type A joint (90^o corner) and 98% for type B joint (interior chamfer).

2. **The use of interior chamfer joint geometry slightly improved the strength of the joint. However, the use of type B geometry prevented the brittle failure exhibited by type A specimens for unconfined and confined cases. The extra material in the interior corner**

provided additional resistance and prevented explosive failure seein in UA-3-6. Although wide cracks were present in the joint region, crushing occurred at the chamfer/column interface.

3. **The reinforcement ratio directly influenced the failure type**

   a) When stresses in the bar exceeded the strength of the bend, failure occurred by rupture of bar at the bend, with no formation of cracks within the diagonal strut.
   b) When stresses in the bar were not exceeded, failure occurred by failure of the diagonal strut and was marked by formation of diagonal cracks in the tensile region of the joint.

4. **Rupture of the bar at the bent portion occurred at a higher stress than the strength reported by the manufacturer. The ultimate strain at the reinforcement bend was at least 161% larger than the strain based manufacturer tests.**

5. **Failure mode was not dictated by the reinforcement ratio of adjoining members. Specimen UA-2-4 failed by bar rupture at the bend despite being designed as over-reinforced. This occurred due to the inherent weakness of the reinforcement bent portion.**

6. **Pseudo-ductility was observed in the confined joint of type B geometry (CB-3-6). At 88% of peak load, there was a marginal increase in load with relatively large displacements. This was not observed in any other specimen (Type A or B).**

6.2 Recommendations for Future Work

To gain a better understanding of knee joints reinforced with GFRP, further investigation is required. The following recommendations for future work:

1. Further investigation regarding the effect of confinement must be conducted. Different confinement techniques ought to be studied, including the typical reinforcement grid as per ACI 352R.

2. Further investigation into other variables should be conducted. This includes studying the effect of the radius of bend, the compressive strength of concrete, and different FRP types including CFRP and GFRP from other suppliers and/or coating types.

3. Different loading configurations should be studied including opening moments and joints subjected to load reversals.

4. An investigation into size effect ought to be conducted since the use of this type of joint is not limited to the size investigated in this experimental program.

References

ACI Committee 440. (2015). Guide for the Design and Construction of Structural Concrete Reinforced with FRP Bars. *ACI 440.1R-15*. Detroit, Michigan: American Concrete Institute.

Ahmed, E. A., El-Sayed, A. K., El-Salakawy, E., & Benmokrane, B. (2010). Bend Strength of FRP Stirrups: Comparison and Evaluation of Testing Methods. *Journal of Composites for Construction, 14*(1), 3-10.

Bai, J. (2013). *Advanced Fibre-Reinforced Polymer Composites for Structural Applications.* Woodhead Publishing.

Bakis, C., Bank, L., Brown, V., Cosenza, E., Davalos, J., Lesko, J., . . . Triantafillou, T. (2002). Fiber-Reinforced Polymer Composites for Construction—State-of-the-Art Review. *Journal of Composites for Construction, 6*(2), 73-87.

Bank, L. C. (2006). *Composites for construction: Structural design with FRP materials.* Hoboken, NJ, USA: John Wiley & Sons.

Benmokrane, B., Chaallal, O., & Masmoudi, R. (1995). Glass Fibre Reinforced Plastic (GFRP) Rebars for Concrete Structures. *Construction and Building Materials, 9*(6), 353-364.

Benmokrane, B., El-Salakawy, E., El-Gamal, S., & Goulet, S. (2007). Construction and Testing of an Innovative Concrete Bridge Deck Totally Reinforced with Glass FRP Bars: Val-Alain Bridge on Highway 20 East. *Journal of Bridge Engineering, 12*(5), 632-645.

Canadian Standards Association. (2004). Design of Concrete Structures. *CAN/CSA A23.3-04*. Mississauga, Ontario, Canada: CSA Group.

Canadian Standards Association. (2012). Design and Construction of Building Components with Fibre Reinforced Polymers. *CAN/CSA S806-12*. Mississauga, Ontario, Canada: CSA Group.

Canadian Standards Association. (2014). Canadian Highway Bridge Design Code (CHBDC). *CAN/CSA S6-14*. Mississauga, Ontario, Canada: CSA Group.

Ehsani, M. R., Saadatmanesh, H., & Tao, S. (1995). Bond of Hooked GFRP Rebars to Concrete. *ACI Materials Journal, 92*(4), 391-400.

Hull, D., & Clyne, T. (1996). *An Introduction to Composite Materials* . Cambridge University Press.

ISIS Canada. (2007). Design Manual No. 3. *Reinforcing Concrete Structures with Fibre Reinforced Polymers*. Winnipeg, Manitoba, Canada: ISIS Canada, Intelligent Sensing for Innovative Structures.

ISIS Educational Committee. (2003). *ISIS Educational Module 2: An Introduction to FRP Composites for Construction*. Winnipeg, Manitoba, Canada: ISIS Canada, Intelligent Sensing for Innovative Structures.

ISIS Educational Committee. (2006). *ISIS Educational Module 8: Durability of FRP Composites for Construction*. Winnipeg, Manitoba, Canada: ISIS Canada, Intelligent Sensing for Innovative Structures.

Johansson, M. (2001). Reinforcement Detailing in Concrete Frame Corners. *ACI Structural Journal, 98*(1), 105-115.

Joint ACI-ASCE Committee 352. (2002). Recommendations for Design of Beam-Column Connections in Monolithic Reinforced Concrete Structures (Reapproved 2010). *ACI 352R-02 (Reapp 2010)*, 38. American Concrete Institute.

Joint Committee on the Detailing of Reinforced Concrete. (1970). Standard Method of Detailing Reinforced Concrete. *(2)*. London: The Concrete Society in conjunction with the Institution of Structural Engineers.

Keller, T. (2003). Use of Fibre Reinforced Polymers in Bridge Construction. *Structural Engineering Documents, 7*. Zurich: International Association for Bridge and Structural Engineering.

Kemp, E., & Mukherjee, P. (1968, October). Inelastic Behaviour of Concrete Knee Joints. *The Consulting Engineer*, 44-48.

Luo, Y. H., & Bai, S. (1988). Concrete Frame Corners. *Pacific Concrete Conference*, *3*, pp. 157-168. Auckland, New Zealand.

Luo, Y. H., Durrani, A. J., Bai, S., & Yuan, J. (1994). Study of Reinforcing Detail of Tension Bars in Frame Corner Connections. *ACI Structural Journal, 91*(4), 486-496.

Maruyama, T., Honma, M., & Okamur, H. (1993). Experimental Study on Tensile Strength of Bent Portion of FRP Rods. *Fibre-Reinforced-Plastic Reinforcement for Concrete Structures: International Symposium. 138*, pp. 163-176. Vancouver: American Concrete Institute.

Mayfield, B., Kong, F.-k., Bennison, A., & Davies, J. C. (1971). Corner Joint Details in Structural Lightweight Concrete. *ACI Journal, 68*(5), 366-372.

Micelli, F., & Nanni, A. (2004). Durability of FRP Rods for Concrete Structures. *Construction and Building Materials, 18*(7), 491-503.

Nilsson, I. H. (1973). *Reinforced Concrete Corners and Joints Subjected to Bending Moment.* Stockholm: National Swedish Institute for Building Research.

Park, R., & Paulay, T. (1975). *Reinforced Concrete Structures.* New York: John Wiley & Sons.

Stroband, J., & Kolpa, J. (1983). The Behavior of Reinforced Concrete Column-to-Beam joints, Part 1: Corners Subjected to Negative Moments. *Report 5-83-9*, 105 pp. Delft, The Netherlands: Delft University of Technology.

Strongwell. (2017). *The Pultrusion Process*. Retrieved May 7, 2017, from Strongwell Website: http://www.strongwell.com/about/the-pultrusion-process

Swann, R. (1969). Flexural Strength of Corners of Reinforced Concrete Portal Frames. *Technical Report TRA/434*. London: Cement and Concrete Association.

Zouzou, A., & Haldane, D. (1993). Detailing Reinforced Concrete Closing Corner Joints for Ductility. *Proceedings of the Institution of Civil Engineers - Structures and Buildings, 99*(1), 43-48.

Appendix A
Specimen Information

A.1 UA-2-6

This was the first specimen tested. It was loaded at a rate of 0.010 mm/second until a load of 25 kN, and then increased to 0.017 mm/second. The failure of this specimen occurred by bar rupture at a peak load of 45 kN, peak bending moment of 62.1 kN.m, and displacement at peak of 120.67 mm.

Table A.1: Properties of Specimen UA-2-6

Adjoining Member Properties	
f'_c	55
$b\ (mm)$	270
$h\ (mm)$	300
$L_{beam}\ (mm)$	1700
$L_{column}\ (mm)$	1000
$d\ (mm)$	246
a_o/d	5.98
ρ_b	0.324 %
ρ	0.858 %
$M_r\ (kN.m)$	98.8
Reinforcement Bar Properties	
$f_{frp,straight}\ (MPa)$	1293
$f_{frp,bent}\ (MPa)$	655
$E\ (MPa)$	53808
$A\ (mm^2)$	570

Table A.2: Strain Gauge Readings, UA-2-6

% of Peak	1	2	3	4	B1	B2	Conc
10	0.000154	0.000025	0.000051	0.000356	0.000227	-0.000018	-0.000076
20	0.000516	0.000042	0.000687	0.000953	0.000668	-0.000034	-0.000187
30	0.001189	0.000070	0.001730	0.002084	0.001378	-0.000033	-0.000288
40	0.003284	0.001647	0.004111	0.003374	0.002376	0.000131	-0.000603
50	0.003911	0.007772	0.005065	0.004276	0.002921	0.000212	-0.000735
60	0.004710	0.009810	0.006114	0.005264	0.003642	0.000300	-0.000881
70	0.005572	0.011950	0.007362	0.006454	0.004448	0.000425	-0.001066
80	0.104212	0.014818	0.008521	0.007544	0.005333	0.000583	-0.001292
90	0.104212	0.017394	0.009625	0.008655	0.006102	0.000714	-0.001502
100	0.104212	0.104216	0.010760	0.010114	0.006878	0.000898	-0.001739

*Strain readings registering ~0.104000 denote failed strain gauge readings

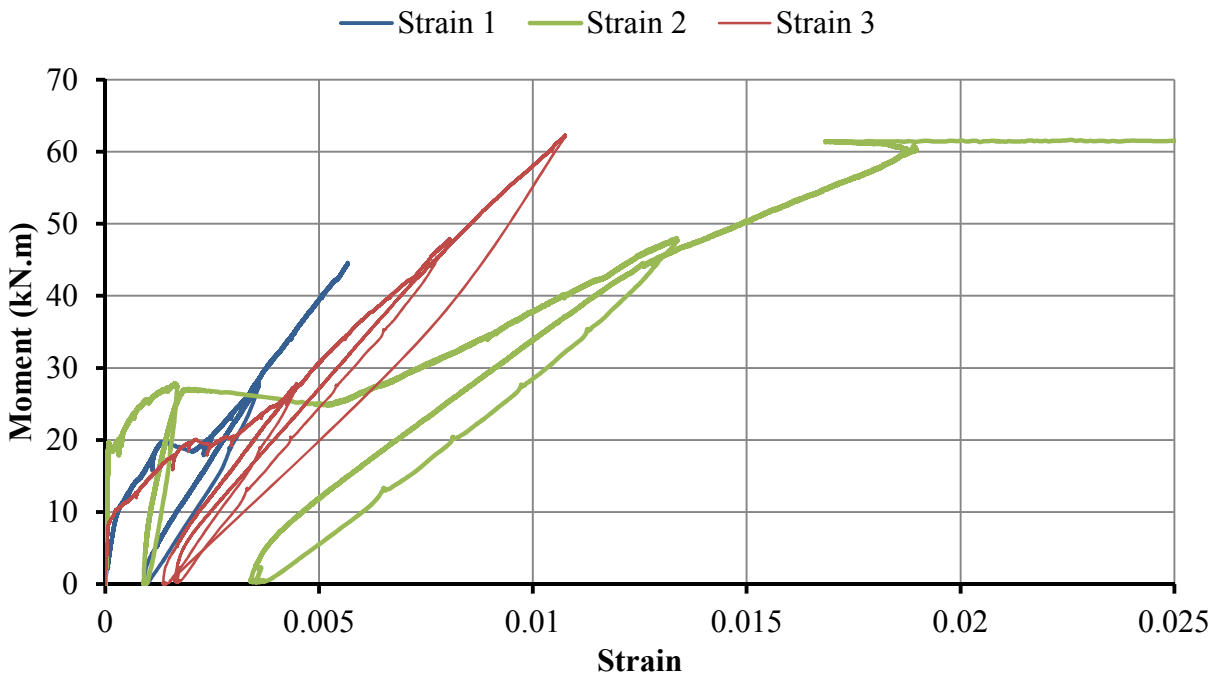

Figure A.1: Moment versus Strain Reading of Gauges 1, 2, and 3, UA-2-6

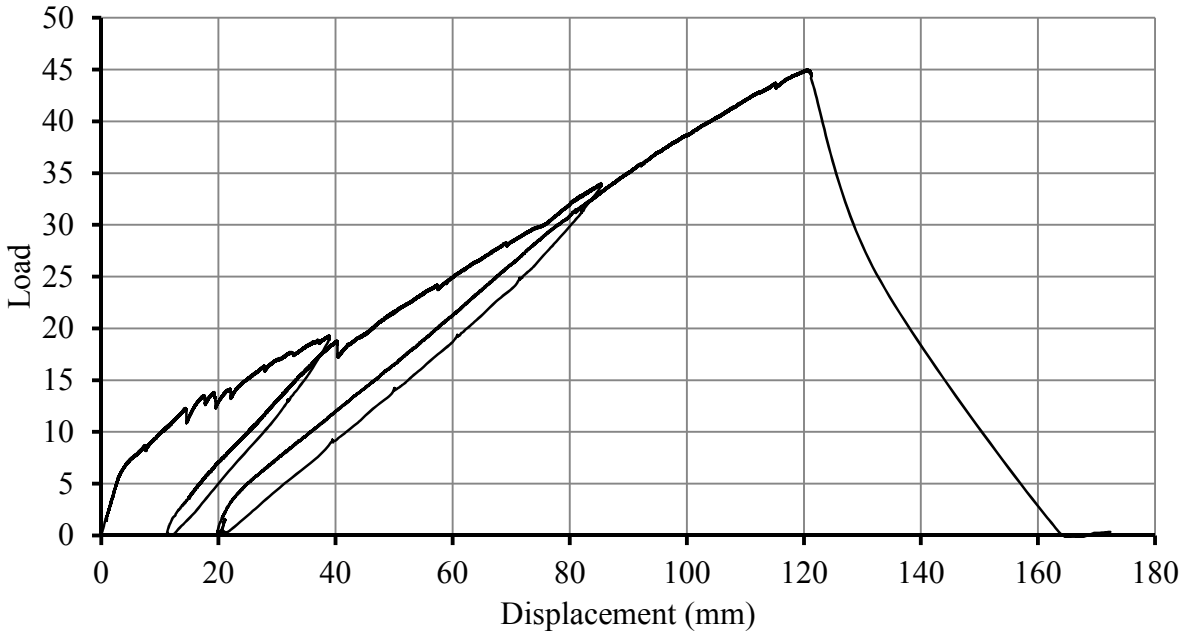

Figure A.2: Load-Deflection Response, UA-2-6

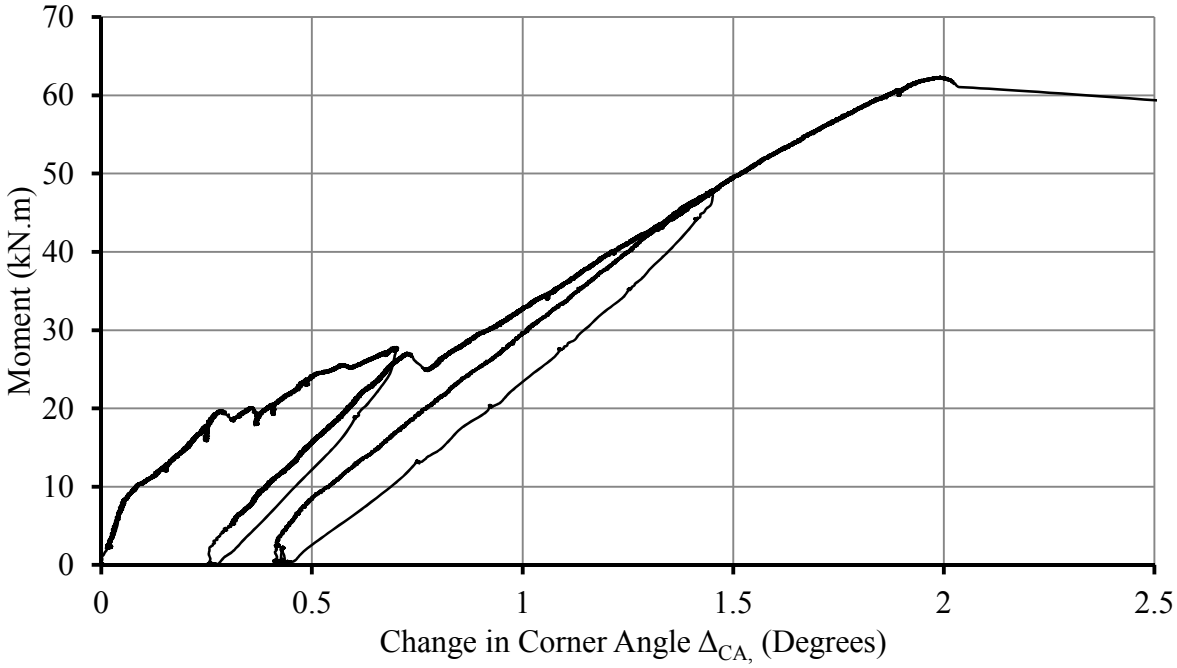

Figure A.3: Moment versus Change in Corner Angle, UA-2-6

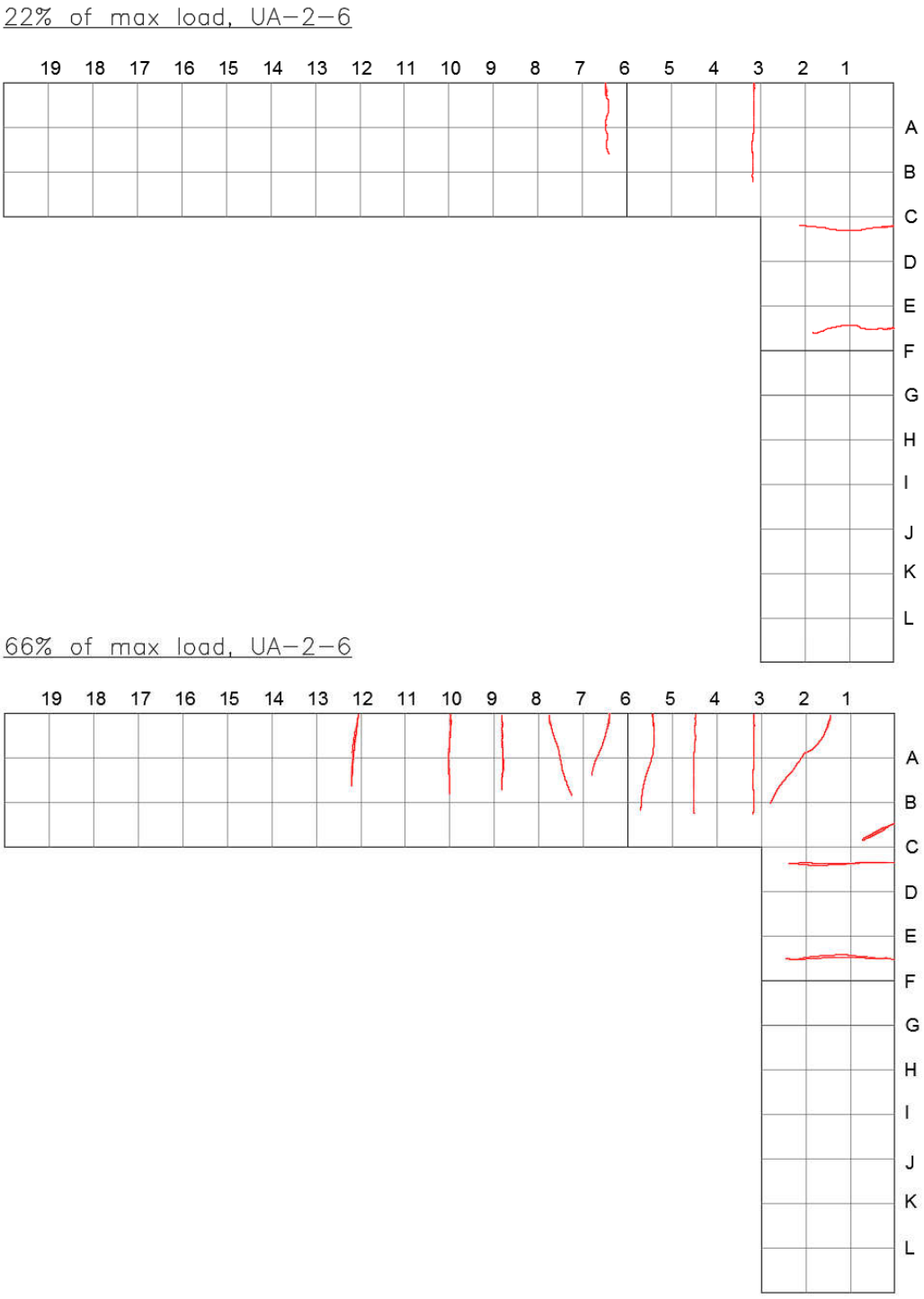

Figure A.4: Crack Progression, Diagram 1, UA-2-6

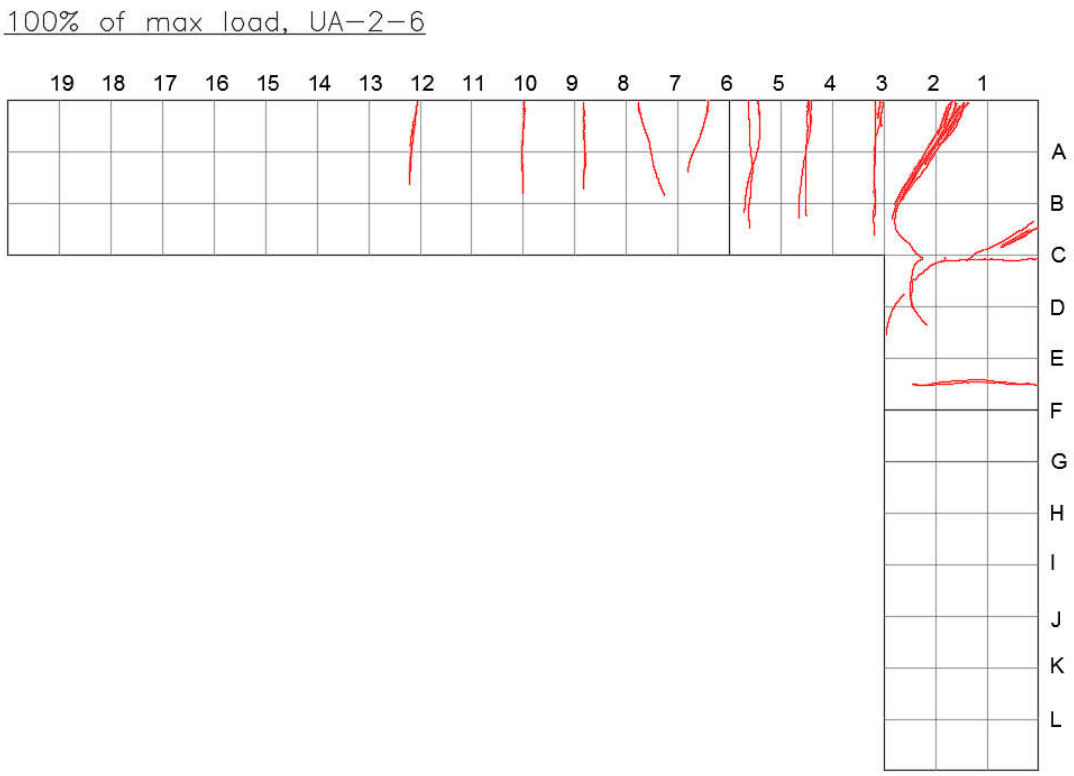

Figure A.5: Crack Progression, Diagram 2, UA-2-6

Figure A.6: Closeup Shots of the Failed Specimen, UA-2-6

A.2 UA-4-6

This was the second specimen tested. It was loaded at a rate of 0.010 mm/second until a load of 25 kN, and then increased to 0.017 mm/second. The failure of this specimen occurred by diagonal strut failure at a peak load of 70.9 kN, peak bending moment of 98.6 kN.m, and displacement at peak of 119.7 mm.

Table A.3: Properties of Specimen UA-4-6

Adjoining Member Properties	
f'_c	55
$b\ (mm)$	270
$h\ (mm)$	300
$L_{beam}\ (mm)$	1700
$L_{column}\ (mm)$	1000
$d\ (mm)$	246
a_o/d	5.98
ρ_b	0.324 %
ρ	1.716
$M_r\ (kN.m)$	129.9
Reinforcement Bar Properties	
$f_{frp,straight}\ (MPa)$	1293
$f_{frp,bent}\ (MPa)$	655
$E\ (MPa)$	53808
$A\ (mm^2)$	1140

Table A.4: Strain Gauge Readings, UA-4-6

% of Peak	1	2	3	4	B1	B2
10	0.0003610	0.0003460	0.0003810	0.0000940	0.0002050	-0.0000380
20	0.0012150	0.0011110	0.0009870	0.0010320	0.0008390	-0.0000520
30	0.0019580	0.0025740	0.0022310	0.0021950	0.0015110	-0.0000380
40	0.0028960	0.0040420	0.0030590	0.0031650	0.0022870	0.0000270
50	0.0038010	0.0057310	0.0039770	0.0041860	0.0030910	0.0001810
60	0.0046730	0.0074340	0.0048580	0.0052110	0.0038640	0.0003010
70	0.0054960	0.0092060	0.0057460	0.0062260	0.0045910	0.0003970
80	0.0063300	0.0111460	0.0066600	0.0072970	0.0052610	0.0005660
90	0.0072020	0.0131010	0.0076260	0.0083610	0.0060180	0.0007730
100	0.0080960	0.0155660	0.0086710	0.0093750	0.0068270	0.0009190

% of Peak	Conc	S1
10	-0.0001090	0.0000020
20	-0.0003710	0.0000400
30	-0.0005580	0.0000360
40	-0.0007970	0.0000290
50	-0.0010460	0.0000290
60	-0.0012530	0.0000410
70	-0.0014450	0.0000510
80	-0.0016560	0.0000520
90	-0.0019170	0.0000540
100	-0.0021400	0.0000540

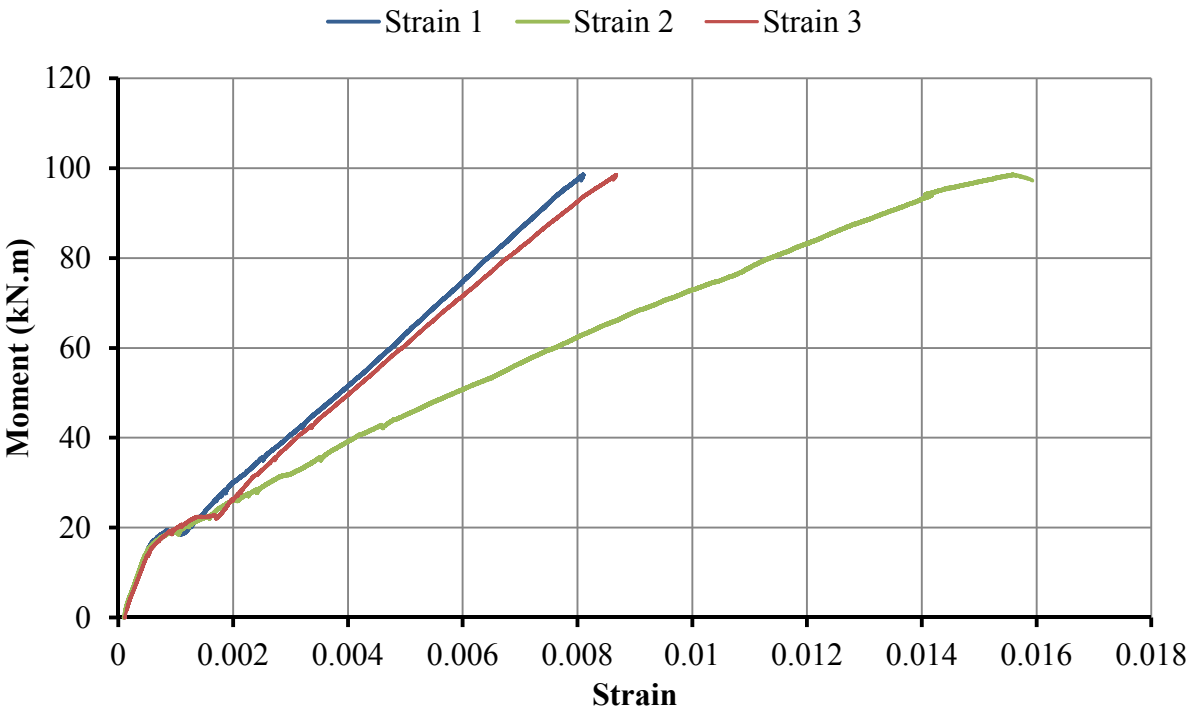

Figure A.7: Moment versus Strain Reading of Gauges 1, 2, and 3, UA-4-6

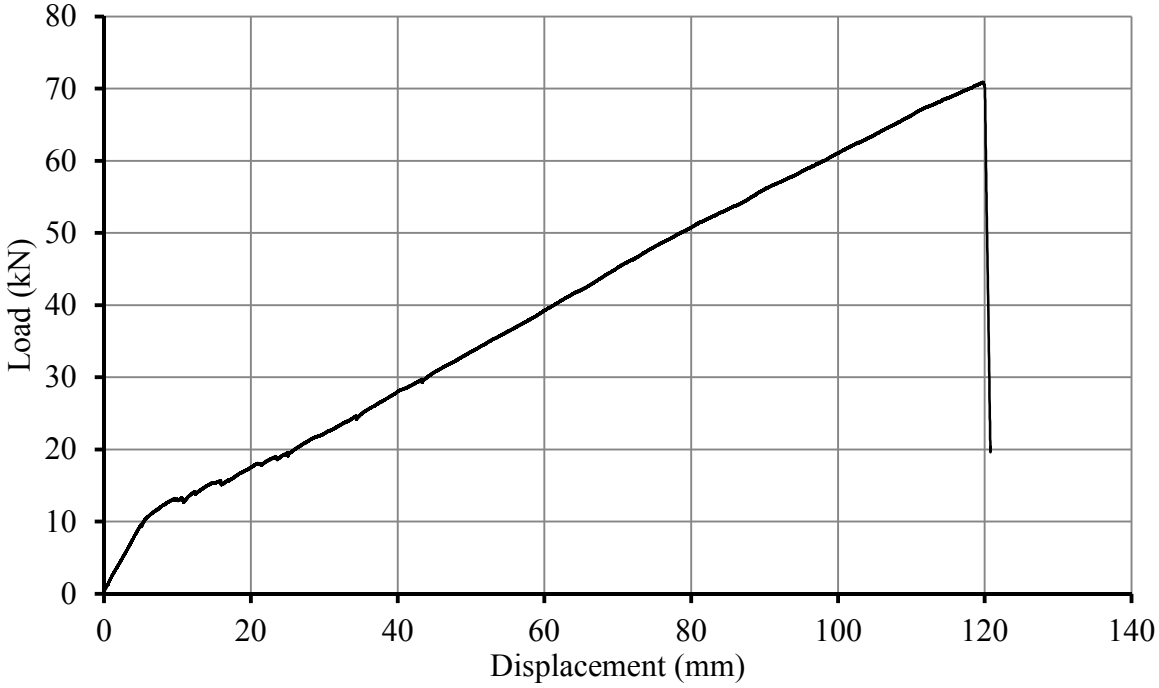

Figure A.8: Load-Deflection Response, UA-4-6

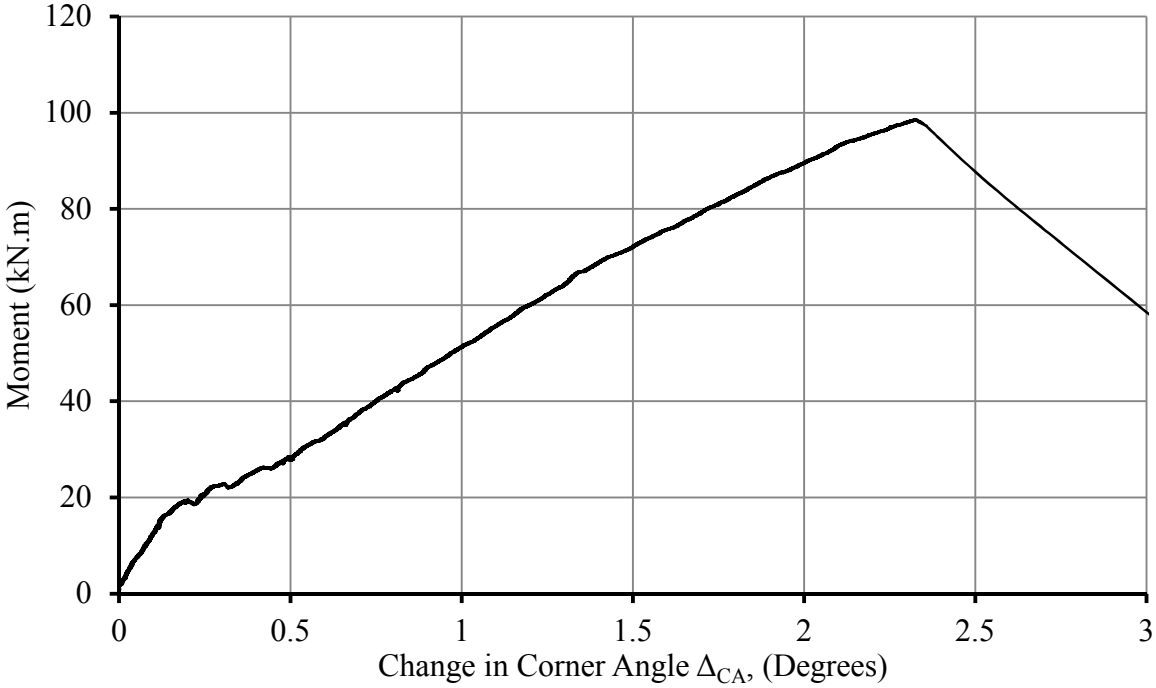

Figure A.9: Moment versus Change in Corner Angle, UA-4-6

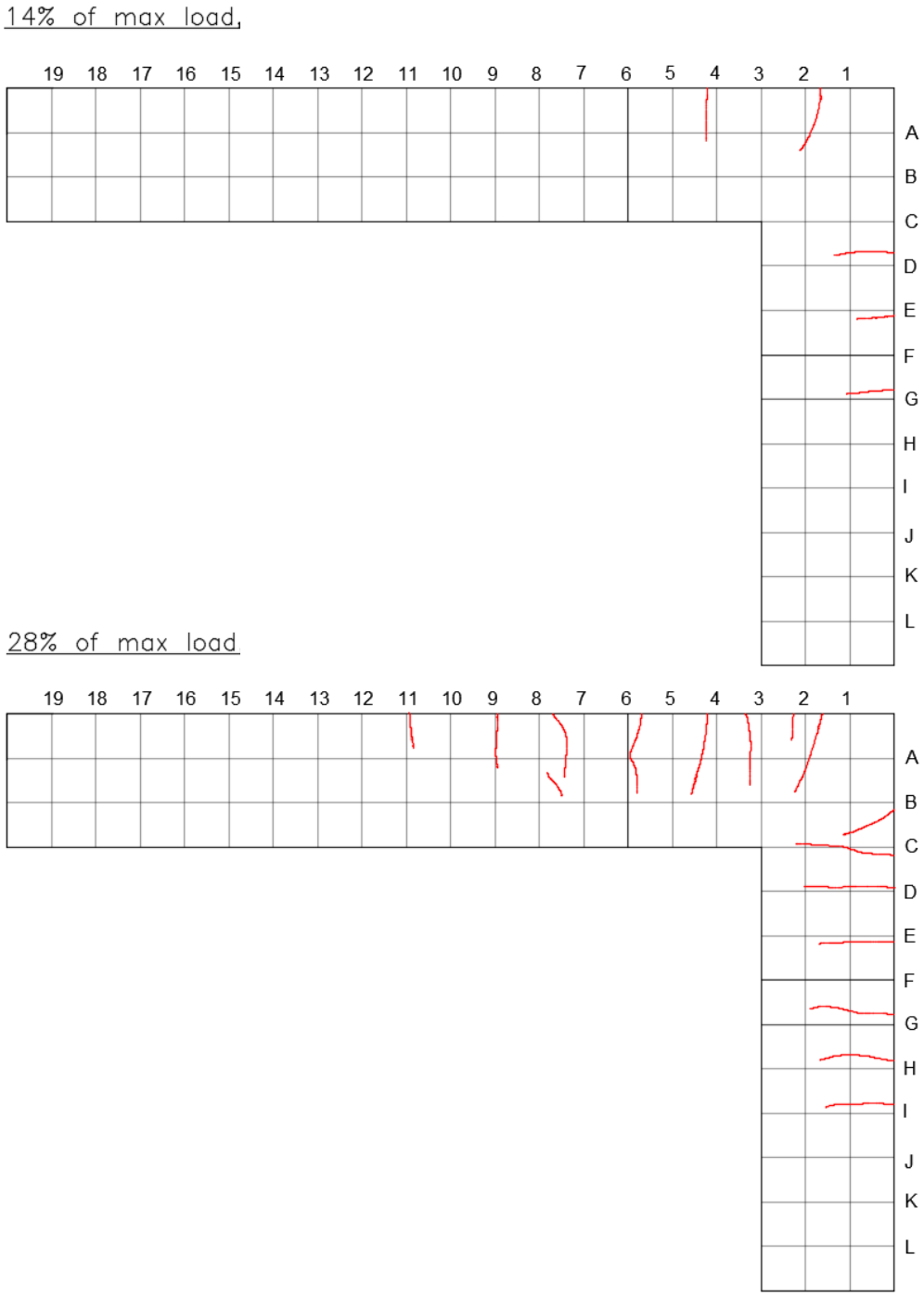

Figure A.10: Crack Progression Diagram 1, UA-4-6

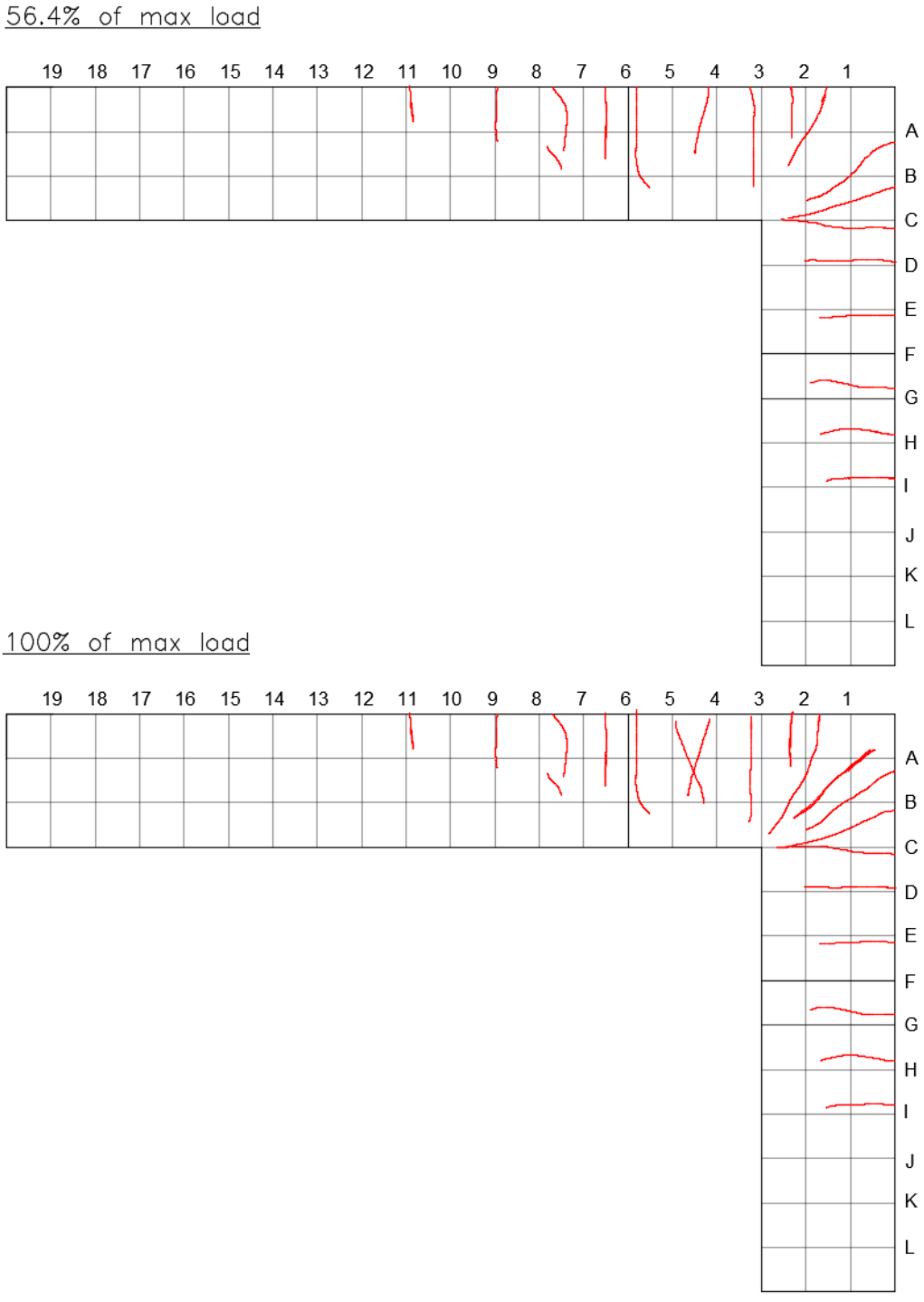

Figure A.11: Crack Progression Diagram 2, UA-4-6

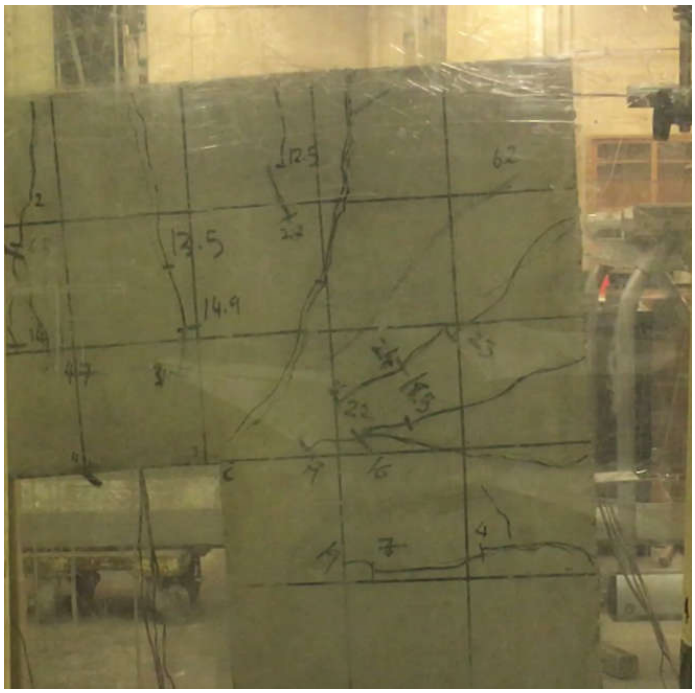

Figure A.12: UA-4-6 Moments Before Failure

Figure A.13: Back Side of Failed Joint, UA-4-6

Figure A.14: Crack in Bent Portion with Waving Also Visible, UA-4-6

A.3 UA-3-6

This was the third specimen tested. It was loaded at a rate of 0.010 mm/second until a load of 25 kN, and then increased to 0.017 mm/second. The failure of this specimen occurred by diagonal strut failure at a peak load of 53.7 kN, peak bending moment of 75.2 kN.m, and displacement at peak of 119.7 mm.

Table A.5: Properties of Specimen UA-3-6

Adjoining Member Properties	
f'_c	55
$b\ (mm)$	270
$h\ (mm)$	300
$L_{beam}\ (mm)$	1700
$L_{column}\ (mm)$	1000
$d\ (mm)$	246
a_o/d	5.98
ρ_b	0.324 %
ρ	1.287 %
$M_r\ (kN.m)$	116.3
Reinforcement Bar Properties	
$f_{frp,straight}\ (MPa)$	1293
$f_{frp,bent}\ (MPa)$	655
$E\ (MPa)$	53808
$A\ (mm^2)$	855

Table A.6: Strain Gauge Readings, UA-3-6

% of Peak	1	2	3	4	B1	B2
10	0.000164	0.000539	0.000057	0.000093	0.000073	-0.000033
20	0.001096	0.001412	0.000770	0.000913	0.000567	-0.000061
30	0.002267	0.002461	0.002009	0.002143	0.001482	0.000029
40	0.003212	0.004029	0.002836	0.003091	0.002176	0.000145
50	0.003992	0.006228	0.003722	0.004036	0.002842	0.000291
60	0.004791	0.008022	0.004591	0.004949	0.003535	0.000468
70	0.005591	0.010084	0.005427	0.005961	0.004241	0.000651
80	0.006392	0.012024	0.006262	0.007016	0.004945	0.000818
90	0.007168	0.013922	0.007121	0.008079	0.005577	0.001018
100	0.008008	0.016948	0.008022	0.009068	0.006168	0.001267

% of Peak	Conc	S1	S2
10	-0.000030	-0.000007	0.000032
20	-0.000227	0.000077	0.000077
30	-0.000509	0.000097	0.000454
40	-0.000689	0.000114	0.000588
50	-0.000876	0.000106	0.000816
60	-0.001077	0.000107	0.001083
70	-0.001278	0.000111	0.001336
80	-0.001461	0.000151	0.001547
90	-0.001660	0.000203	0.001680
100	-0.001866	0.000316	0.001692

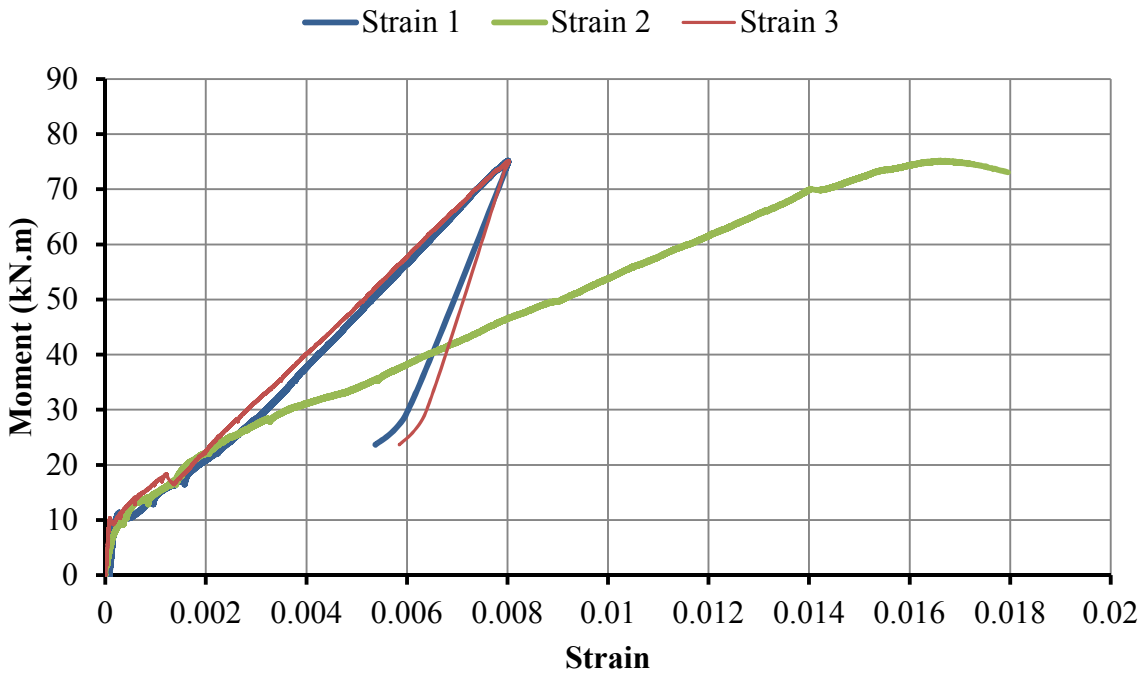

Figure A.15: Moment versus Strain Reading of Gauges 1, 2, and 3, UA-3-6

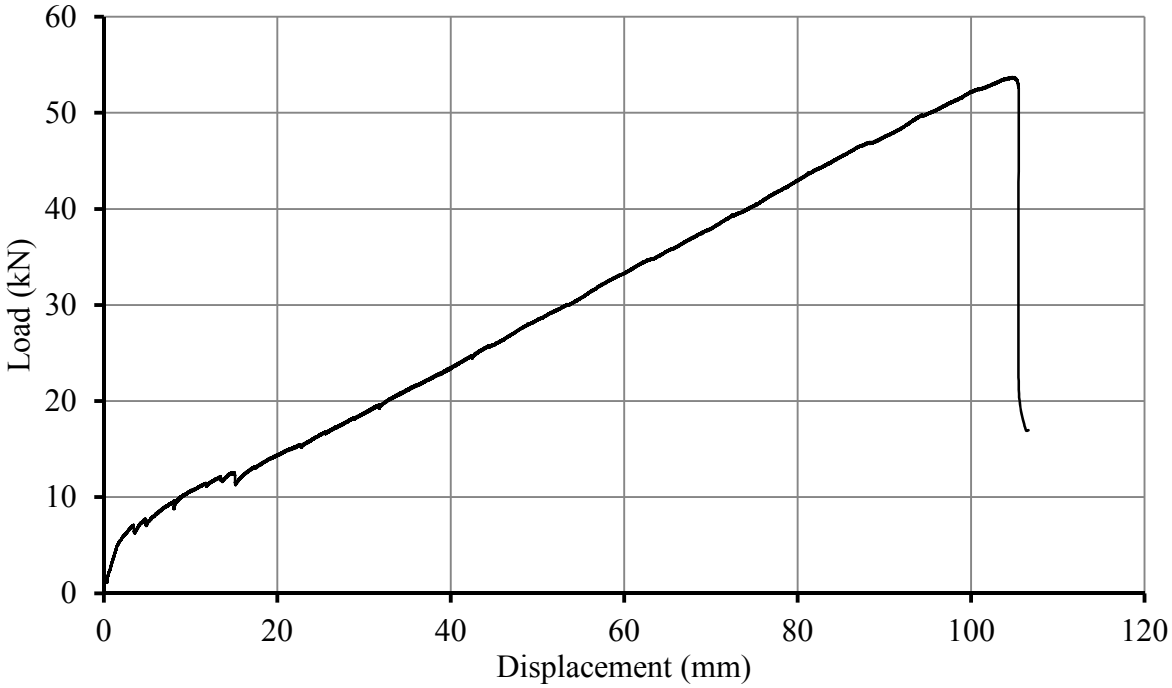

Figure A.16: Load-Deflection Response of UA-3-6

Figure A.17: Moment versus Change in Corner Angle, UA-3-6

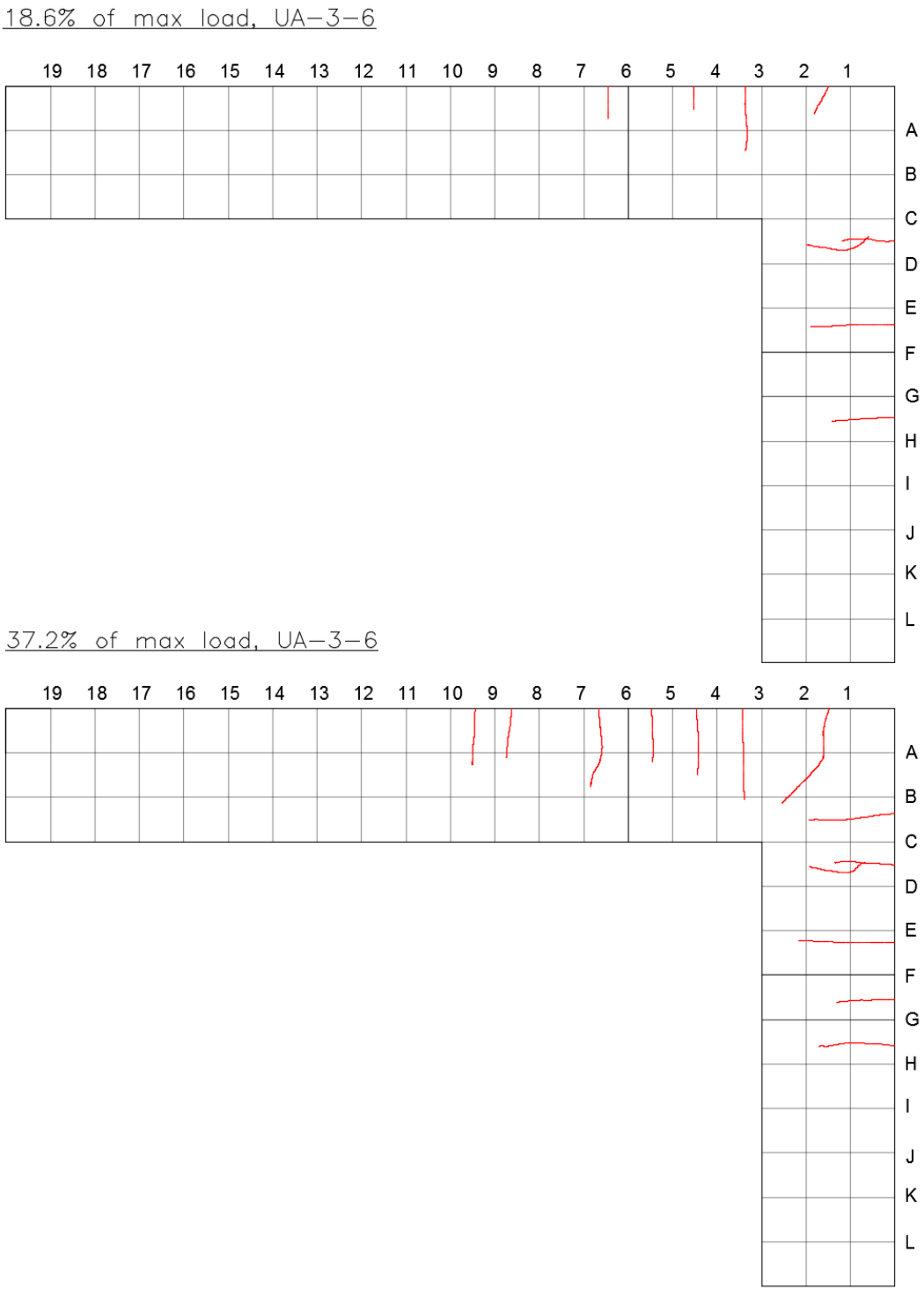

Figure A.18: Crack Progression Diagram 1, UA-3-6

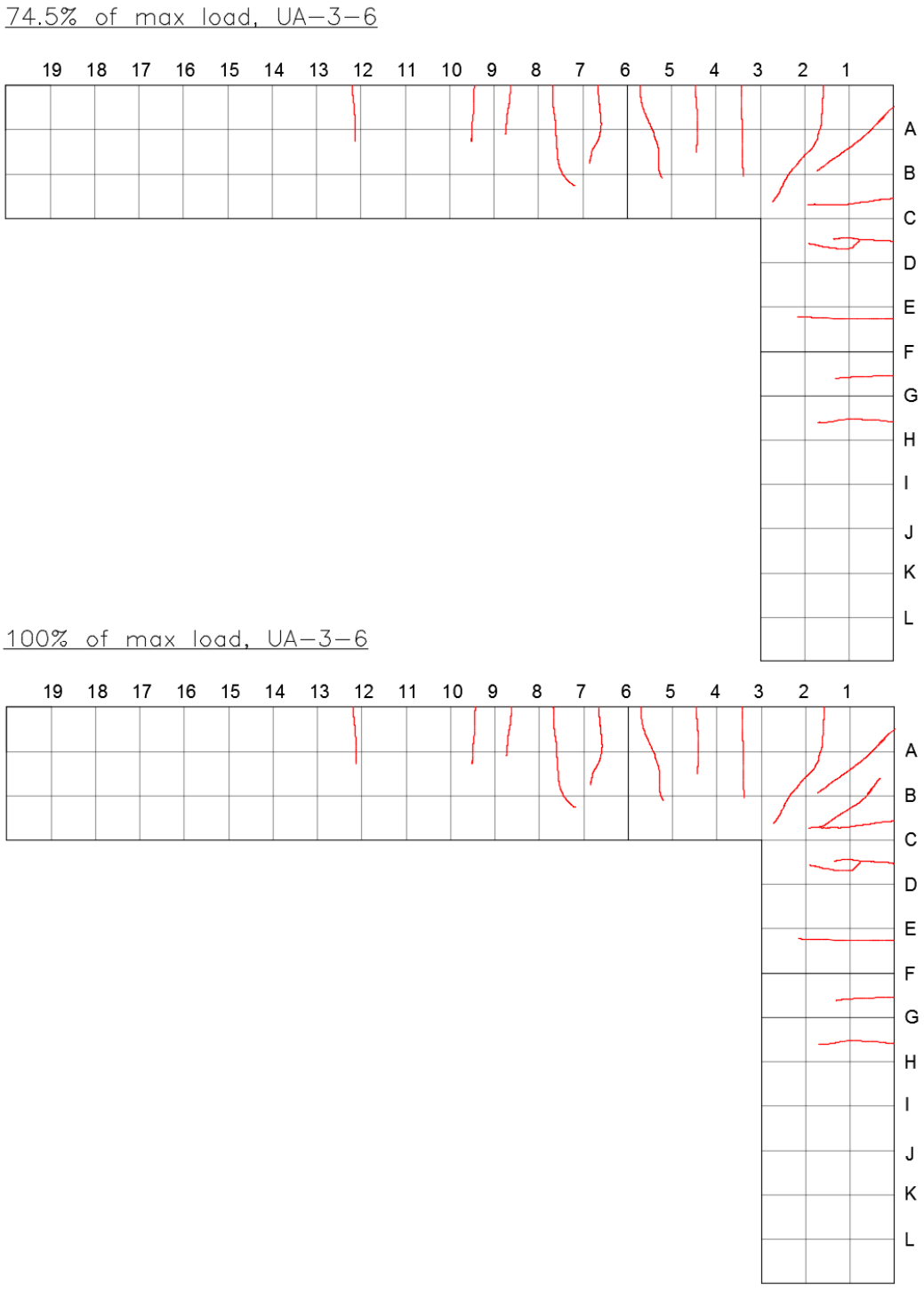

Figure A.19: Crack Progression Diagram 2, UA-3-6

Figure A.20: Joint UA-3-6 Moments Before Failure

Figure A.21: North Side of Failed Joint, UA-3-6

Figure A.22: Crack in Bend, UA-3-6

A.4 UB-3-6

This was the fourth specimen tested. It was loaded at a rate of 0.010 mm/second until a load of 25 kN, and then increased to 0.017 mm/second. The failure of this specimen occurred by crushing of interior corner, at column/chamfer interface, at a peak load of 61 kN, peak bending moment of 76.2 kN.m, and displacement at peak of 91.5 mm.

Table A.7: Properties of Specimen UB-3-6

Adjoining Member Properties	
f'_c	55
$b\ (mm)$	270
$h\ (mm)$	300
$L_{beam}\ (mm)$	1550
$L_{column}\ (mm)$	850
$d\ (mm)$	246
a_o/d	5.98
ρ_b	0.324 %
ρ	1.287 %
$M_r\ (kN.m)$	116.3
Reinforcement Bar Properties	
$f_{frp,straight}\ (MPa)$	1293
$f_{frp,bent}\ (MPa)$	655
$E\ (MPa)$	53808
$A\ (mm^2)$	855

Table A.8: Strain Gauge Readings, UB-3-6

% of Peak	1	2	3	4	B1	B2
10	0.000013	0.000004	0.000013	0.000118	0.000052	-0.000025
20	0.000023	0.000006	0.000042	0.001209	0.000183	-0.000092
30	0.000042	0.000013	0.000179	0.002190	0.000892	-0.000088
40	0.000071	0.000016	0.000656	0.003009	0.001543	-0.000048
50	0.000852	0.000039	0.003046	0.003924	0.002254	0.000015
60	0.002092	0.001032	0.005449	0.004831	0.002925	0.000114
70	0.002822	0.003236	0.006364	0.005694	0.003565	0.000206
80	0.003514	0.004422	0.007312	0.006699	0.004321	0.000355
90	0.004113	0.005643	0.008374	0.007790	0.004960	0.000513
100	0.004982	0.006963	0.009796	0.009241	0.005584	0.000672

% of Peak	Conc	S1	S2	C1	C2
10	-0.000034	0.000002	0.000016	0.000002	-0.000019
20	-0.000175	-0.000020	0.000070	-0.000075	-0.000078
30	-0.000421	-0.000018	0.000248	-0.000003	-0.000108
40	-0.000636	0.000035	0.000443	-0.000029	-0.000135
50	-0.000825	-0.000006	0.000800	-0.000024	-0.000167
60	-0.001030	0.000047	0.001053	-0.000019	-0.000204
70	-0.001205	0.000083	0.001277	-0.000017	-0.000296
80	-0.001412	0.000101	0.001463	0.000009	-0.000316
90	-0.001620	0.000197	0.001587	0.000010	-0.000329
100	-0.001833	0.000211	0.001703	0.000033	-0.000335

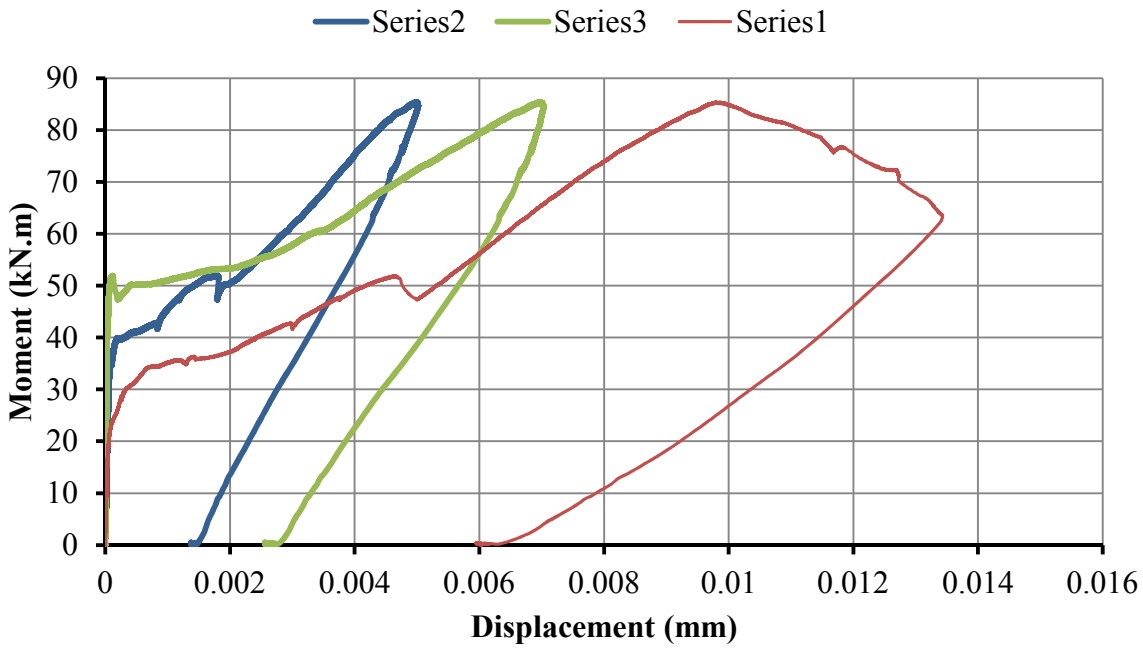

Figure A.23: Moment versus Strain Reading of Gauges 1, 2, and 3, UB-3-6

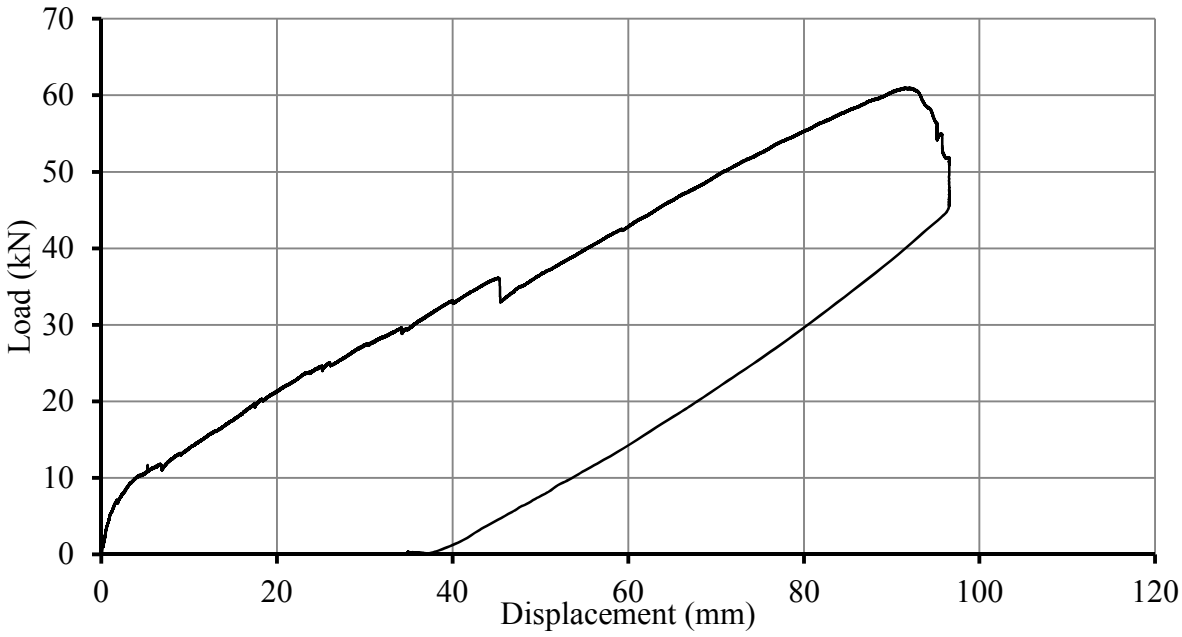

Figure A.24: Load-Deflection Response of UB-3-6

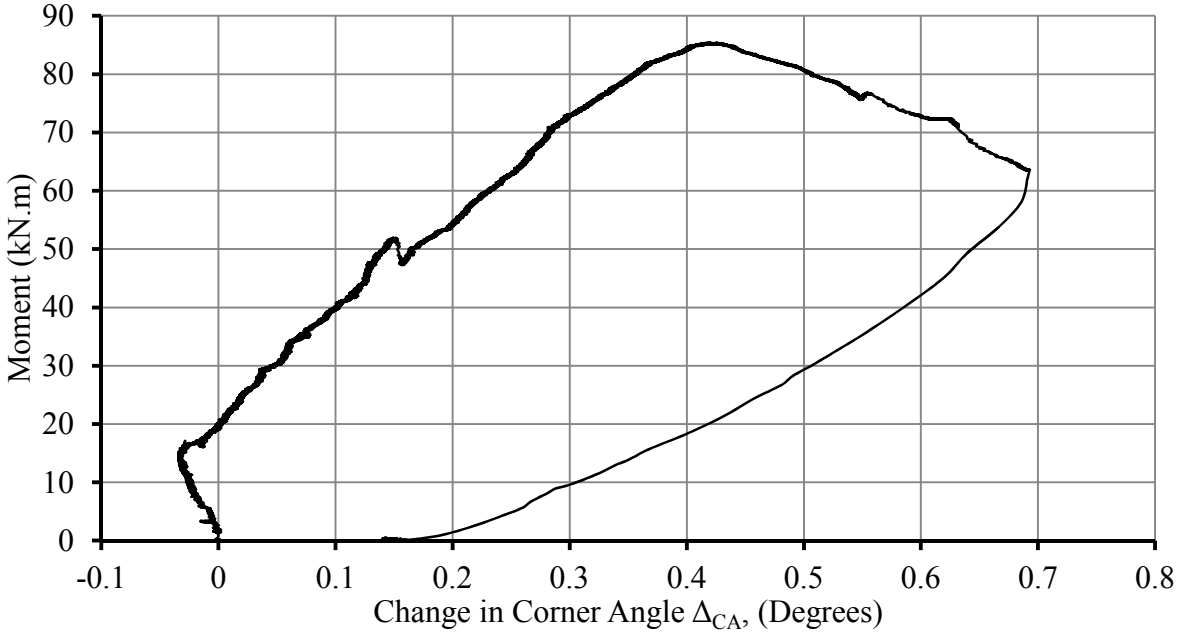

Figure A.25: Moment versus Change in Corner Angle, UB-3-6

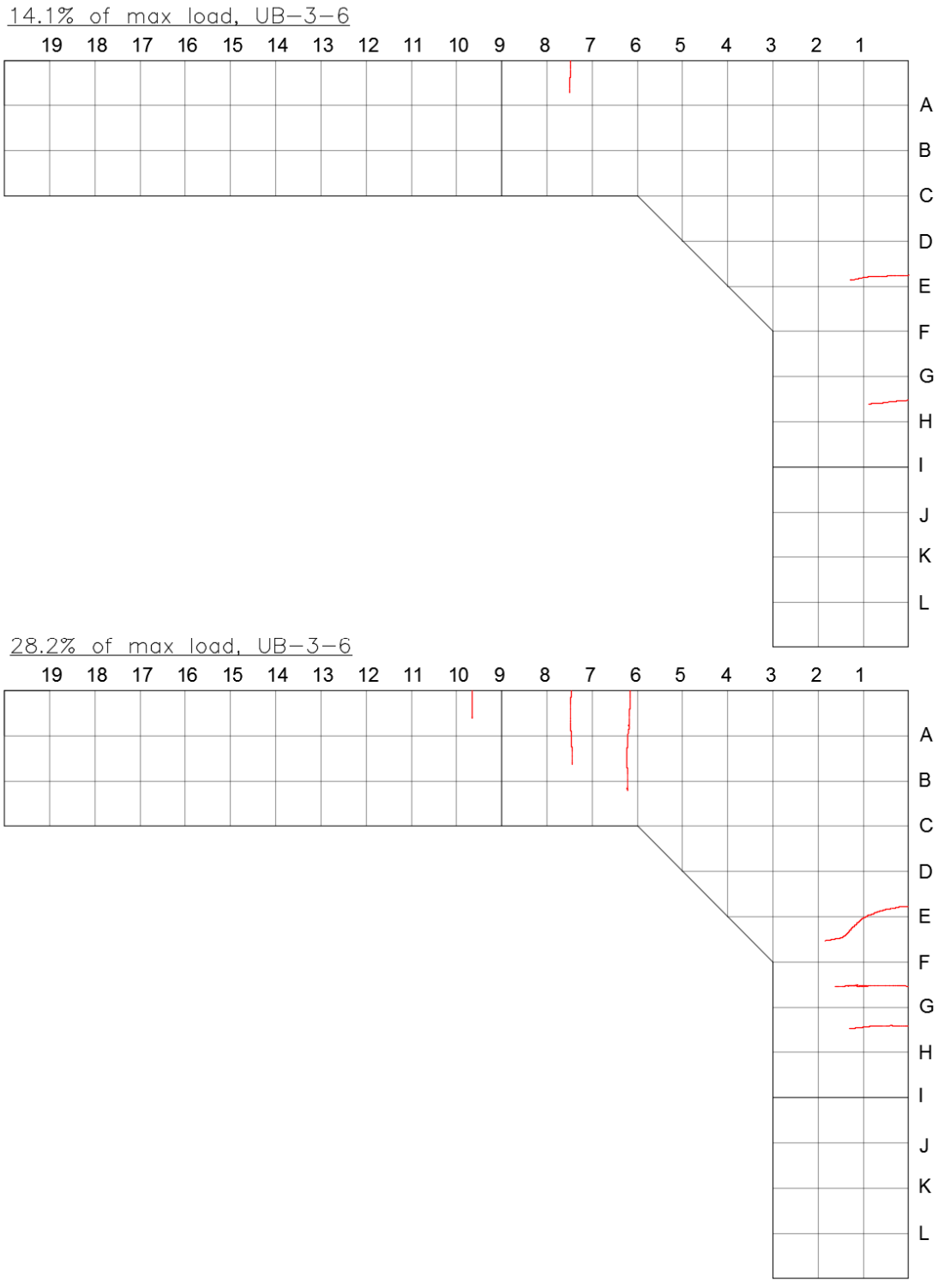

Figure A.26: Crack Progression Diagram 1, UB-3-6

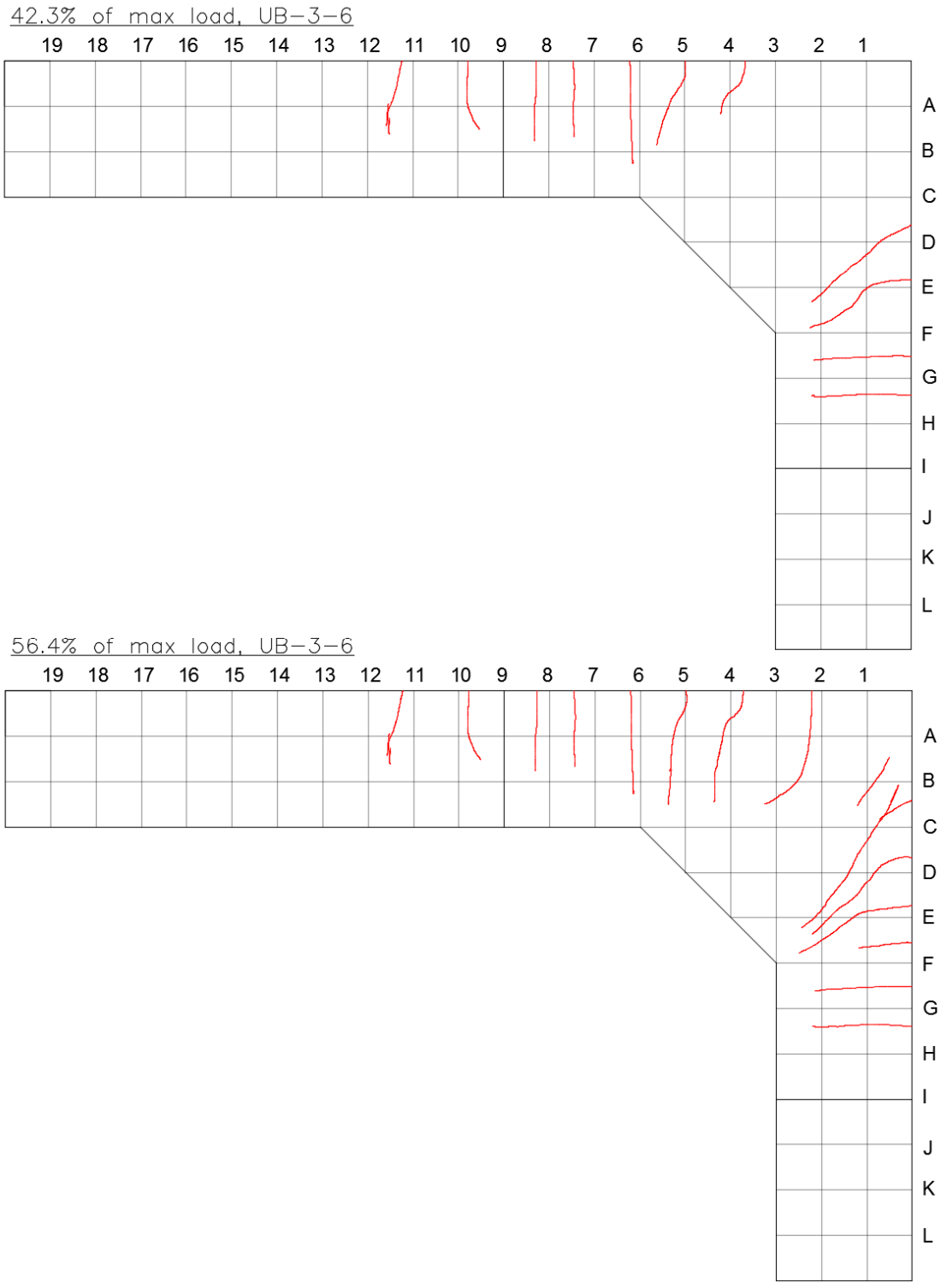

Figure A.27: Crack Progression Diagram 2, UB-3-6

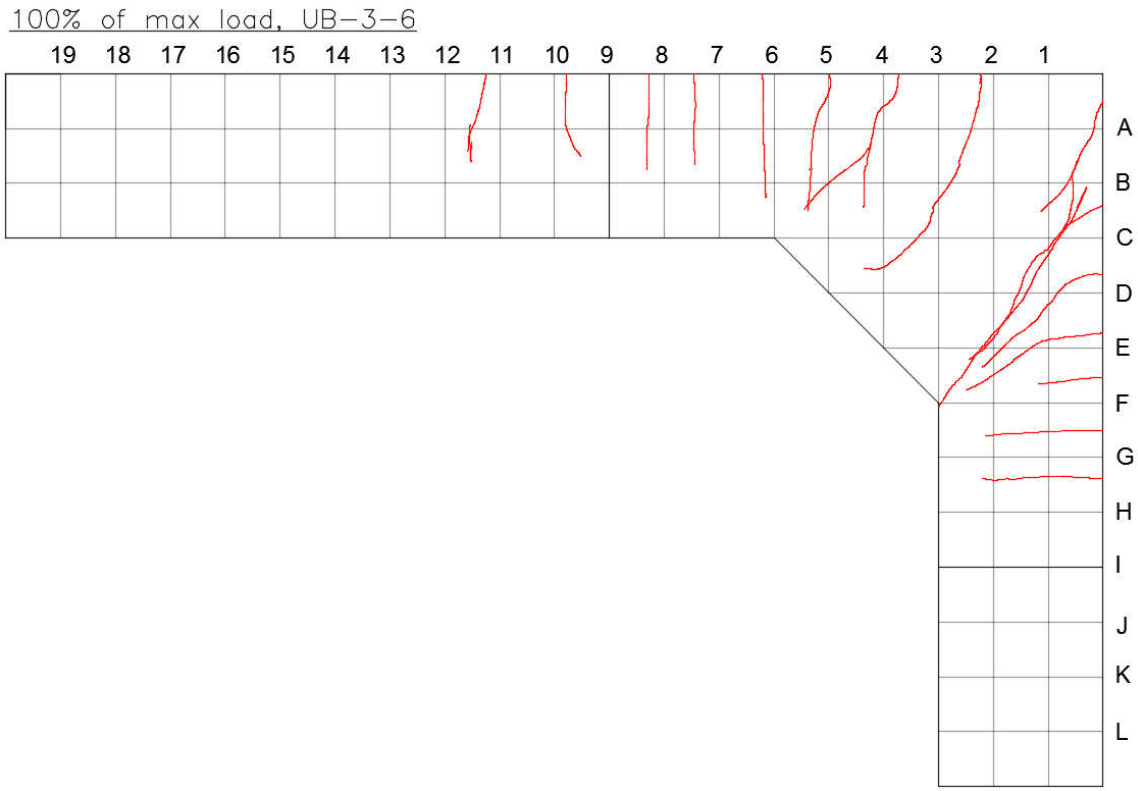

Figure A.28: Crack Progression Diagram 3, UB-3-6

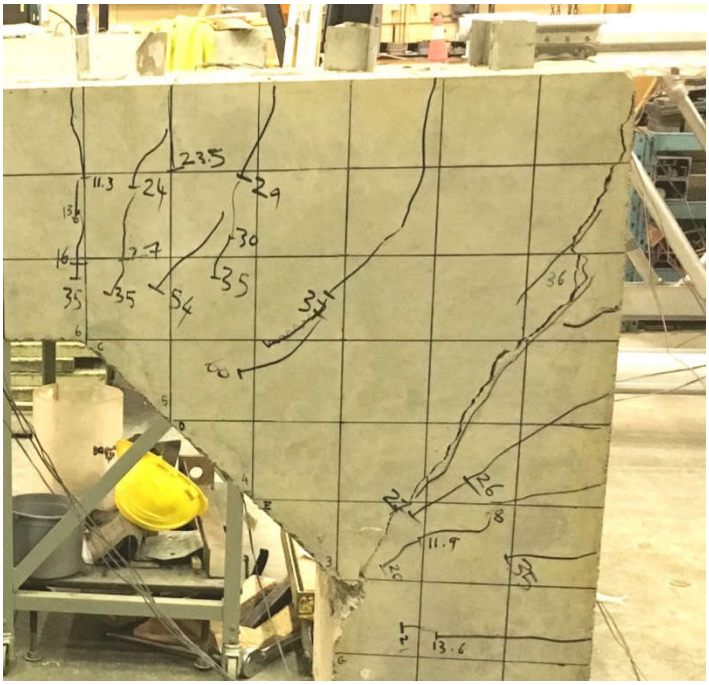

Figure A.29: Closeup of Joint at Failure, UB-3-6

Figure A.30: Extent of Crushing, UB-3-6

A.5 CA-2-6

This was the fifth specimen tested. It was loaded at a rate of 0.010 mm/second until a load of 25 kN, and then increased to 0.017 mm/second. The failure of this specimen failed due to bar anchorage at the column base. After the formation and widening of the crack in the column base, the bars experienced debonding. This specimen attained a peak load of 55 kN, peak bending moment of 75 kN.m, and displacement at peak of 155 mm.

Table A.9: Properties of Specimen CA-2-6

Adjoining Member Properties	
f'_c	48
$b\ (mm)$	270
$h\ (mm)$	300
$L_{beam}\ (mm)$	1700
$L_{column}\ (mm)$	1000
$d\ (mm)$	246
a_o/d	5.98
ρ_b	0.293 %
ρ	1.287 %
$M_r\ (kN.m)$	109.1
Reinforcement Bar Properties	
$f_{frp,straight}\ (MPa)$	1293
$f_{frp,bent}\ (MPa)$	655
$E\ (MPa)$	53808
$A\ (mm^2)$	855

Table A.10: Strain Gauge Readings, CA-2-6

% of Peak	1	2	3	4	B1	B2
10	0.001177	-	0.000990	0.001110	0.001160	-0.000335
20	0.002503	-	0.002807	0.002255	0.002153	-0.000393
30	0.003488	-	0.004184	0.003683	0.003127	-0.000284
40	0.004512	-	0.005345	0.004825	0.004050	-0.000128
50	0.005611	-	0.006478	0.005893	0.004981	0.000035
60	0.006962	-	0.007766	0.007082	0.006005	0.000216
70	0.008240	-	0.009007	0.008354	0.006998	0.000375
80	0.009535	-	0.010236	0.009792	0.008031	0.000545
90	0.010864	-	0.011489	0.011165	0.009099	0.000701
100	0.012354	-	0.012823	0.012918	0.010309	0.000834

% of Peak	Conc	S1	S2	D1	D2
10	0.000051	0.000110	0.000005	0.000031	0.000074
20	-0.000184	0.000128	-0.000012	0.000032	0.000090
30	-0.000561	0.000025	0.000028	0.000055	0.000168
40	-0.000823	0.000052	0.000044	0.000082	0.000310
50	-0.001055	0.000062	0.000046	0.000119	0.000537
60	-0.001297	0.000078	0.000050	0.000196	0.001844
70	-0.001556	0.000080	0.000039	0.000250	0.002699
80	-0.001800	0.000086	0.000047	0.000322	0.003584
90	-0.002078	0.000095	0.000044	0.000407	0.004339
100	-0.002420	0.000070	0.000036	0.000741	0.005473

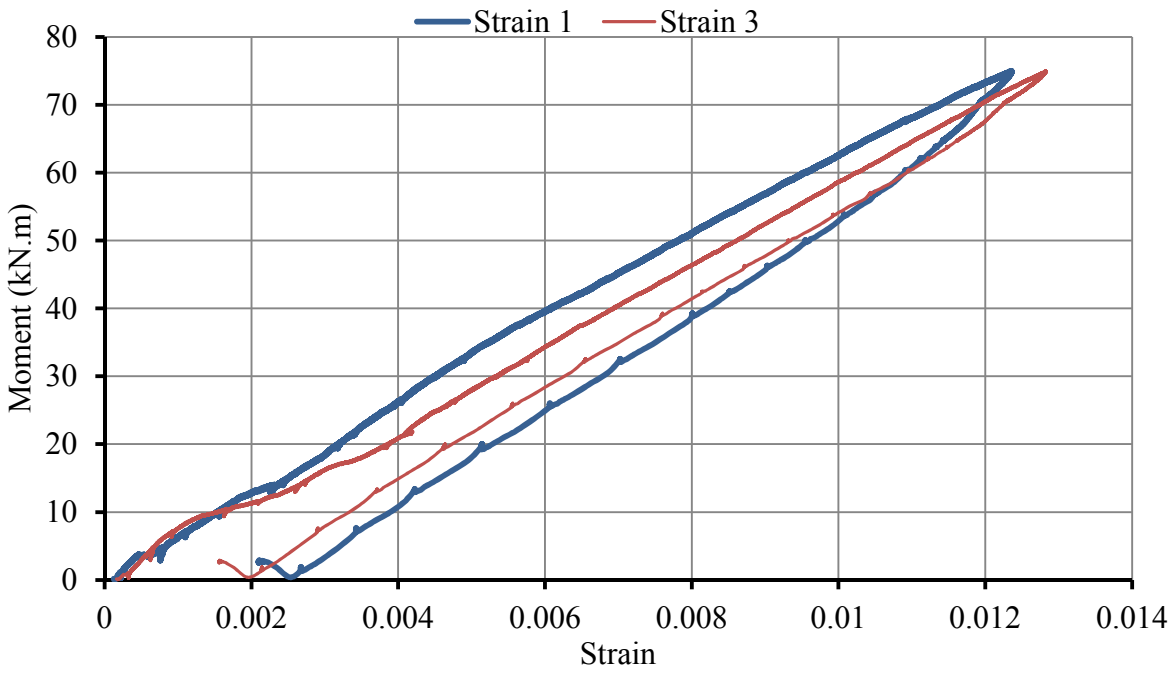

Figure A.31: Moment versus Strain Reading of Gauges 1, 2, and 3, CA-2-6

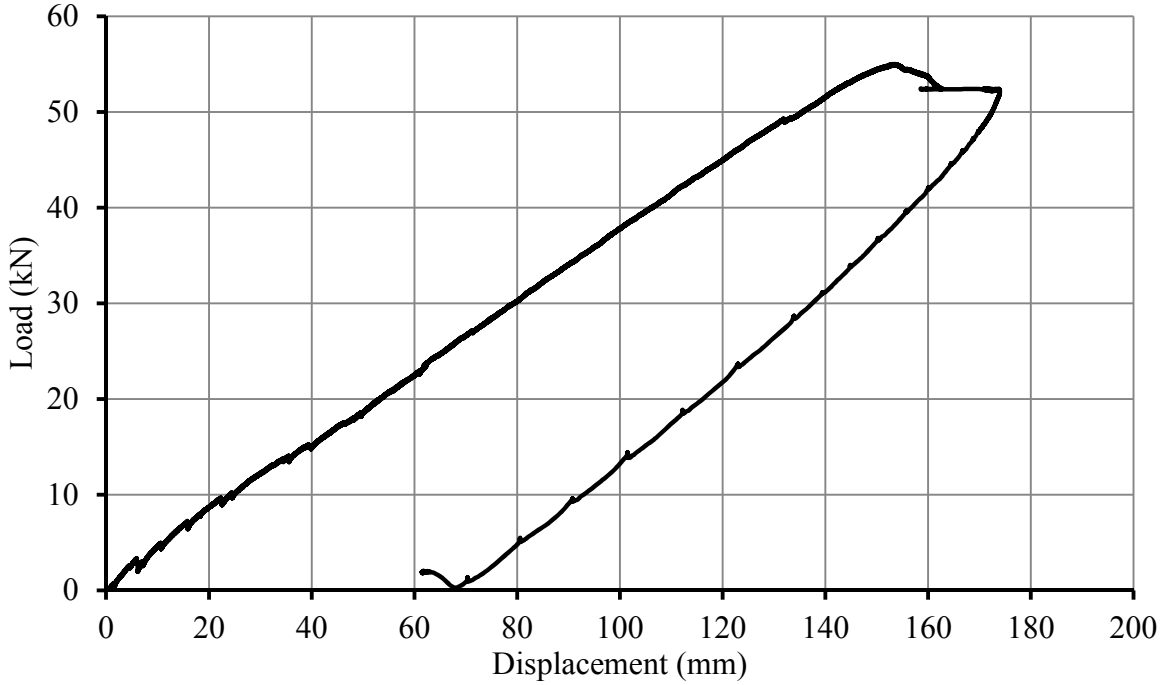

Figure A.32: Load-Deflection Response of CA-2-6

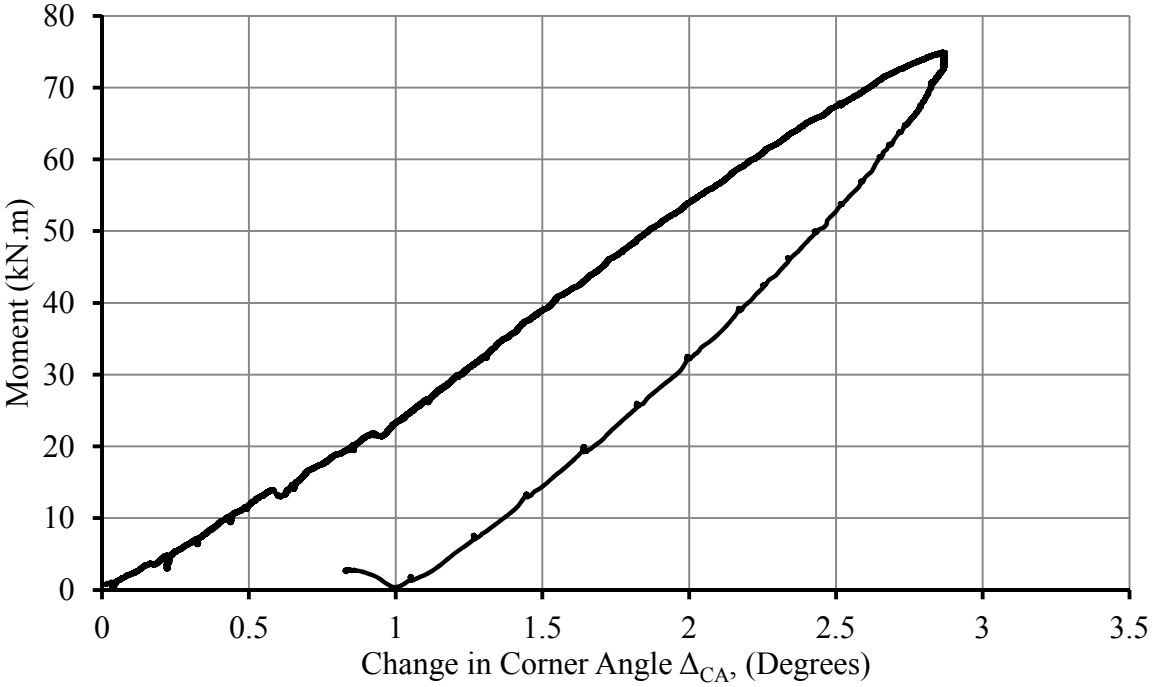

Figure A.33: Moment versus Change in Corner Angle, CA-2-6

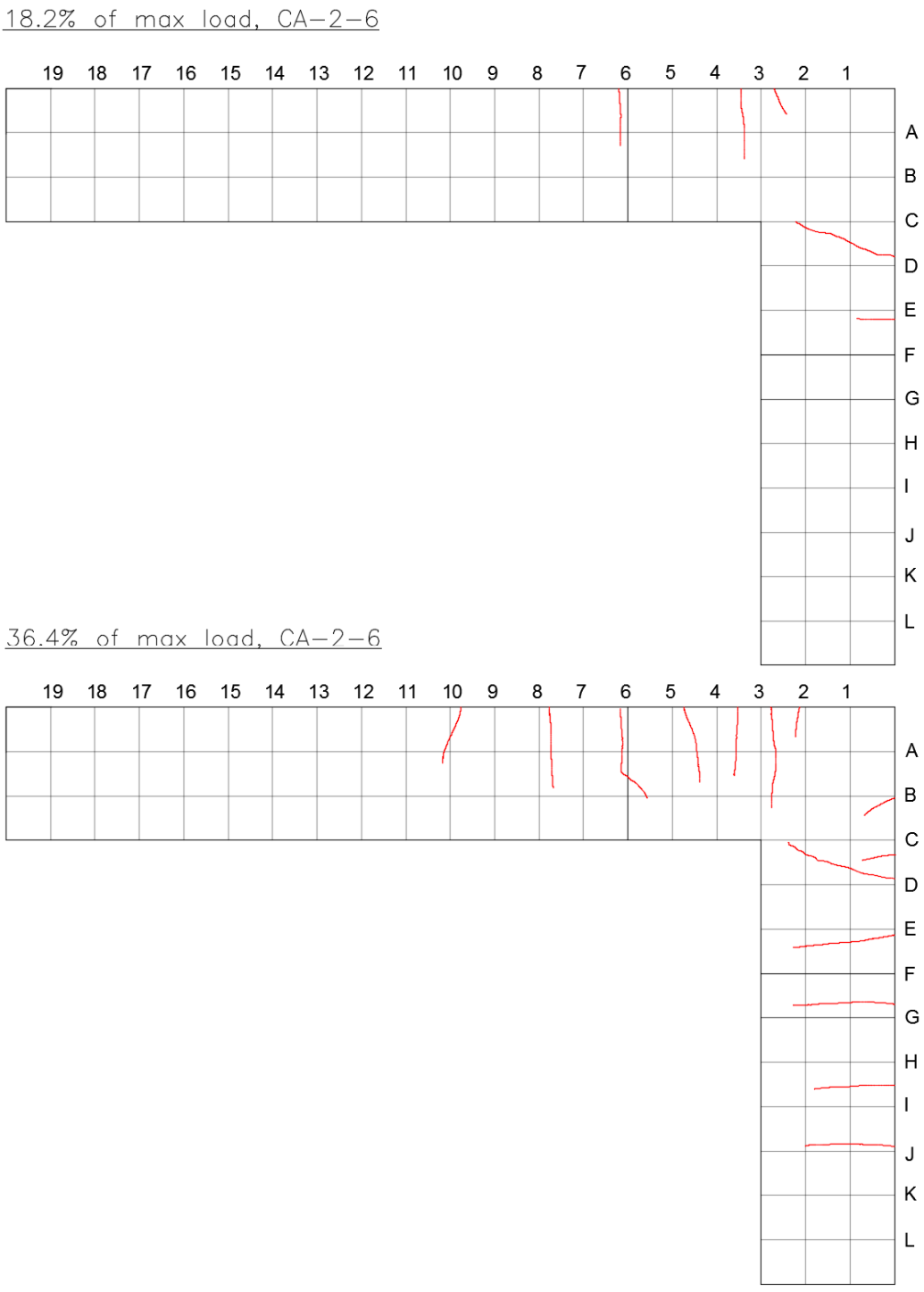

Figure A.34: Crack Progression Diagram 1, CA-2-6

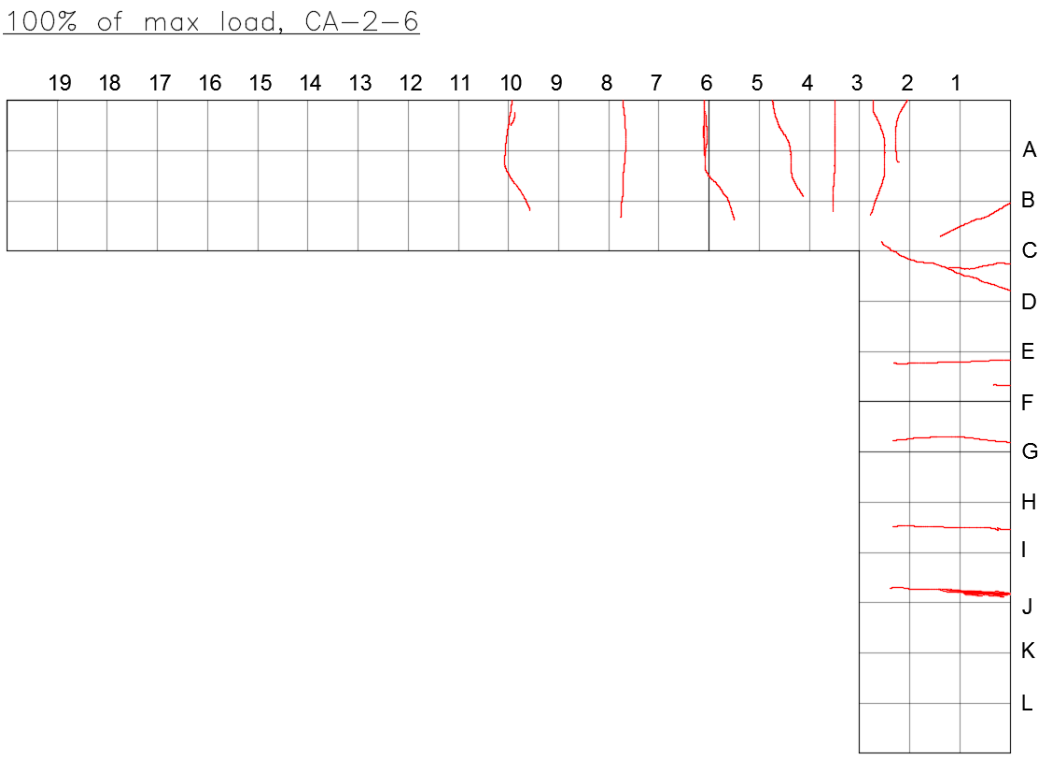

Figure A.35: Crack Progression Diagram 1, CA-2-6

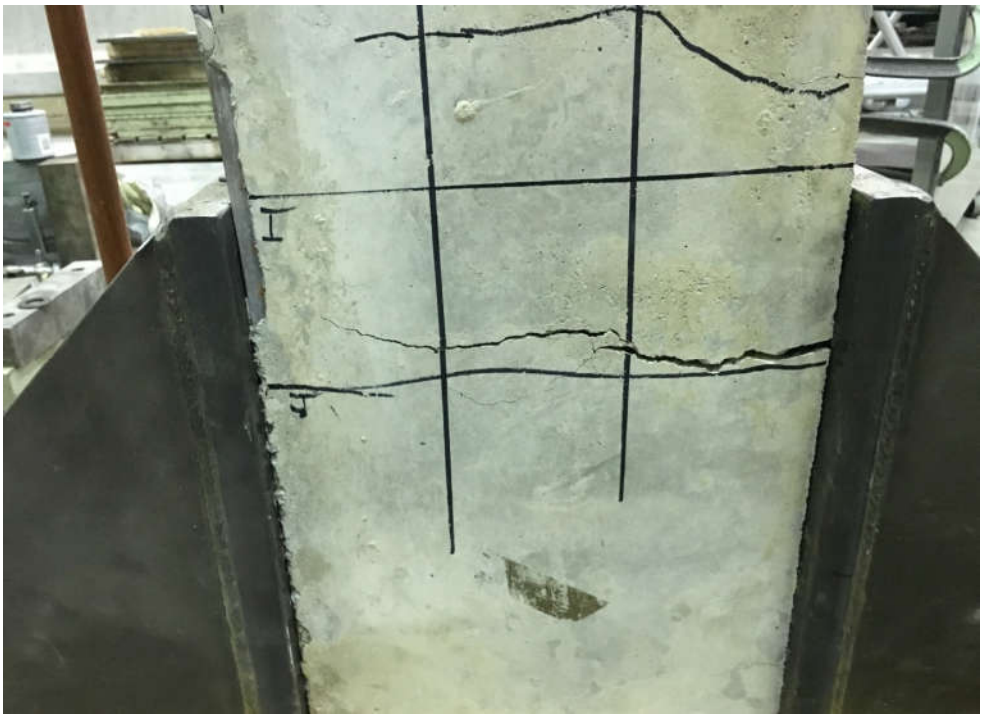

Figure A.36: Wide Crack in Column Base Causing Debonding. CA-2-6

A.6 CA-3-6

This was the sixth specimen tested. It was loaded at a rate of 0.010 mm/second until a load of 25 kN, and then increased to 0.017 mm/second. The failure of this specimen initiated by crushing of interior corner, however ultimate failure occurred by strut failure and bar rupture. This specimen attained a peak load of 84.9 kN, peak bending moment of 115.2 kN.m, and displacement at peak of 182.1 mm.

Table A.11: Properties of Specimen CA-3-6

Adjoining Member Properties	
f'_c	48
$b\ (mm)$	270
$h\ (mm)$	300
$L_{beam}\ (mm)$	1700
$L_{column}\ (mm)$	1000
$d\ (mm)$	246
a_o/d	5.98
ρ_b	0.293 %
ρ	1.287 %
$M_r\ (kN.m)$	109.1
Reinforcement Bar Properties	
$f_{frp,straight}\ (MPa)$	1293
$f_{frp,bent}\ (MPa)$	655
$E\ (MPa)$	53808
$A\ (mm^2)$	855

Table A.12: Strain Gauge Readings, CA-3-6

% of Peak	1	2	3	4	B1	B2
10	0.000886	0.000056	0.000854	0.000512	0.104050	-0.000058
20	0.002289	0.000894	0.002055	0.002343	0.104050	-0.000009
30	0.003477	0.003655	0.003358	0.003802	0.104050	0.000064
40	0.004657	0.005553	0.004638	0.005103	0.104050	0.000204
50	0.005881	0.007407	0.006062	0.006521	0.104050	0.000424
60	0.007034	0.009282	0.007462	0.007989	0.104050	0.000727
70	0.008203	0.011148	0.008963	0.009500	0.104050	0.001173
80	0.009376	0.013260	0.010476	0.010938	0.104050	0.001732
90	0.010683	0.015904	0.012150	0.013077	0.104050	0.002248
100	0.012279	0.022608	0.014460	0.104316	0.104050	0.002134

% of Peak	Conc	S1	S2	D1	D2
10	-0.000100	-0.000024	-0.000021	0.000028	0.000124
20	-0.000470	-0.000004	-0.000024	0.000055	0.000454
30	-0.000697	-0.000012	-0.000029	0.000096	0.000814
40	-0.000956	-0.000014	-0.000046	0.000217	0.001222
50	-0.001274	-0.000008	-0.000050	0.000476	0.001707
60	-0.001602	-0.000011	-0.000047	0.001509	0.002664
70	-0.001948	-0.000006	0.000047	0.002429	0.003512
80	-0.002241	-0.000004	0.000200	0.003257	0.004310
90	-0.002483	-0.000015	0.001629	0.004375	0.005415
100	-0.002814	-0.000022	0.003342	0.005297	0.006614

Figure A.37: Moment versus Strain Reading of Gauges 1, 2, and 3, CA-3-6

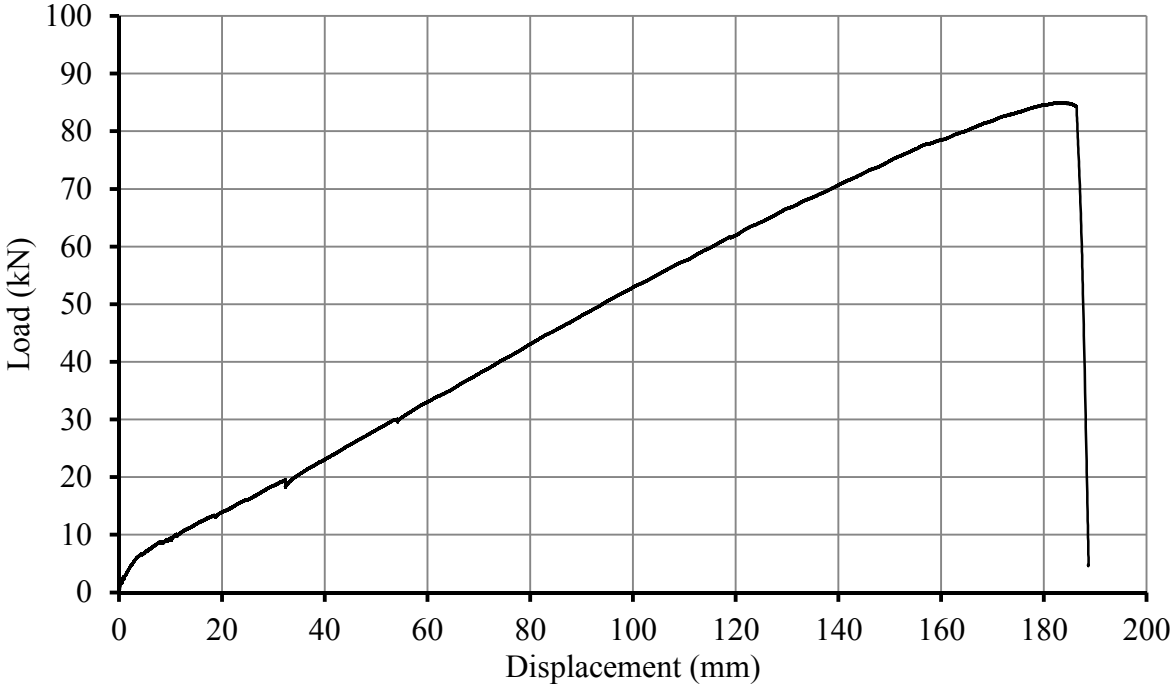

Figure A.38: Load-Deflection Response of CA-3-6

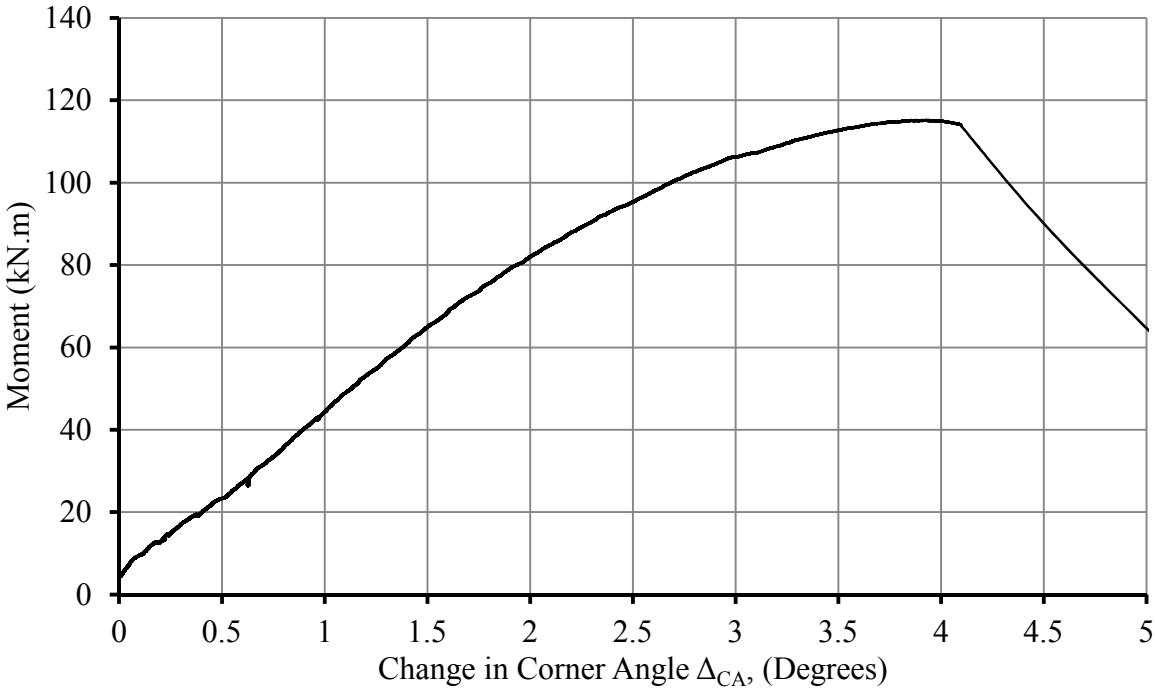

Figure A.39: Moment versus Change in Corner Angle, CA-3-6

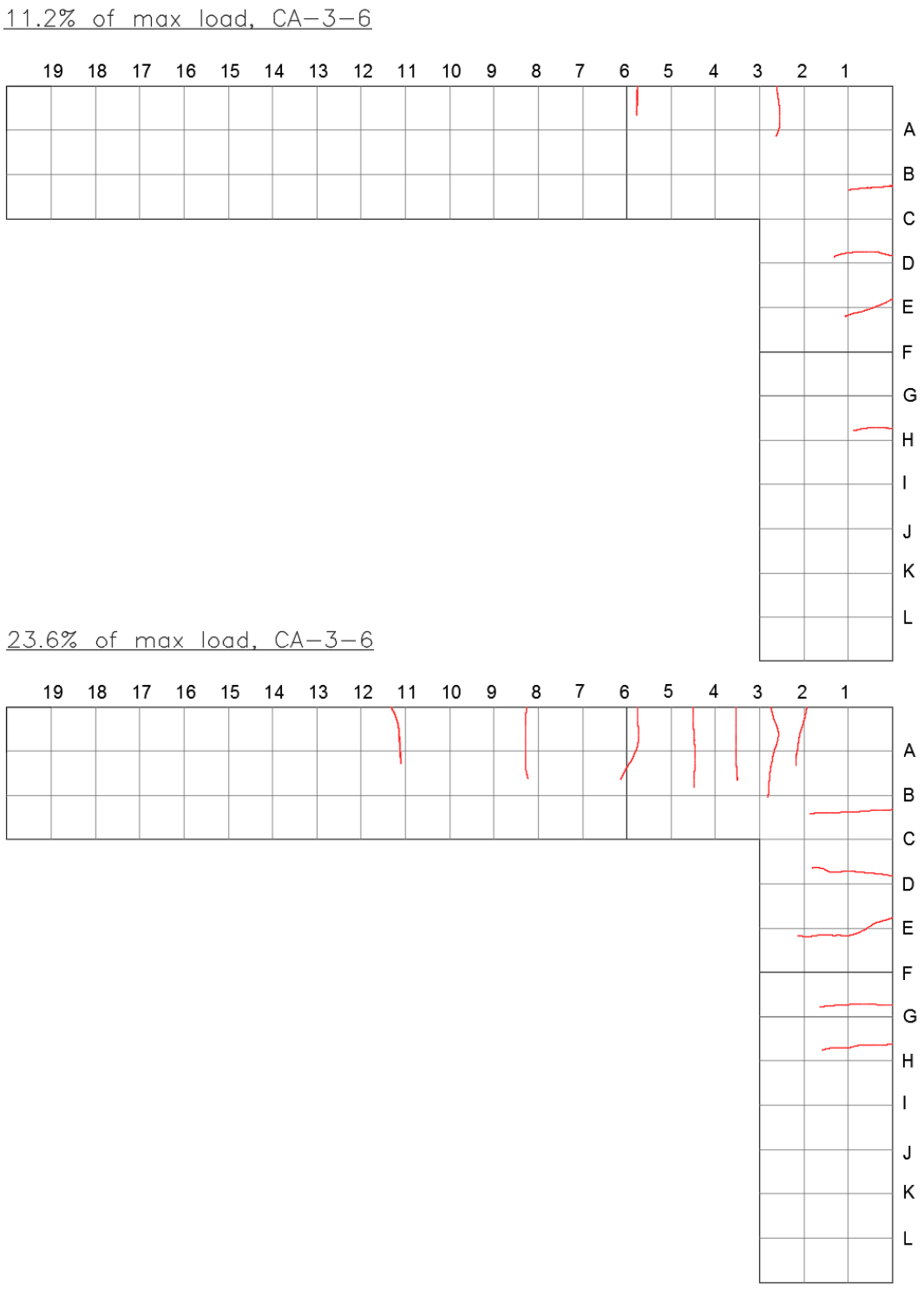

Figure A.40: Crack Progression Diagram 1, CA-3-6

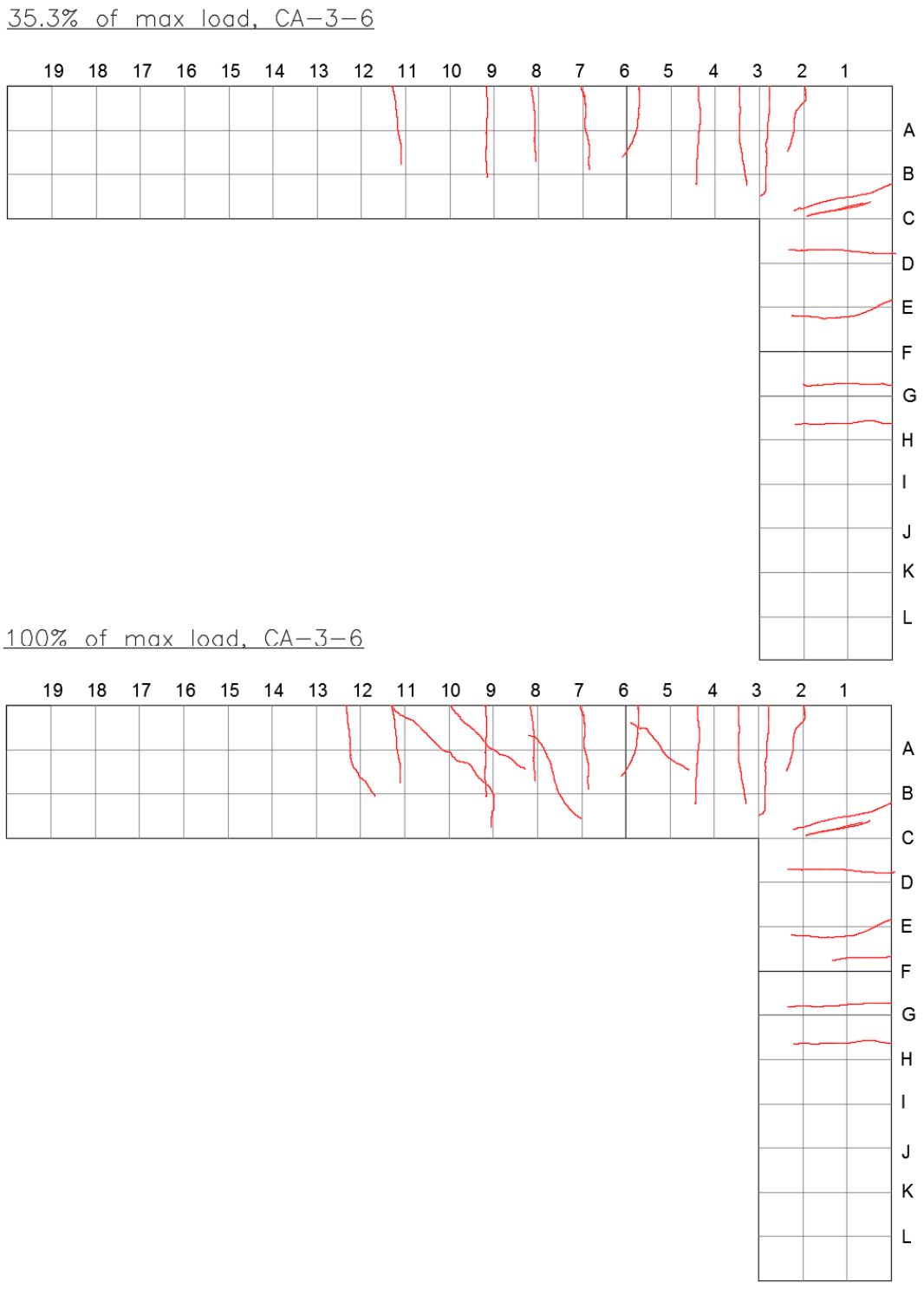

Figure A.41: Crack Progression Diagram 2, CA-3-6

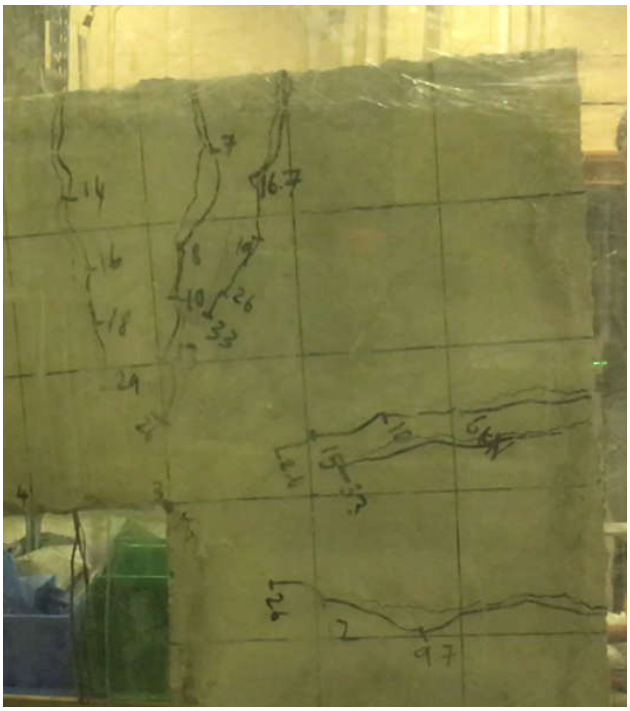

Figure A.42: CA-3-6 Moments Before Failure

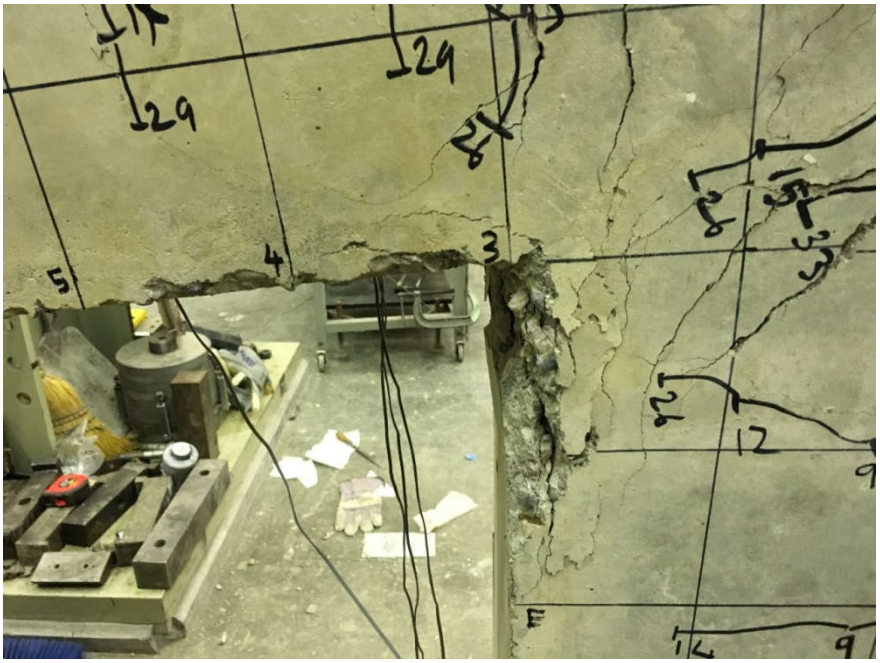

Figure A.43: The Extent of Crushing, CA-3-6

Figure A.44: Bar Rupture and Bar Shifting, CA-3-6

A.7 UA-2-4

This was the seventh specimen tested. It was loaded at a rate of 0.010 mm/second until a load of 15 kN, and then increased to 0.017 mm/second. The failure of this specimen occurred by bar rupture at a peak load of 28.5 kN, peak bending moment of 39.2 kN.m, and displacement at peak of 140.26 mm.

Table A.13: Properties of Specimen UA-2-4

Adjoining Member Properties	
f'_c	48
$b\ (mm)$	270
$h\ (mm)$	300
$L_{beam}\ (mm)$	1700
$L_{column}\ (mm)$	1000
$d\ (mm)$	246
a_o/d	5.98
ρ_b	0.290 %
ρ	0.376 %
$M_r\ (kN.m)$	66.8
Reinforcement Bar Properties	
$f_{frp,straight}\ (MPa)$	1287
$f_{frp,bent}\ (MPa)$	634
$E\ (MPa)$	53942
$A\ (mm^2)$	253.4

Table A.14: Strain Gauge Readings, UA-2-4

% of Peak	1	2	3	4	B1	B2
10	0.000024	0.000011	0.000019	0.000029	0.000024	-0.000008
20	0.000057	0.000024	0.000047	0.000060	0.000051	-0.000026
30	0.002550	0.000030	0.000081	0.001357	0.001179	-0.000037
40	0.004824	0.000039	0.003071	0.002672	0.003177	0.000162
50	0.006395	0.004938	0.005730	0.005430	0.004183	0.000353
60	0.007521	0.007412	0.008477	0.006702	0.005332	0.000487
70	0.008699	0.010636	0.009970	0.008005	0.006366	0.000665
80	0.010239	0.015155	0.011254	0.009269	0.007449	0.000872
90	0.011632	0.104098	0.012586	0.010518	0.008553	0.001122
100	0.012927	0.104098	0.013916	0.011675	0.009579	0.001434

% of Peak	Conc	S1	S2
10	-0.000012	0.000008	0.000011
20	-0.000036	0.000006	0.000015
30	-0.000248	0.000112	0.000016
40	-0.000602	0.000059	0.000039
50	-0.000759	0.000055	0.000059
60	-0.000923	0.000046	0.000054
70	-0.001117	0.000112	0.000046
80	-0.001310	0.000204	0.000045
90	-0.001536	0.000287	0.000042
100	-0.001776	0.000392	0.000039

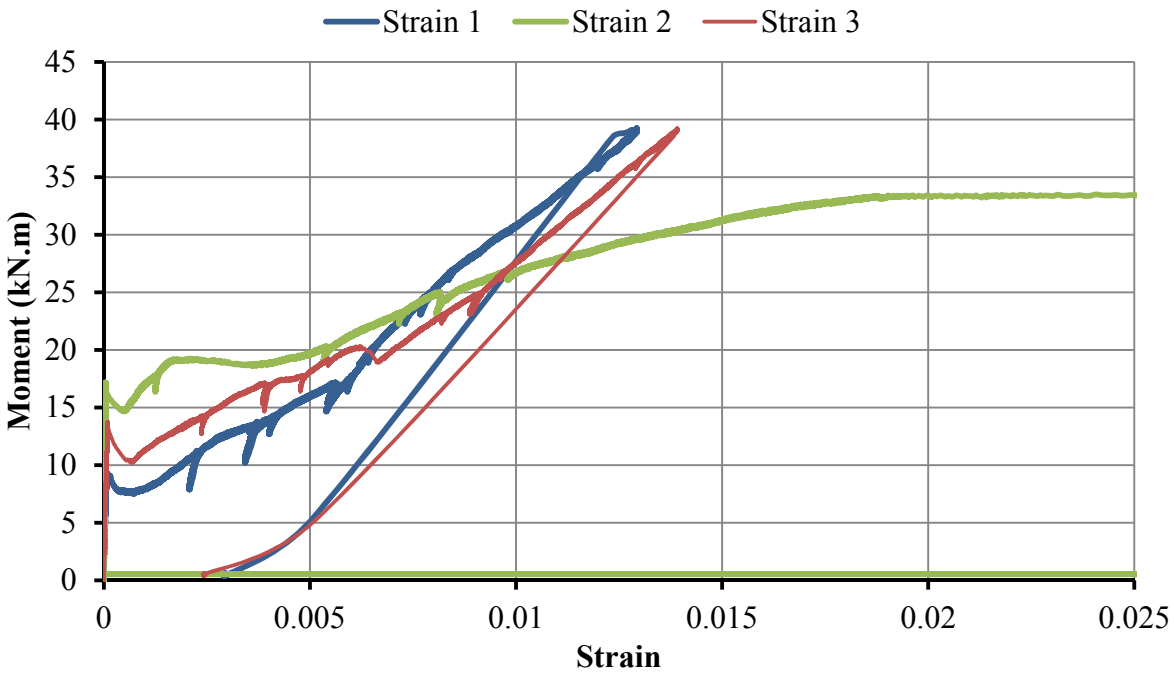

Figure A.45: Moment versus Strain Reading of Gauges 1, 2, and 3, UA-2-4

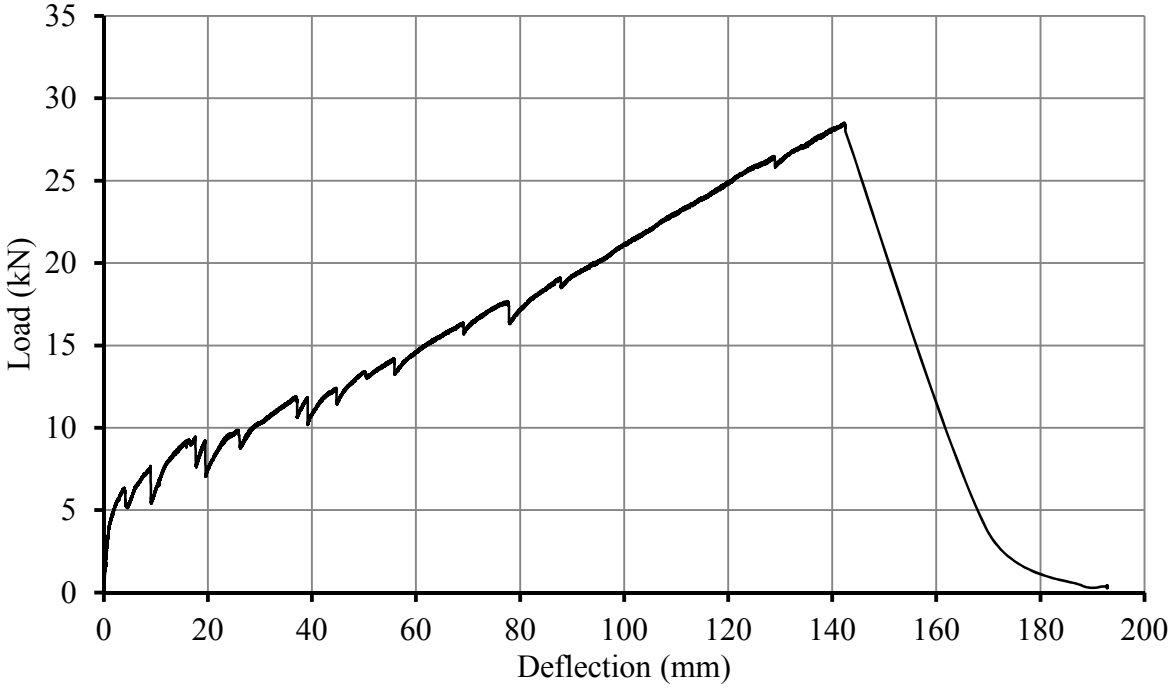

Figure A.46: Load-Deflection Response of UA-2-4

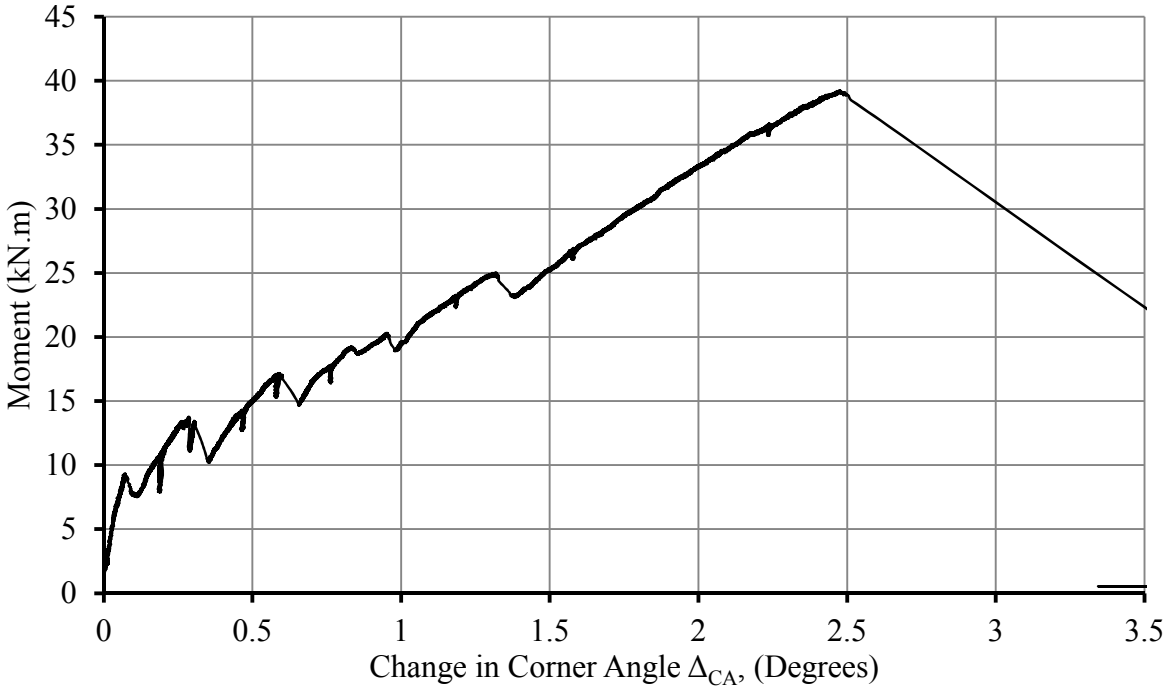

Figure A.47: Moment versus Change in Corner Angle, UA-2-4

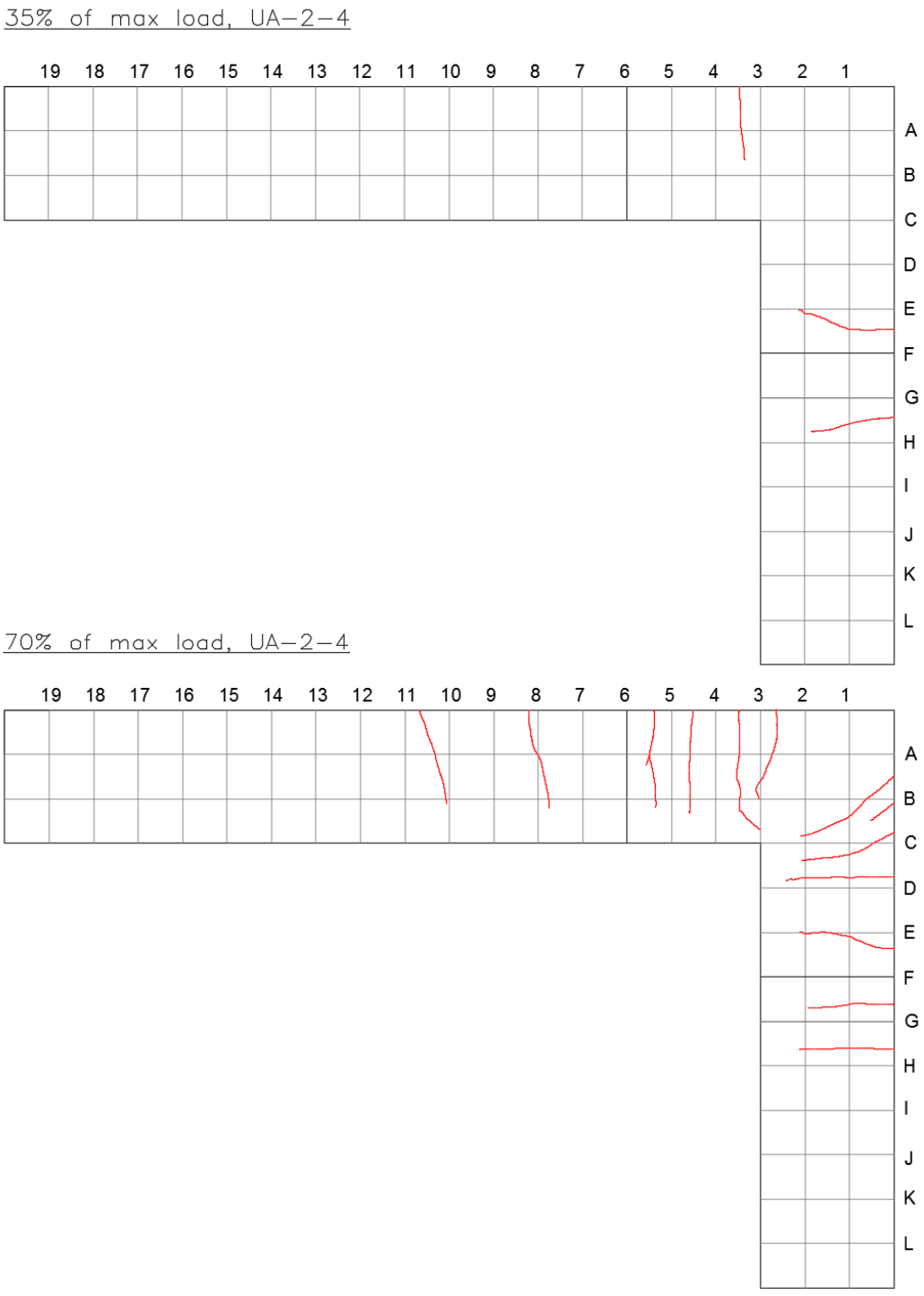

Figure A.48: Crack Progression Diagram 1, UA-2-4

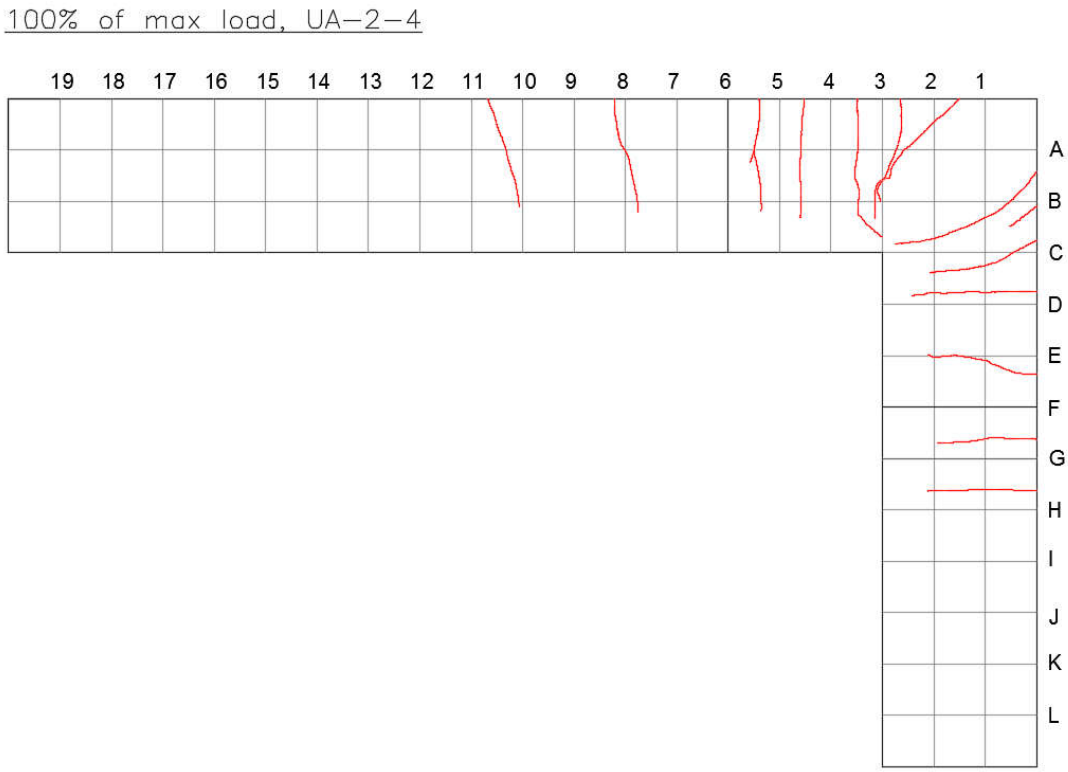

Figure A.49: Crack Progression Diagram 2, UA-2-4

Figure A.50: Closeup of Bar Rupture, UA-2-4

Figure A.51: Top View of UA-2-4, Showing Spalling on One Side

A.8 CB-3-6

This was the eighth specimen tested. It was loaded at a rate of 0.010 mm/second until a load of 15 kN, and then increased to 0.017 mm/second. The failure of this specimen occurred by crushing of interior corner, at column/chamfer interface, at a peak load of 88.8 kN, peak bending moment of 119.9 kN.m, and displacement at peak of 186.8 mm.

Table A.15: Properties of Specimen CB-3-6

Adjoining Member Properties	
f'_c	48
$b\ (mm)$	270
$h\ (mm)$	300
$L_{beam}\ (mm)$	1700
$L_{column}\ (mm)$	1000
$d\ (mm)$	246
a_o/d	5.98
ρ_b	0.293 %
ρ	1.287 %
$M_r\ (kN.m)$	109.1
Reinforcement Bar Properties	
$f_{frp,straight}\ (MPa)$	1293
$f_{frp,bent}\ (MPa)$	655
$E\ (MPa)$	53808
$A\ (mm^2)$	855

Table A.16: Strain Gauge Readings, CB-3-6

% of Peak	1	2	3	4	B1	B2	Conc
10	0.000022	0.000006	0.000024	0.000224	0.000066	-0.000080	-0.000062
20	0.000059	0.000009	0.000071	0.001519	0.000920	-0.000071	-0.000431
30	0.000270	0.000026	0.002207	0.002673	0.002084	0.000301	-0.000666
40	0.002229	0.000134	0.003586	0.003850	0.002860	0.000642	-0.000890
50	0.003738	0.000556	0.004551	0.005196	0.003701	0.001043	-0.001118
60	0.004805	0.001170	0.005473	0.006405	0.004453	0.001574	-0.001338
70	0.005678	0.003669	0.006582	0.007649	0.005265	0.002166	-0.001554
80	0.006573	0.004564	0.007828	0.009000	0.006081	0.002749	-0.001791
90	0.007528	0.006048	0.009786	0.011760	0.007019	0.003406	-0.002105
100	0.008325	0.007716	0.013001	0.015840	0.007816	0.003923	-0.002374

% of Peak	S1	S2	D1	D2	C1	C2
10	-0.000006	0.000024	0.000010	0.000023	0.000024	-0.000077
20	-0.000002	0.000085	0.000012	0.000031	0.000094	-0.000212
30	-0.000007	0.000704	0.000018	0.000037	0.000368	-0.000284
40	0.000083	0.001898	0.000025	0.000050	0.001542	-0.000361
50	0.000479	0.002345	0.000047	0.000074	0.002058	-0.000444
60	0.000948	0.002664	0.000073	0.000107	0.002324	-0.000514
70	0.001249	0.002823	0.000106	0.000302	0.002554	-0.000674
80	0.001433	0.002784	0.000139	0.000412	0.002773	-0.000710
90	0.001841	0.002649	0.000208	0.000748	0.002866	-0.000696
100	0.002082	0.002708	0.000525	0.104193	0.002897	-0.000573

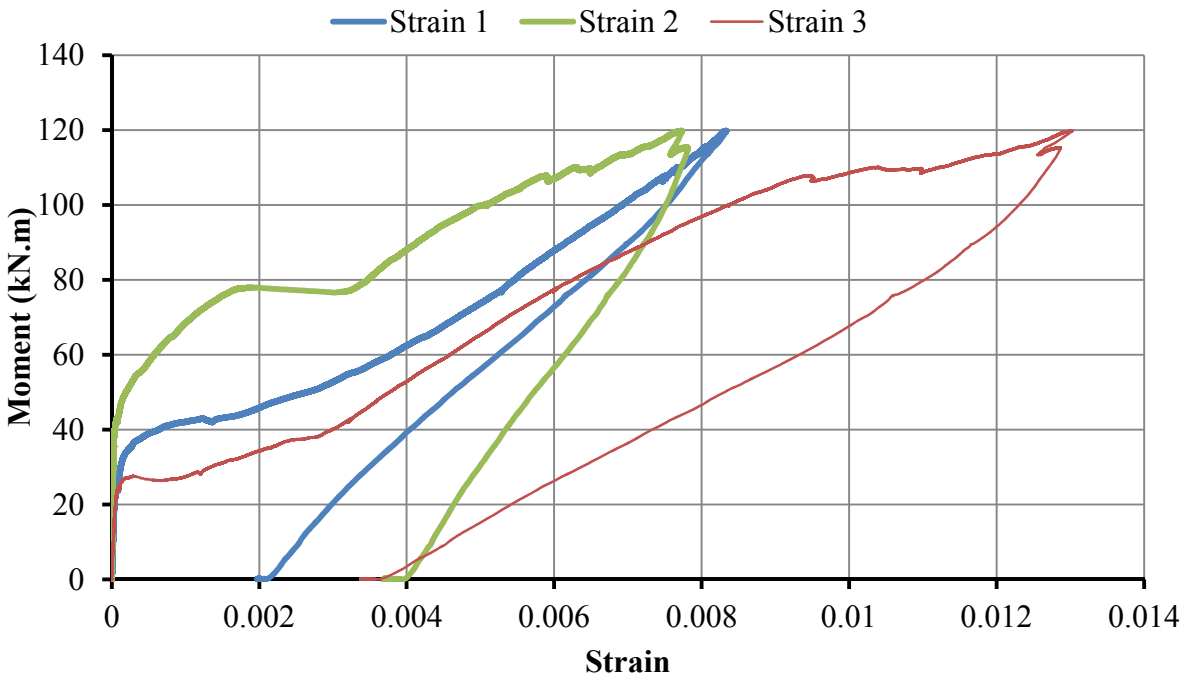

Figure A.52: Moment versus Strain Reading of Gauges 1, 2, and 3, CB-3-6

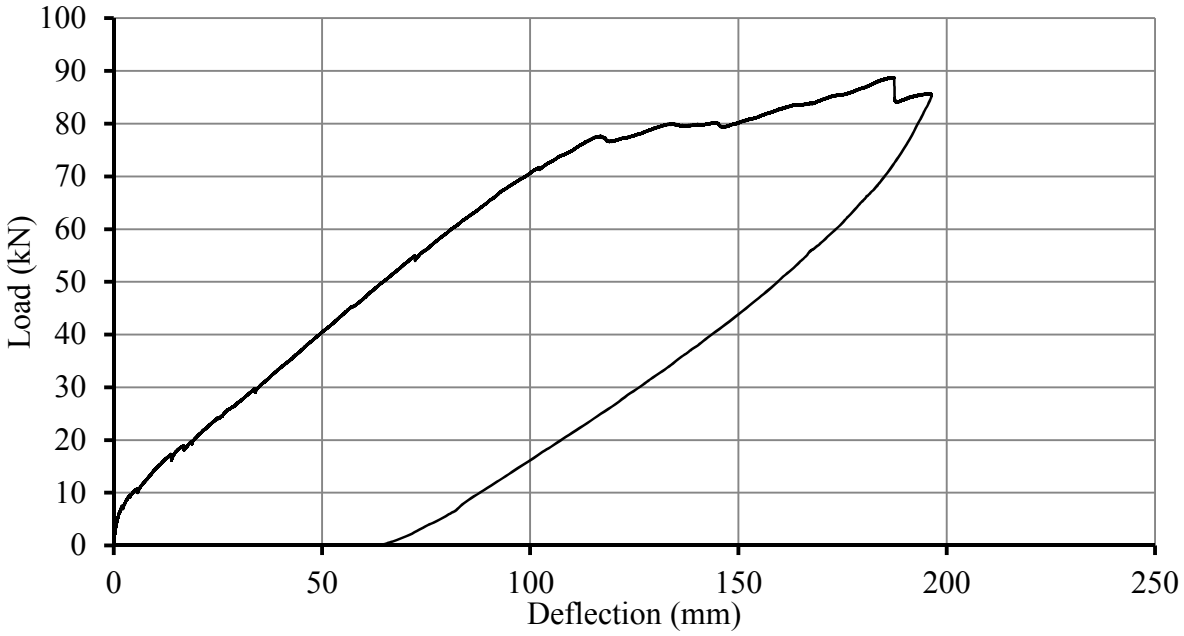

Figure A.53: Load-Deflection Response of CB-3-6

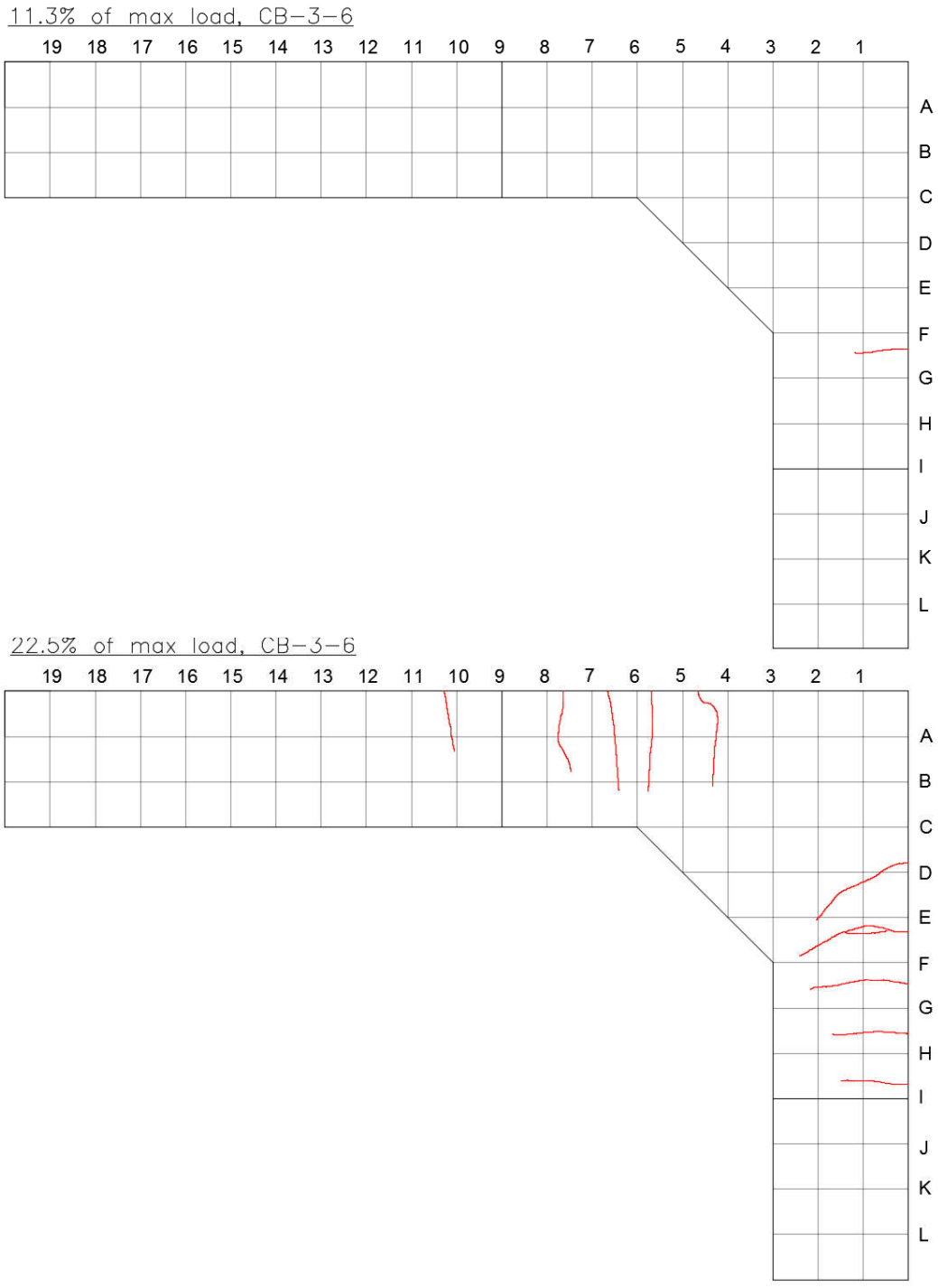

Figure A.54: Crack Progression Diagram 1, CB-3-6

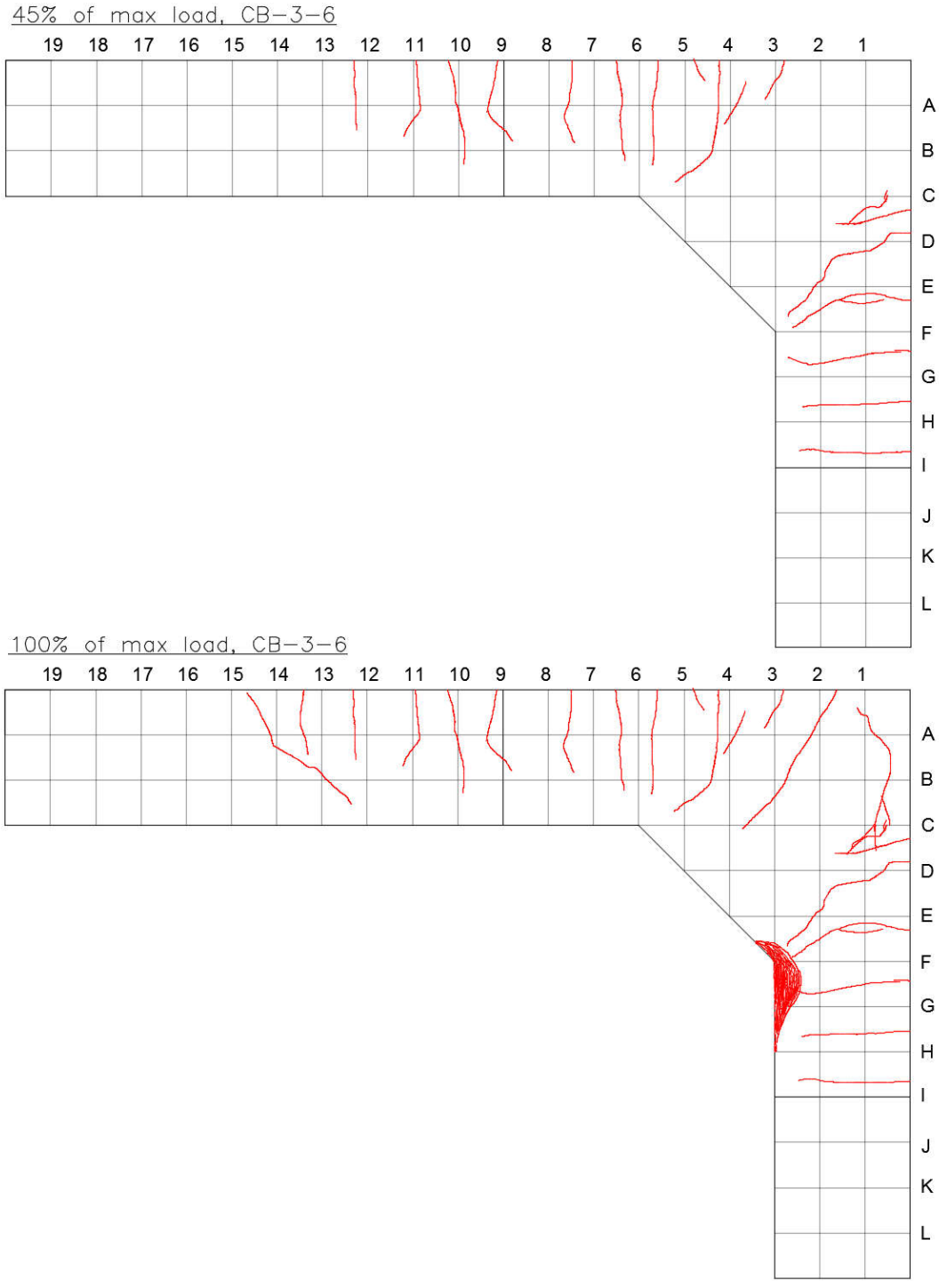

Figure A.55: Crack Progression Diagram 2, CB-3-6

Figure A.56: Extent of Crushing on Interior Corner, CB-3-6

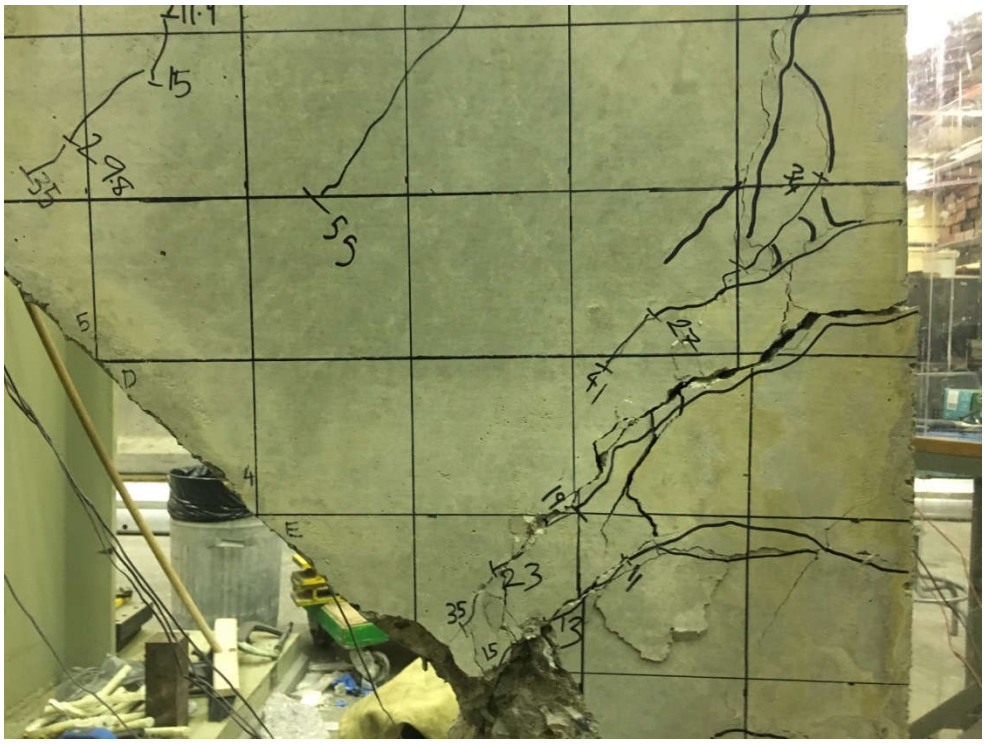

Figure A.57: Significant Crack Width, East Face CB-3-6

Appendix B
Support Apparatus

The following appendix presents figures outlining the dimensions of the steel support.

B.1 Support System

The support system consists of two stiffened angles that clamp the column base to the support beam. The support beam is affixed to the laboratory floor, as shown in Figure B.1.

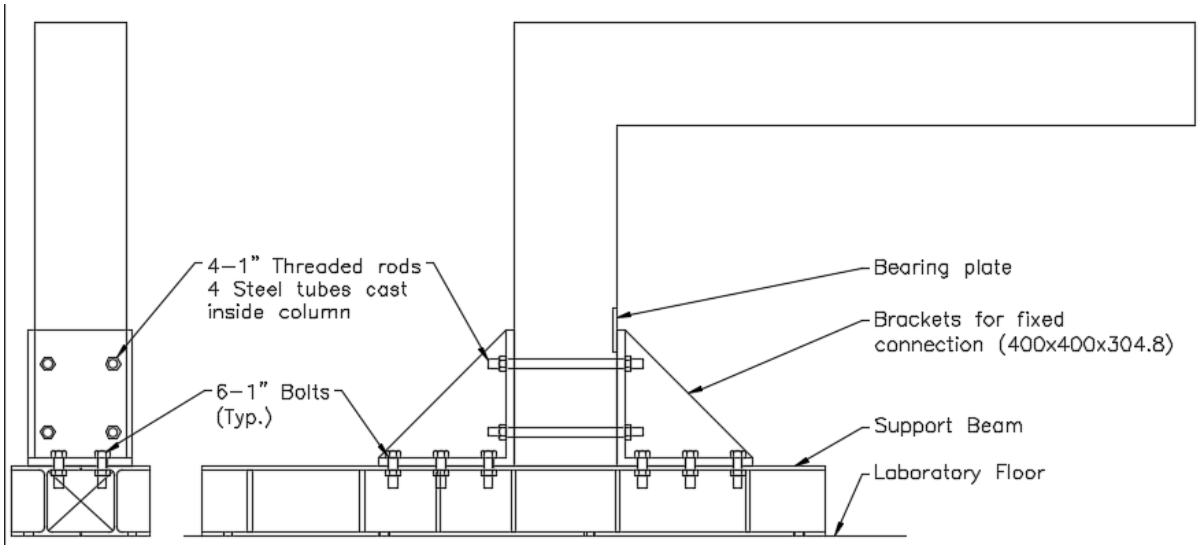

Figure B.1: Steel Support System

Four holes are cast within the column base as part of the specimen clamping. It was important to choose correct hole location to avoid interference with the reinforcement bars.

B.2 Holes Within Column

Threaded rods must run through the specimen and also avoid the longitudinal reinforcing bars encased in the concrete. Matching the plate width to the width of the column, 270mm, would not be sufficient for providing the minimum edge distance from the plate edge to the bolt hole. Thus, extending the plate width on both sides is required. A 304.8mm (12 inch) plate width was chosen. Figure B.2 shows an overlay of the steel plate ontop of the North

side of the column. The holes must be placed such that they do not interfere with the reinforcement bars.

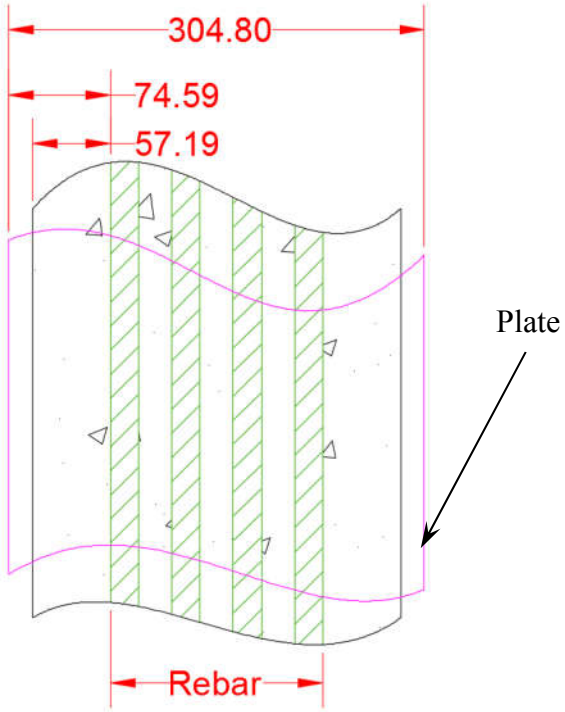

Figure B.2: Plate Edge Clearance for Bolt Holes

B.3 Detailed Drawings

B.3.1 Stiffened Brackets

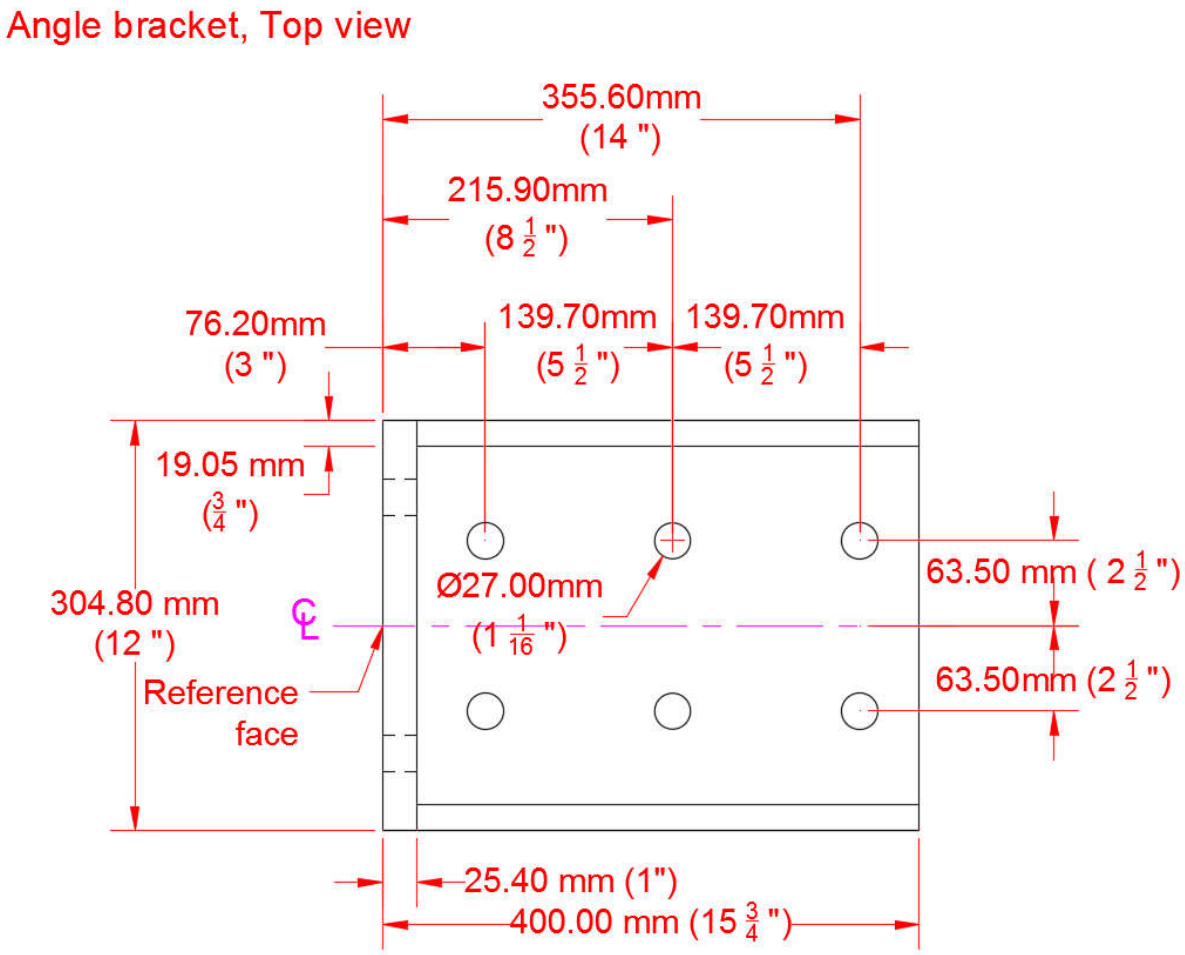

Figure B.3: Steel Bracket Details, Top View

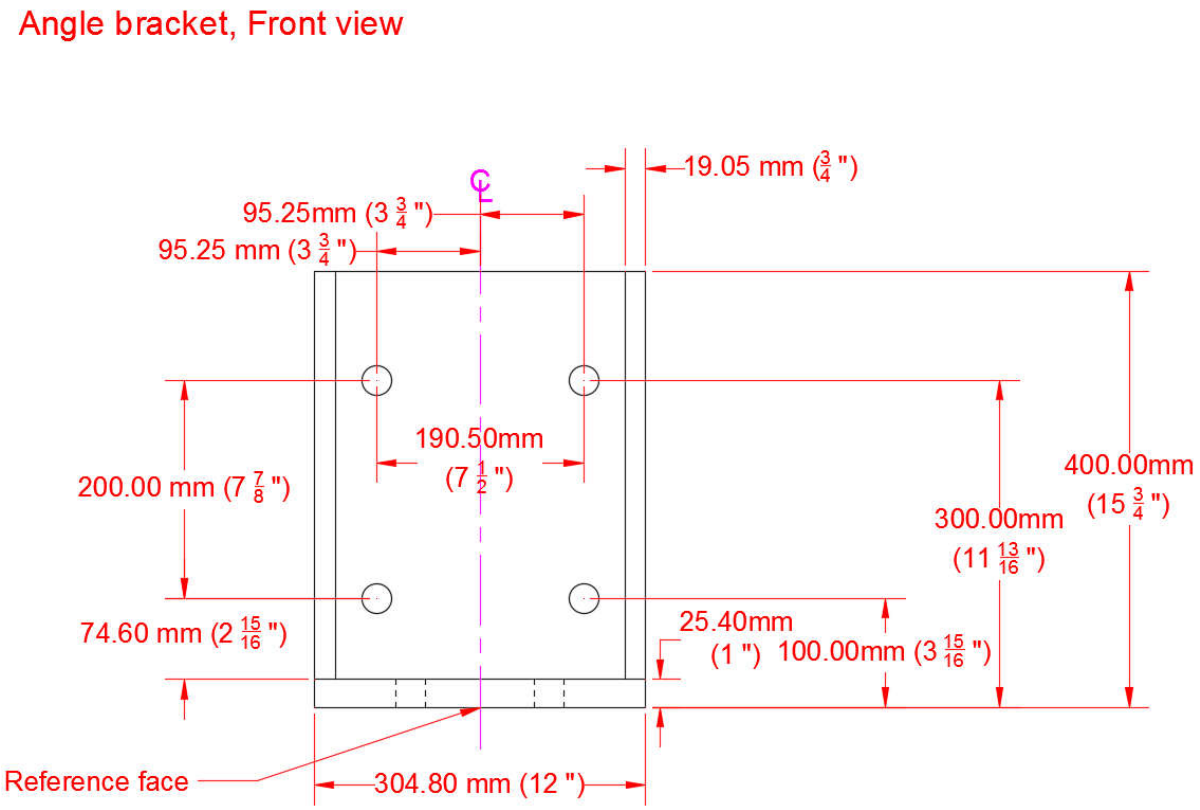

Figure B.4: Steel Bracket Details, Front View

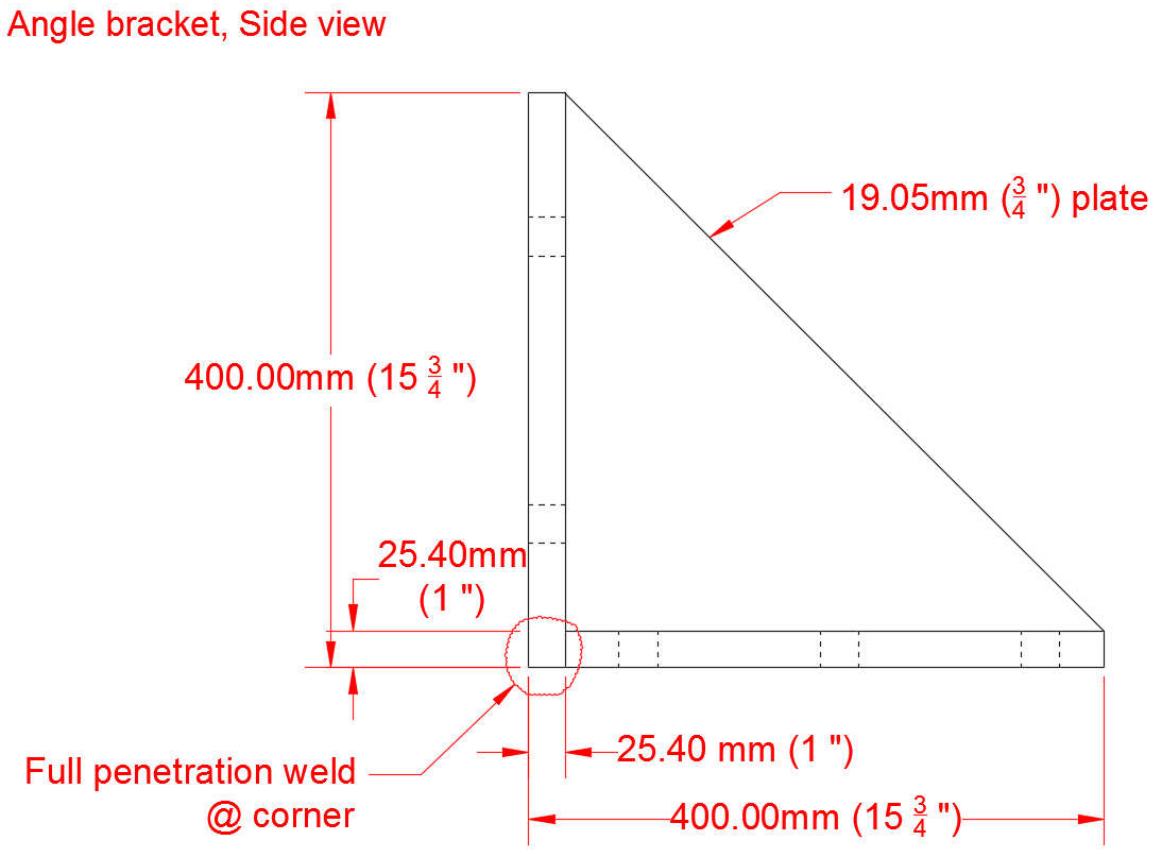

Figure B.5: Steel Bracket Details, Side View

B.3.2 Support Beam

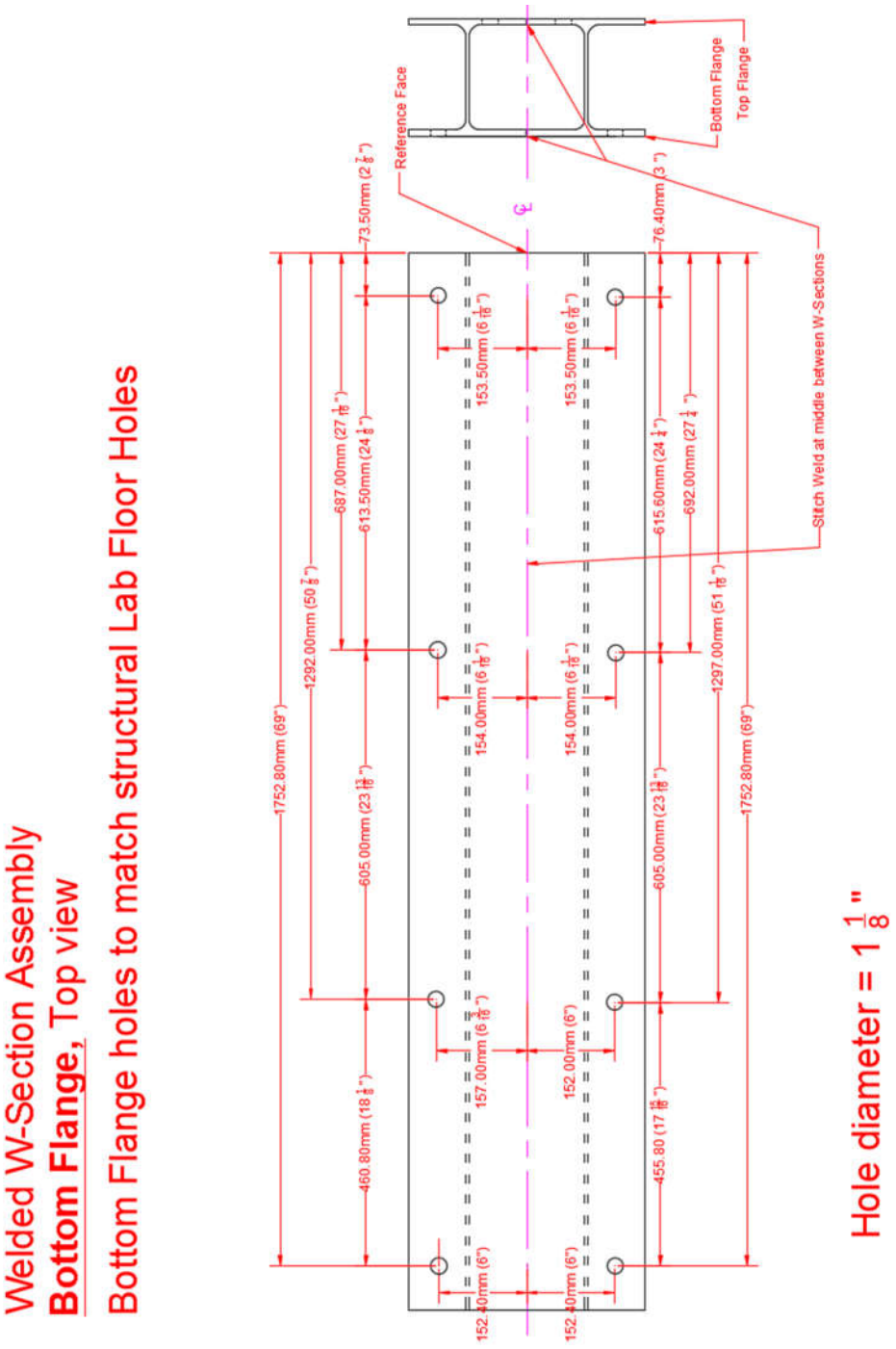

Figure B.6: Support Beam Hole Locations, Bottom Flange

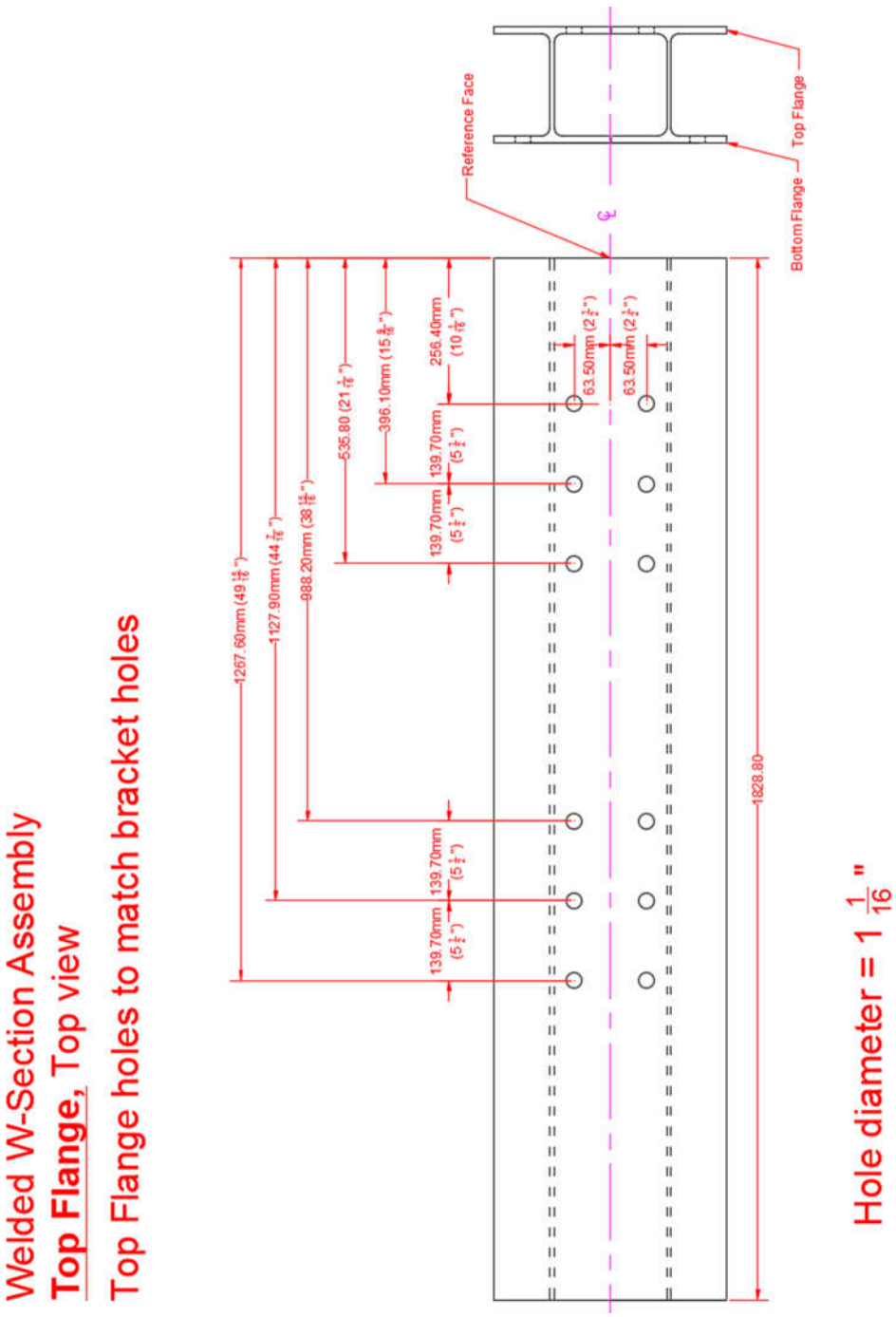

Figure B.7: Support Beam Hole Locations, Top Flange

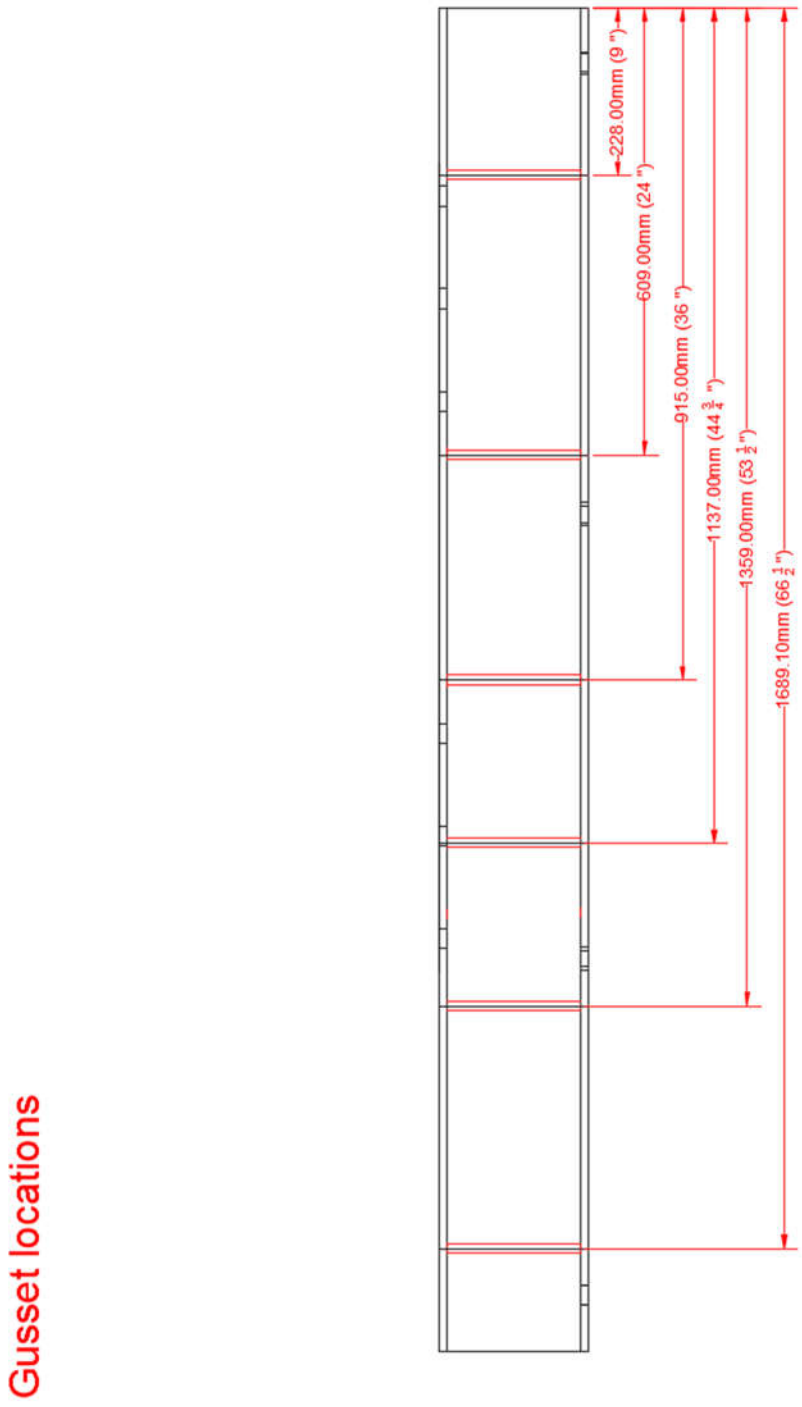

Figure B.8: Support Beam Gusset Locations